Assessment of the potential of selected adsorbents for use in small-scale systems for the removal of uranium from mine-impacted water

By

Kgaugelo Ishmael Smiley Mabape

A dissertation submitted to the Faculty of Science, University of the Witwatersrand, Johannesburg, in fulfilment of the requirements for the degree of Masters of Science

WITS University, Johannesburg, 2017

Declaration

I declare that this dissertation is my own, unaided work. It is being submitted for the Degree of Masters of Science in Chemistry at the University of the Witwatersrand, Johannesburg, South Africa. It has not been submitted before for any degree or examination in any other University.

_____

Signature of candidate

This 28th day of February 2017, Johannesburg

Abstract

The tailoring of zeolites surface properties using organic functionalising agents displaying higher binding affinity for metal ions is a widely explored approach for water treatment. In this study, amine functionalised zeolites and phosphate functionalised zeolites were separately synthesised from similar natural zeolite precursors using reflux methods. The surface composition and morphological elucidations were achieved by characterising the adsorbents using Fourier Transform Infra-red spectroscopy (FTIR), thermogravimetric analysis (TGA), Zeta potential, Point of zero charge (pH_{PZC}), and the Brunauer, Emmett and Teller analysis (BET).

In case study 5.1, the sorption mechanisms of the uranyl ion onto amine functionalised zeolites (AMZ), activated carbon (AC) and natural zeolite (NZ) were studied as function of various environmental batch parameters. There was effective adsorption when uranium existed as uranyl ions: UO_2^{2+} and UO_2OH^+. The data fitted numerous kinetic and isotherm models suggesting that the equilibrium mechanisms were characteristic of a combination of chemisorption and physisorption for these three adsorbents. The Dubinin-Radushkevich (D-R) model did not fit the data and therefore the energy values derived from it were not used to predict the mechanisms involved. However, the thermodynamic evaluations of parameters ΔH, ΔG and $\Delta S°$ showed that equilibrium mechanisms were exothermically, randomly and spontaneously favoured for all adsorbents at temperatures ranging between 22 and 40^oC. The adsorption capacity of 0.452 mg g^{-1} was achieved at pH 3 by 500 mg AC dosage using 20 mL volume of 10 mg L^{-1} uranyl ion solution after equilibrating for 6 h within the temperature ranges of 22 to 30^oC. Under the same conditions of sorbent dosage of 500 mg, uranyl solution volume of 20 mL and 10 mg L^{-1} U(VI) solution concentration, the maximum adsorption capacity of 0.506 mg g^{-1} for NZ and 0.480 mg g^{-1} for AMZ were both achieved at pH 4 after equilibration time of 21 h and 6 h with the optimum temperature range of 22 to 30^oC, respectively. The model results predict that intraparticle diffusion thorough pores decreased in the order AC > NZ > AMZ while estimating that chemisorption occurred in a reverse order. On the basis of the modelled data, it was deduced that amine functionalisation of natural zeolites improves their chemisorption capability for uranyl ion and can therefore be used as a cost efficient adsorbent for small-scale remediation of contaminated aquatic systems.

In another case study 5.2, the surface properties of successfully prepared aminomethyl phosphonic acid functionalised natural zeolite (APZ) were compared to those of commercial silica polyamine composites (SPC) for uranium uptake in batch aqueous solutions. The FTIR spectrum revealed that (3-aminotrimethyl) phosphonic acid functional groups were successfully grafted onto natural zeolite. The TGA analysis showed that the APZ had higher thermal stability and fewer active sites compared to SPC. The optimum adsorption capacity (q_e) of 49 mg g^{-1} and 44 mg g^{-1} uranium was achieved using 25 mg SPC and 100 mg APZ, respectively at pH 4, 25^{o}C after 1 and 6 h equilibrating time. The data best fitted the pseudo second-order kinetic model and Freundlich isotherm model. The thermodynamic studies showed that adsorption occurred chemically and exothermically for both APZ and SPC. The overall selectivity order for APZ was; Na > Mn ≥ U > Ca > Fe and for SPC was; Fe > Mn ≥ Ca > U> Na.

The findings showed that phosphate- and amine-functionalised zeolite bind strongly to uranium compared to the unmodified natural zeolite and other conventional adsorbents such as activated carbon. Their selectivity for this element was commendable. With further improvements in the synthetic protocols e.g. by using microwave-based methods, it should be possible to obtain functionalised zeolite that has superior properties to SPC.

Conference presentations

1. **Kgaugelo Mabape and Hlanganani Tutu,** *Removal of uranium from .polluted water; comparative study using activated carbon, natural zeolite and amine functionalized zeolite* SACI 2015 Conference, 27 November - 1 December 2015, Durban, Republic of South Africa, *Oral presentation*.

Dedication

To my mom; Agnes Mabape and my siblings Daisy, Thato and Naledi Mabape, I am grateful for being part of my family.

To my uncle; Masilo Phosa, I could not have asked for a wiser uncle.

Acknowledgements

I would like to convey in so many ways my sincere gratitude to Prof. Hlanganani Tutu for his supervision, mentorship and efforts executed to avail financial support for my studies.

Many thanks go to the past and present fellow Environmental Analytical Chemistry Research group members at the University of Witwatersrand. However, I would like to pay special thanks to Joy Mokone and Somandla Ncube for their academic and life advices as well as jokes shared that made this research work a journey joyfully travelled.

To Nikita Tavengwa, Kgabo Manamela, Pfano Nekhunguni and Kitondo Mwelwa, my appreciation for your inputs to my work remain second to none. To Tshegofatso Mabilane, I am truly grateful and honoured to have worked and co-supervised an inspirational student like you as my first ever honours student.

To Chimangadzo Munonde and Penny Mathumba from the University of Johannesburg, I thank you my friends for your limitless heaven sent research discussion and write up advices through those midnight calls and emails.

My extended gratitude goes to Prof N. Coville for assistance with BET and TGA data acquisition, Mr Chuene Mogehle for ICP-OES analysis, Mr Tebogo Mokhele for FTIR data acquisition and Ms Khumalo Ignatia for access and use of analytical balance. I would like to further give many thanks to Mr Famanda Valoyi and Mr David Moloto for their help with supply of gas cylinders.

I would like to thank the National Academy of Science USA (PEER) and National Research Funding (NRF) of South Africa for their financial support towards this project.

Above all I would like to thank God for the gift of life shared on his beautifully created world.

Table of Contents

Declaration i

Abstract ii

Conference presentations iv

Dedication v

Acknowledgements vi

Table of Contents vii

List of figures x

List of tables xii

Acronyms and abbreviations xiii

Chapter 1 1

Introduction: 1

1.1. General background 2

Chapter 2 6

Literature review: 6

2.1. The formation of acid mine drainage (AMD) 7

2.2. Uranium (U) background 9

2.3. Uranium speciation and complexation 10

2.4. Uranium in mining industry 12

2.5. Uranium applications 13

2.6. Uranium health hazards 13

2.7. Legislative restrictions on uranium 15

2.8. Uranium water remediation techniques 15
2.9. Background of adsorbents: 17
2.10. Activated carbon 17
2.11. Zeolite 18
2.12. Zeolite functionalisation 19
2.13. Silica Polyamine Composites 21
2.14. Principle of various technologies used for characterisation 22
2.15. Environmental data modelling 23
Chapter 3 25
Research aim and objectives: 25
3.1. Aim 26
3.2. Objectives 26
3.3. Questions 26
3.4. Significant indicators of the study purpose 27
3.5. Hypothesis 28
3.6. Novelty 28
Chapter 4 29
Research Methodology: 29
4.1. Chemicals and reagents 30
4.2. Preparation of solutions 30
4.3. Adsorbent preparation 31
4.3.1. 3-aminomethyltriethoxysilane zeolite functionalisation 31

4.3.2. (Aminomethyl) phosphonic acid functionalised zeolite 31
4.4. Instrumentation and characterisation of sorbents 32
4.5. Batch adsorption studies 33
4.5.1. Sample preparation 33
4.5.2. Parameter optimisation 33
4.5.3. Batch adsorption competition studies 34
4.6. ICP-OES analysis 34
4.7. Data treatment 35
4.7.1. Data processing 35
4.7.2. Data validation 38
4.7.2. Adsorption data modelling 41
4.7.3. Geochemical modelling 46
Chapter 5 48
Results and Discussion 48
5.1. Results and discussion 49
5.2. Results and discussion 70
Chapter 6 89
Summary of general conclusions and future work 89
6.1. Summary of general conclusions 90
6.2. Future work 91
6.3. References 92

List of figures

Figure 2.1: The AMD introduction into aquatic systems through surface water (route 1) and aquifer (route 2).

Figure 5.1: Adsorption of U(VI) from 10 mg L^{-1} U aqueous solution at different pH and T = 25 ± 1°C over 24 h mixing time at 150 rpm shaking speed.

Figure 5.2: Effect of adsorbent dosage increase on adsorption efficiency of 10 mg L^{-1} uranium(VI) using AC, NZ and AMZ as the adsorbents at pH 3, 4 and 4, respectively.

Figure 5.3: The plot of time versus adsorption efficiency as function of contact time

Figure 5.4 (a): Linearised Pseudo first-order for activated carbon on uranium

Figure 5.4 (b): Linearised Pseudo second-order for activated carbon on U

Figure 5.4 (c): Linearised Pseudo first-order for natural zeolite on U

Figure 5.4 (d): Linearised Pseudo second-order for natural zeolite on U

Figure 5.4 (e): Linearised Pseudo first-order for amine zeolite on U

Figure 5.4 (f): Linearised Pseudo second-order for amine zeolite on U.

Figure 5.5: Effect of U(VI) concentration on adsorption capacity and adsorption efficiency.

Figure 5.7: Adsorption efficiency of AC (t = 6 h), NZ (t = 21 h) and AMZ (t = 6 h)for uranium(VI) in 10 mg L^{-1} aqueous solution.

Figure 5.8: The FTIR spectrum profile of NaZ (NaOH), APZ and SPC.

Figure 5.9: Thermogravimetric curves of NZ, APZ and SPC

Figure 5.10: Effect of pH_i on 10 mg L^{-1} U adsorption capacity at room temperature for 24 h (n=3, SD =RSD × q_e).

Figure 5.11: Speciation of U in 10 mg L^{-1} U aqueous solution at T = 25 °C, Eh = 4 using Phreeqc code interactive modelling version.

Figure 5.12: Effect of dosage on 10 mg L^{-1} U adsorption capacity at T =25°C, pH_i 4 and t = 24 h (n = 6, sd = rsd × qe, p-value at 95% confidence level)

Figure 5.13: The plot of 10 mg L^{-1} U(VI) concentration adsorption efficiency versus contact time (n = 3, sd = rsd ×qe, p value at 95 %).

Figure 5.14: Effect of initial uranium (IV) concentration on adsorption capacity of 100 mg APZ (at t = h) and 20 mg SPC (at t = 1 h) at pH 4, 25^{o}C and 150 rpm.

Figure 5.15: Effect of temperature on 30 mg L^{-1} uranium removal efficiency and adsorption capacity (n = 3, sd =e_4 ×q_e, p –value at 95% confidence level)

List of tables

Table 2.1: The admissible limit of uranium in different countries

Table 2.2: Some metal ion removal techniques.

Table 4.1: Some operating conditions for ICP-OES parameters

Table 5.1: Mineralogical composition of natural zeolites and amine functionalised zeolites.

Table 5.2: Some of the important physicochemical properties displayed by natural zeolite, activated carbon and amine zeolites.

Table 5.3: kinetic models calculated parameters for U sorption onto AC, NZ and AMZ.

Table 5.4: The adsorption isotherm parameters calculated for AC, NZ and AMZ.

Table 5.5: Thermodynamic parameters of U adsorption using AC, NZ and AMZ adsorbent

Table 5.6: Physicochemical properties of aminophosphonated zeolite and Silica polyamine composite before batch adsorption studies

Table 5.7: Kinetic parameters of U adsorption using SPC and APZ adsorbents

Table 5.8: Isotherm parameter of U adsorption using SPC and APZ adsorbent

Table 5.9: Thermodynamic parameters of U adsorption using SPC and APZ

Table 5.10: The metal ion distribution coefficient and selectivity coefficient

Acronyms and abbreviations

AC	Activated carbon
AMD	Acid mine drainage
AMZ	3-aminopropyltriethoxysilane functionalised natural zeolites
ANOVA	Analysis of variance
APTES	3- aminopropyltriethoxysilane
APZ	Aminomethyl phosphonic acid functionalised natural zeolites
BET	Brunauer-Emmett-Teller
CNS	Central nervous system
DNA	Deoxyribonucleic acid
D-R	Dubinin–Radushkevich
DU	Depleted uranium
FTIR	Fourier transformer-infrared
GDR	German Democratic Republic
ICP-OES	Inductively coupled plasma-optical emission spectroscopy
LOD	Limit of detection
LOI	Loss on ignition
LOQ	Limit of quantification
MDL	Method detection limit
MOFs	Metal-organic frameworks
Na-Z	Sodium hydroxide modified zeolites
NZ	Natural zeolites
pH_{pHz}	Point of zero charge
PHREEQC	pH Redox Equilibrium computer code
SA	South Africa
SPC/BPAP	Silica polyamine composite
TDS	Total dissolved solutes
TGA	Thermogravimetric analysis
U	Uranium

USEPA	United States Environmental Protection Agency
WHO	World health organisation
XRF	X-ray florescence
Sd	standard deviation
3- MPTMS	3-mercaptopropyltrimethoxysil

Chapter 1

Introduction:

This introductory chapter highlight the potential hazards of elevated amounts of trace metals causing environmental water pollution. Emphasis is also made on the importance of mine impacted small-scale water remediation techniques.

1.1. General background

Water pollution is ubiquitous. According to United States Environmental Protection Agency – USEPA (Azarch, 2011) and Li (Li, 2015), water is ranked second global challenge. In developing countries (e.g. South Africa) that thrive on mining for their economic stability, water problem is exacerbated by mining activities in addition to low rainfall (Saad, 2013). Mining industry utilize 6% of water yearly (Azarch, 2011) and this may directly or indirectly deteriorate water quantity (Tutu *et al*., 2008) and quality. The inorganic water pollution occurs as a consequence of acid mine drainage (AMD) (Groudev *et al*., 2008), a phenomenon whereby elevated concentrations of sulphide metal rich effluents leached from mining industries are introduced into the aquatic environment (Johnson and Hallberg, 2005).

The AMD poses extensive environmental threat to aquatic ecosystem, animals and human beings (Ríos et al., 2008). The toxicity (Tutu *et al*., 2013) and exposure level of environmental inorganic pollutants (Monser and Adhoum, 2002) may cause acute or chronic morbidity, mortality and other varied human physiological responses associated with inorganic pollutants, hence these environmental risks makes water purification a universal concern.

In South African mine fields, in particular at Wits basin, the phenomenon of AMD has been extensively studied and reported (McCarthy, 2011; Naicker *et al*., 2003; Rosner and van Schalkwyk, 2000). The Wits basin is the major source of the estimated 40% gold global contribution from the South African mine fields (Grové and Harris, 2010). During or after gold mining most trace metals, for instance mercury (Leigh, 1995) and uranium are left at the gold mining tailings as mine wastes that oxidises and become potential agents of AMD. Thus, wastes from Wits basin epitomise significant source of trace metal impacting enormously on the quality of the surrounding water, therefore may pose health defects to aquatic ecosystem. Nonetheless, designing solution strategies to the problem of AMD remains a complex challenge.

In order to design a plausible water treatment method material, it is important to first gain knowledge about the source of pollution and possible contaminants. According to literature (Rui-Zhong et al., 2002) uranium mostly coexist with gold in ores. Similar declarations were made for Witwatersrand basin (Tucker et al., 2016). Uranium is characterised by wide oxidation states range, high toxicity, bioaccumulation and radioactivity. Hence their high mobility through (Blood brain barrier) causes acute diseases such as brain impairments and cancers, in addition to kidney complications, cell necrosis (Wan et al., 2006) and cancer (Saccomanno et al., 1988). Therefore, uranium removal from polluted water is a major health concern.

Different methods known to treat radioactive metal ions have been compared for removal efficiency of uranium. The techniques are ion-exchange, precipitation (Saad *et al*., 2014), reverse osmosis (Monser and Adhoum, 2002), electrolytic (Faur-Brasquet, 2002), coagulation, nanofiltration (Sprynskyy *et al.*, 2011), solvent extraction (Mellah et al., 2006), intracellular sequestration of plants (Kalin *et al.*, 2004) and adsorption (Kütahyalı and Eral, 2004). However, most methods lack selectivity for metals such as uranium. The large amounts of the competing ions in the effluent volumes result in binding site competition (Kalin *et al*., 2004).

Adsorption is generally preferred owing to cost efficiency (Faur-Brasquet *et al.*, 2002; Motsi *et al*., 2009), easy applicability and regeneration (Ríos *et al*., 2008), environmentally friendly (Jamil *et al*., 2011) and availability of wide range of adsorbents materials to choose from (Zhang *et al*., 2009; Mellah *et al.*, 2006; Babel and Kurniawan, 2003)**.**

Since industrialization and mining left legacy of tailings which leaches metal ions into water resources, it is therefore necessary to remedy water at both large and small scale water systems. A few large scale solutions have been put in place in the Central and West Rand Goldfields of the basin. In these basins, the remediation processes relies upon the application of the neutralisation process whereby the inorganic polluted water is treated with limestone and lime. One such plant is located in Boksburg where the East Rand Proprietary Mine had a shaft.

Water is pumped out of the disused shaft and mine voids, treated and discharged into the Elsburgspruit, a tributary of the Klip River.

The common and widely used adsorbent; activated carbon has lost interest for use in small scale water resources due to cost inefficiency and low affinity for inorganic contaminants (Babel and Kurniawan, 2003). Therefore, the need for cost effective adsorbents for use in small-scale water resources to remove toxic trace metals (especially radioactive) causing detrimental diseases to human and animals remains a major concern throughout the world.

Therefore, according to the knowledge of the author, not much attention has been paid to small scale solutions such as treatment of contaminated mine water at the point of use. Thus, this study was aimed at assessing selected adsorbent materials for their potential for use in small scale applications to clean up contaminated mine water. Water treatment material such as natural zeolites will be modified to target certain important inorganic contaminants such as uranium since apart from being non-biodegradable, uranium is also characterised by radiotoxicity. The zeolites are chosen as priority solid material adsorbent for small scale water remediation investigations because of their high stability, abundance and easy modifications for better cation capturing.

1.2. Dissertation Overview

Pollution and scarcity of water contribute to the worldwide absolute concern for water quality and quantity. In this study, the problem of water pollution caused by mining activities was addressed. In general, the study focused on developing cheap adsorbent for trace metal ion removal from contaminated water. However, the main specific objective of this research was to develop functionalised zeolites displaying high affinity for uranium. The work was divided such that the focus was put onto the importance of applying different zeolite functionalisation routes, functionalisation reagents and varied adsorption parameters optimisation designs. The methods employed in order to achieve the goals of the study are based on previously used techniques.

Changes and additions made were aimed at providing suitable methodology that will enhance the possibilities of achieving the ultimate goals of the study. Both the developed and untreated material were characterised using a variety of characterisation techniques in order to understand the properties of the material used as adsorbents. In our study, the zeolites were calcined using NaOH- before being functionalised with amine-, and phosphate groups using corresponding capping agents. The resulting functionalised zeolites hybrids were evaluated for removal of uranium from aqueous solution. The experimental procedures were performed in batch analysis. Data processing was done using mathematical adsorption models that are rigorously explained in chapter 4. In chapter 5, a brief background for case study 5.1, is followed by a detailed section of the results and discussions of uranium batch adsorption study using activated carbon (AC), natural zeolite (NZ) and amine functionalised zeolite (AMZ) as adsorbents. Similarly, in chapter 5.2 a brief background precedes the discussions based on the use of phosphonated zeolite and silica polyamine composites for uranium sorption. The summary of conclusions and possible work for undertaking as future research objectives is separately documented in chapter 6.

Chapter 2

Literature review:

This chapter gives a literature background on chemistry and treatment methods of uranium in mine drainage and other forms of polluted water. A brief description on human health hazard owing to uranium is succeeded by an in-depth discussion on the type of adsorbents used in this study. The chapter concludes by highlighting the general zeolite functionalisation for water remediation.

2.1. The formation of acid mine drainage (AMD)

In South Africa the AMD phenomenon is evident at the Witwatersrand basin which encompasses seven (7) goldfields (Feather, 1975) consisting of over 70 minerals (Pretorius, 1989) from the ores. Minerals identified includes gold, a variety of silicates, pyrite (FeS_2), cobaltite (CoAsS), sphalerite (ZnS), chalcopyrite ($CuFeS_2$), arsenopyrite (FeAsS), uraninite (U_3O_8), and brannerite ($UO_3Ti_2O_4$) (Tutu et al., 2009; Feather, 1975;) . Gold mining at the basin commenced in 1886 (Falconer *et al.*, 2006) with the aid of mercury amalgam extraction method (Bakatula et al., 2012). As mining got deeper, a lot more pyrite was encountered; competing reaction between mercury and sulphur (Naicker *et al.*, 2003) made mercury amalgamation method less economic. It has been over a century since amalgamation method was then replaced by the cyanidation method (MacArthur-Forrest process) (Yazici *et al.*, 2009) which showed abundant availability, strong affinity for gold (Dash et al., 2009) and complexing capability leading to effective low cost extraction (Yazici *et al.*, 2009). Cyanidation gold extraction method equations equation 2.1 (Fagan and Haddad, 1991):

$$4Au + 8CN^- + O_2 + 2H_2O \rightarrow 4Au(CN)_2^- + 4OH^- \quad (2.1)$$

Cyanidation is quite selective for gold and silver making the other elements to largely remain as sulphates (Tutu et al., 2008) wastes discarded in the porous mine tailing (Johnson and Hallberg, 2005). These sulphides (mainly pyrite) oxidizes on exposure to oxygenated water (Akcil and Koldas, 2006) forming acid mine drainage.

AMD formation can be briefly described by the following equations (Akcil and Koldas, 2006; Ríos *et al.*, 2008;):

$$FeS_2 + {}^7/_2O_2 + H_2O \rightarrow Fe^{2+} + 2SO_4^{2-} + 2H^+ \quad (2.2)$$

$$Fe^{2+} + {}^1/_4O_2 + H^+ \rightarrow Fe^{3+} + {}^1/_2H_2O \quad (2.3)$$

$$Fe^{3+} + 3H_2O \rightarrow Fe(OH)_3 + 3H^+ \quad (2.4)$$

$$FeS_2 + 14Fe^{3+} + 8H_2O \rightarrow {}^{15}/_2Fe_{2+} + 2SO_4^{2-} + 16H^+ \quad (2.5)$$

Equation 2.2 shows oxidation of FeS_2 leading to high total dissolved solutes (TDS) and acidity characterized by high levels of Fe^{2+}, SO_4^{2-}, and H^+; (2.3) is the oxidation of Fe^{2+} in the presence of O_2, microbial activity and low pH conditions. In (2.4) oxidation of iron (Fe) from Fe^{2+} to Fe^{3+} leads to ferric iron (Fe^{3+}) precipitation as $Fe(OH)_3$ in water with some Fe^{3+} remaining precipitated. In (2.5), the precipitated Fe^{3+} from (2.4) oxidizes more FeS_2 resulting in elevated total dissolved solutes (TDS) consisting the AMD.

The AMD composition largely depends on pollution sources. Sources of AMD or inorganic wastewater includes but not limited to mining, sewage (Tutu *et al.*, 2013), metal finishing (Monser and Adhoum, 2002), galvanic process (Johnson and Hallberg, 2005), electroplating (Mugisidi *et al.*, 2007), agricultural fertilizers and pesticides (Saeed and Shaker, 2008), petroleum refining, and steel manufacturing (Inglezakis and Grigoropoulou, 2004).

Furthermore, the availability of oxidising agents (Johnson and Hallberg, 2005), microbes (Akcil and Koldas, 2006), historic mining operations (Leigh, 1994), climate and geomorphological conditions (McCarthy, 2011) determine both the nature and distribution of TDS or trace metals (Akcil and Koldas, 2006) forming part of the AMD. The trace metals content in polluted water also depends on the water contamination path undertaken and the activeness of the mine (Johnson and Hallberg, 2005) introducing the mine effluents into water streams. There is two most common AMD pathways into aquatic environmental systems. Oxidised trace metals from tailings may cause AMD water contamination principally during high rainfall through a continuous flow of surface water into water streams (Egiebor, 2007) such as borehole, rivers and dams as shown by route 1 (Fig.1.1). In Route 2, AMD water contamination pathway involves transportation of TDS through groundwater system or aquifer (Johnson and Hallberg, 2005). From the diagram it is shown that wide range of tailings constituting metals ores left as wastes during mining largely accounts for introduction of inorganic TDS into environmental water systems through surface or aquifer transportation.

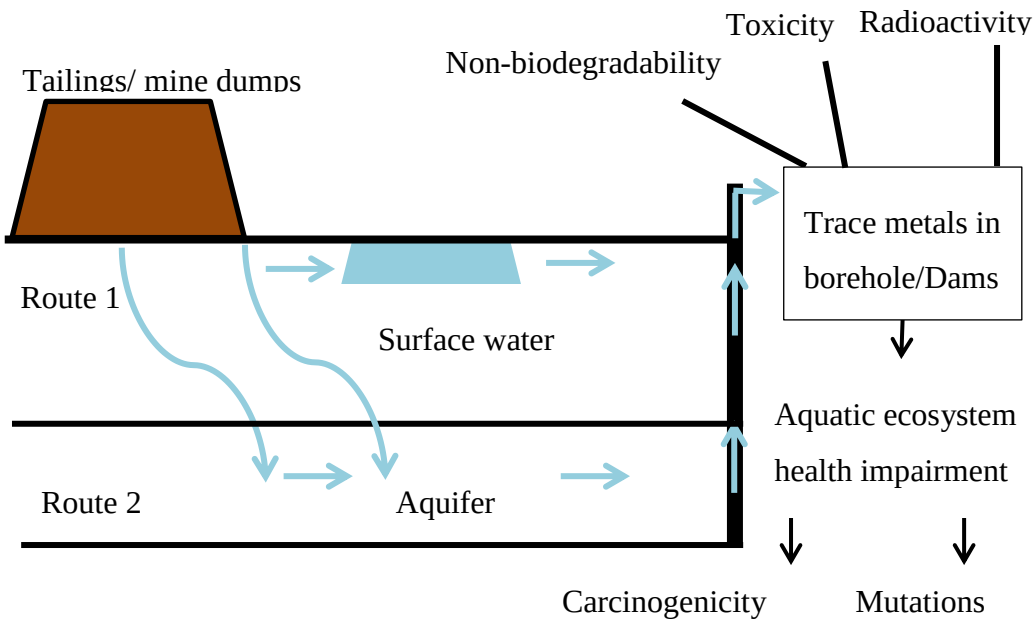

Figure 2.1: the AMD introduction into aquatic systems through surface water (route 1) and aquifer (route 2).

2.2. Uranium (U) background

Uranium is a naturally occurring chemical element (Kraemer and Evans, 2012) with atomic number 92. This element is the heaviest trace metal (Zamora *et al.*, 2009) and has the heaviest nucleus found in the environment (Vidaud *et al.*,2005). Uranium display radionuclide properties (Horzum *et al.*, 2012), hence it forms part of actinides series. Actinides refer to radioactive transition metals with 5f orbital; they are placed at the bottom of the transition metal groups due to their chemical behavioural similarities to other transition metals and they are arranged along the periodic table according to the strength of their radioactivity. Actinides are so named as a consequence of their series first element known as actinium. Scientists often refer to actinides as uraninides (actinides elements from uranium) or transuranium due to the production of transient amount of other actinides from uranium decay and also the predominant occurrence of uranium juxtaposed to any group member of actinides elements (Zhao *et al.*, 2010). A decade ago, uranium constituted about 160 mineral species (Yang and Volesky, 1999) that accounted for one twentieth ($1/20^{th}$) of all identified minerals (Kalin *et al.*, 2004).

Despite its abundance on the earth's crust, naturally occurring uranium rarely enters the environment in significant quantities. Noticeable uranium concentrations enter the environment anthropogenically. Mining and nuclear industry are the main human sources of uranium. Industrial operation such as burning of coal and some fossil fuels also add uranium content in the environment (Sprynskyy *et al*., 2015). Human induced uranium concentrations often reach levels capable of endangering the exposed human, fauna and biota.

Ordinarily uranium is converted into ^{238}U before use as nuclear energy and nuclear weapon production source (Zhao *et al*., 2010). During these nuclear productions a uranium by-product known as depleted uranium (DU) is produced. DU is 40% less radioactivity than natural uranium. In human DU biochemically combines to insulin receptors specific sites, citrate , carbonates or in most cases replace calcium in bones leading to body dysfunctionalities such as lung cancer, distorted vision, birth defects in offspring, lymphoma, nephrotoxicity, osteoporosis and kidney malfunction (Zamora *et al*., 2009).

Speciation of uranium at pH 7.4 in biological medias is complicated by its interactions with small ligands such as phosphate bases in addition to few proteins (lipoproteins, enzymes and hormones) Phosphorus is a micronutrient without any known alternative, therefore its reaction to uranium at pH near neutral causes a potentially abnormal human urinary system functioning and bone fragmentation (Elser and Bennett, 2011; Vidaud *et al*., 2005).

2.3. Uranium speciation and complexation

Knowledge about uranium speciation in aqueous solutions provides the basis for determining a suitable uranium water remediation techniques (Bernhard *et al*., 1998) because speciation regulates physical and chemical processes responsible for uranium transportation (Belli *et al*., 2015; Martinez-Torrents *et al.*, 2013) and mine wastes into the environmental formation. Environmental migration and distribution of U is also dependent on the interactions of uranyl ion with organic ligands (e.g carboxylic acids) (Sladkov, 2013; Deepatana and Valix, 2008).

Nonetheless, the transportation and interaction strength are dependent on the oxidation of the available uranium species in solution(Arnold et al., 2011). Uranium can exists in water as: +2,+ 3, +4, +5 and +6 oxidation state (Shrivastava *et al.*, 2013). The oxidation state of U^{6+} is the most stable state of uranium under a wide pH range. Water rich in organic material may primarily contains uranium in a tetravalent oxidation state (Shrivastava *et al*., 2013).

Uranium strongly binds to oxygen rich ligands such as carbonate (CO_3^{2-}), humic acid, flavonoids (Alberti *et al*., 2007), phosphates ($H_xPO_4^{(3-x)}$) (Wang *et al*., 2014; Liu, 2013), CO_2 (Gregusova, 2011), nitrate (NO_3^-), sulphate (SO_4^{2-}), silicate ($Si(OH)_4$), acetate (CH_3COO^-) and electron rich halides [fluorine (F^-), and chlorine (Cl^-)] owing to the predominant existence of uranium in aquatic environments as a mobile hydrated hexavalent uranyl dication (UO_2^{2+}) (Bargar *et al*., 1999; Ulrich *et al*., 2006) that displays a hard Lewis acid metal properties (Vidaud *et al*., 2005). Uranium also reacts with small carboxylic acids to form different metal complexes. For instance uranium can react with acetate to form UO_2Ac, UO_2Ac_2 and $UO_2(Ac)_3^-$ (Sladkov, 2013).

The metal-ligand interaction strength, metal selectivity for ligands and number of possible binding sites for complex formation depends largely on metal ion coordination numbers (Dudev *et al*., 2006). This coordination number and geometry can be controlled by modifications of metals or ligands (Lee *et al*., 2004).

In addition the complexes formation, uranium mobility, and sorption in aquatic solutions dependents on solution pH, concentration and the presence competing metals such as; Mg (Fox *et al*., 2006), Ca, Fe, Al (Ulrich *et al*., 2006) 20), Zn, Mn, and Hg. Moreover, competing metals may bind to ligands to form bulky metal complexes that lead to reduced metal availability for adsorption by the ligand already occupied by the competing metals. Uranium complexes identified in different mine waters systems includes; UO_2SO_4 (aq) in sulphate rich acidic medium, $Ca_2UO_2(CO_3)_3$ (aq) in calcium-carbonate rich neutral medium and $UO_2(CO_3)_3^{4-}$ (aq) in calcium-carbonate rich medium (Bernhard *et al.*, 1998).

Other studies (Langmuir, 1978; Sanding and Bruno, 1992) reported that the presence of phosphate in water of pH range 4-9 lead to the predominance of uranium species such as UO_2HPO_4, $UO_2(HPO_4)_2^{2-}$, (aq) and $UO_2PO^-_4$. The presences of sulphuric acid and iron pyrite in uranium mine water lead to the formation of complexes such as uranyl-bisulphates ($UO_2(HSO_4^+)$) (Nguyen Trung *et al*., 1992) and $UO_2(SO_4)_3^{4-}$ (Ladeira and Gonçalves, 2007), respectively. In summary, Uranium speciation, the presences of microbes, organic and inorganic ligands determine the removal percentage and phases of uranium onto materials used for uranium water decontamination (Semião *et al*., 2010; Wall and Krumholz, 2006).

2.4. Uranium in mining industry

Over 70 years ago, Uranium was mostly mined for use as a colouring agent. It was in 1940s that uranium gained its use for nuclear fuel and economic purposes. Today uranium mining can be done in three basic methods, namely; surface, underground, and solution mining. The choice of extraction is governed by the deposit grade, size, geology and economic reflections (Campbell *et al*., 2015). The abundant uranium availability was recorded in countries such as German Democratic Republic (GDR) (Bister *et al*., 2015), USA *(*Fox *et al.*, 2006*;* Samet *et al*., 1984) and South Africa.

In uranium concentrations were ruled to be above admissible limits in some mining areas such as Minas Genais – Brazil (Ladeira and Gonçalves, 2007). The studies (Lundin Jr *et al*., 1969; Samet *et al*., 1984) respectively showed that uranium underground mining was responsible for the two separate cases of 62 from 3414 and 11 from 780 lives terminated due to malignant respiratory system lung cancer infection. In South Africa 78 cases associated with uranium caused lung cancer were previously reported out of 2260 gold miners and 380 controls (Hnizdo *et al*., 1997). The studies further reported an increasing probability of uranium caused lung cancer in smoking miners.

The increasingly uranium lung cancer cases reported from different health and medical research institutions led to the closing down on most uranium mining in most countries. However, in South Africa uranium from mine areas remains a treat to human and other living organisms owing mostly to two factors, (1) uranium has a longer half live enough to exist for more future millions of years, (2) Uranium is continuously leached into the environmental systems through abandoned and operating gold mine tailings. Henceforth, uranium removal at low acidic pH solutions is appropriate as uranium contaminated water characterised by low pH is expected to leach into water streams at the point of use rather than the main pollution site. Different uranium removal techniques have primarily involved sorbents whereas general method for bulk mine water remediation involved liming using $CaCO_3$.

2.5. Uranium applications

As previously mentioned that uranium use for colouring was halted decades ago, the application of uranium oxides to produce orange colours for fiestaware or tableware also ended around 1960s (Sutton and Burastero, 2004). Decades ago uranyl salts were also reported to enhance sample sustainability during electromagnetic microscopy analysis of DNA(Zobel and Beer, 1961).

However, currently uranium gains its abundant use in nuclear fuel manufacturing, nuclear research and weapon production (Gregusova and Docekal, 2011; Mellah *et al*., 2006). Other applications of uranium are in the form of depleted uranium in military (Kraemer and Evans, 2012) to provide stability of transport aircrafts and watercrafts. It is also reported that uranium can be used for radiation shielding for radiopharmaceuticals, armor plating and armor penetrating munitions during war (Sutton and Burastero, 2004).

2.6. Uranium health hazards

Uranium threatens the health of organisms owing to its high toxicity and radioactivity (Alberti *et al*., 2007). Therefore, its environmental and geochemical behavioural analysis is important (Wang *et al*., 2014).

Human organs reported to be affected by uranium high levels include; kidney (Neves *et al*., 2012), lungs, brains, bones (Vidaud *et al*., 2005) and liver. As shown in Fig.1.1 a lung cancer is among the most acute diseases emanating from high levels of trace metals in water (Davidescu, 2013).

Other disease may include; renal malfunctioning, acute tubular necrosis, red blood cell immune system disorder, bone cancer and neurotoxins. These health risks can emanate from uranium extraction and subsequent exposure of organisms to uranium radiations in the environment (Scislewski and Zuddas, 2013). Consumption of food substances made from radioactive contaminated fish may also be responsible for radioactive health defects (Karpas, 2014; Environment, 2014).

Uranium is a carcinogenic radioactive metal capable of causing biochemical and genetic damages in addition to liver and kidney diseases that may subsequently lead to death (Shrivastava *et al*., 2013). Uranium binds strongly to iron metal. In human body this may affect the amount of free iron available for binding to haemoglobin which is responsible for transportation of oxygen and carbon dioxide to and from body cell and tissues respectively. Other proteins that are susceptible to the raise in uranium body levels include transferrin.

The binding of uranium to transferrin affects the transportation of the transportation of metabolites from liver and brain where transferrin is produced (Chung, 1984). This results in human vulnerability to microbes infections due to reduced microphage production. Irrespective of the method of uranium introduction to human body, only less than 1% amounts of uranium are retained in body systems after 5 days, with about 40 % of the remaining amounts in blood streams being deposited equally to kidney and bones (Adams and Spoor, 1974).

Uranium problem was identified in countries such as Iraq, Serbia and USA as wars repercussion. In Helsinki region, south of Finland, uranium content above exceeding 10 mg L^{-1} was reported (Asikainen and Kahlos, 1979).

2.7. Legislative restrictions on uranium

Health hazards of trace metals lead to tightening of the environmental policies towards industries (Crafford, 2010). Currently, various state environmental regulations agencies enforce mine water treatment before its release into the environment. In an endeavour to limit uranium consumption from water, World Health Organisation (WHO) and USEPA set the admissible uranium daily intake of 0.6 and 3 μg kg^{-1}, respectively (Neves et al., 2012). An example of a significant regulation impact on uranium content occurred in Portugal were about 60 uranium mines were abandoned in the past century. Table 2.1 display the optimum permissible levels of uranium in drinking water as per different regulatory bodies.

Table 2.1: The admissible limit of uranium in different countries

Country	Regulatory body	Admissible uranium limit	Environmental system	Literature sources
USA	USEPA	0.02 μg L^{-1}	Drinking water	(Shrivastava *et al*., 2013)
Canada	-	20 μg L^{-1}	Drinking water	(Karpas, 2014)
Germany	EPA(UBA)	15 μg L^{-1}	Drinking water	(Karpas, 2014)
Across the globe	WHO	9 μg L^{-1} 0.6 μg Kg^{-1}	Drinking water Body weight p/d	(Abdi *et al*., 2014)

2.8.Uranium water remediation techniques

The well documented uranium chemistry in AMD or wastewaters (Kalin et al., 2004; Tutu, 2003) emphasise that uranium chemistry determines its complex removal processes. The nature of the adsorbent, solution pH (Motsi et al., 2009), metal speciation, water composition and complexation affinity (Kalina, 2005) as well as other environmental conditions (Kalin et al., 2004; Tsezos, 1983) are some factors that affect the removal of metals from AMD. Various conventional methods have been used for trace metal removal and recovery from polluted water (Phillips, 2008).

The commonly used uranium contaminated water remediation mechanisms are chemical precipitation, ion exchange, solvent extraction liming, and adsorption. Each of these mechanisms has its own distinct virtues and limitations (Mellah *et al*., 2006). Adsorption is applied in most water treatment studies mainly due to its easy application and better removal efficiency (Li *et al.*, 2011). Adsorption can be performed in batch or column studies. In this study adsorption in batch studies were done within 24 hours with reference to the literature hypothesis that if there is no metal species dissociation within 24 h of equilibration, the metals are considered inert to the technique used (Alberti *et al*., 2007).

Table 2.2: Some metal ion removal techniques.

Technique	Material	Active site	Advantages	Disadvantage
Ion-exchange	Mesoporous material e.g. smectite or clay	Na, Ca and Mg	Easy of operation and cost effective	Introduction of secondary pollutants
Biosorption	Microbes e.g. Bacteria	Exopolymers and negatively charged on the cell walls	Microbes rapidly adjust to climate changes and speed metal reduction rate.	Microbe-metal approaches are applicable in wetlands (Brierley, 1990) than at point of use
Adsorption	Solid material e.g. Zeolites and Activated carbon (AC)	Alkali earth metals, pore size, surface area Specific organic groups	Easy application, high efficiency (Li, 2011) and inexpensive	Zeolites and AC poorly adsorbs oxyanions and cations, respectively (Haggerty, 1994; Chen, 2003).

2.9.Background of adsorbents:

Adsorbents are solid material that displays surface properties capable of promoting small particles adherence on the surface of the material. Although the knowledge about uranium chemistry provides the basis for determination of suitable remediation techniques, it is the adsorbent properties that enhance the uranium removal feasibility of the mechanism. The adsorbents used in this study are granular activated carbon, natural zeolites (untreated and functionalised) and silica polyamine composite.

2.10. Activated carbon

Activated carbon is widely used for adsorption of both organic and inorganic water pollutants. The use of activated carbon for sorption of water contaminants is attributed to its rigid porosity, large surface area (Mugisidi et al., 2007), high thermos/radiation stability (Kütahyalı and Eral, 2004), chemical stability (Mellah et al., 2006) and the presence of wide range of reactive surface functional groups (Zhao et al., 2010). However, activated carbon use for AMD treatment is often criticised due to its production and regeneration expenditure (Ibrahim et al., 2010; Ríos et al., 2008).

There is differing views about the classification of activated carbon as a cost effective or cost ineffective adsorbent (Ibrahim et al., 2010; Ríos et al., 2008; Mellah et al., 2006; Kütahyalı; Eral, 2004; Babel and Kurniawan, 2003;). Other major conflicting reports about activated carbon as a water purification and separation technique are related to the potential of this adsorbent for uranium uptake in aqueous solutions. Some studies reported that activated carbon can effectively remove uranium (Kütahyalı, 2004; Mellah, 2006) whereas other studies reported the opposite. Hence, further assessments of activated carbon adsorption capacity for uranium are necessary. However, it is a general view that activated carbon is a common prolific adsorbent for most trace metals (Sandhya, 2003).

2.11. Zeolite

Zeolites occurs naturally around the globe (Englert and Rubio, 2005; Wang and Zhu, 2006) and synthetically (Donat, 2009). Over 41 natural zeolites (Haggerty and Bowman, 1994) and 150 synthetic zeolites have been reported to date. These hydrated aluminosilicates crystalline lattice of three dimensional tetrahedron cage-like structures characterised by microporosity (Barquist, 2009; Haggerty and Bowman, 1994; Barquist, 2009) are classified under "tectosilicates" minerals (Ibrahim *et al*., 2010).

Zeolite contains exchangeable cations such as sodium, calcium, strontium, barium, and magnesium (Englert and Rubio, 2005) that counter balance the net negative charge provided for by the isomorphic replacement of Si^{4+} with the presence of Al^{3+} (Cozmuta *et al*., 2012) in the central lattice position. The stable capturing of the mentioned alkali and alkali earth cations is provided for by the presence of the cages and channels interconnected by the oxygen atoms at the vertices of each continuously joined tetrahedral structure (Englert and Rubio, 2005). The general formula for zeolite composition is mathematically given by equation 2.6 (Barquist, 2009):

$$Mx/n[(AlO2)x(SiO2)y]mH_2O \quad (2.6)$$

Zeolite differ on the basis of morphology, pore size and Al/Si composition ratio as displayed by the cliptinolite $(Ca, K_2,Na_2)_3[Al_6Si_{30}O_{72}].24H_2O$ (Haggerty and Bowman, 1994) and chemical formulas.

In general, variations of zeolite composition, structure, and morphology offer this aluminosilicates an extensive versatile application for scientific purposes (Asakura *et al.*, 2014). It is particularly the easy of the silica separation from reaction mixture in addition to high surface area and shape/size selectivity that offers zeolite such enormous industrial applications (Mandal *et al.*, 2004). The reported uses of zeolite include but not limited to water treatment (Oliveira et al., 2004), catalysis (Shin et al., 2000; Margolese, 2000), building stone, cement pozzolan, oil spill clean-up (Wang and Zhu, 2006), mining, paper products, gas and petroleum separations (Englert and Rubio, 2005).

The wide effective use of zeolites in water treatment techniques in particular adsorption of inorganic pollutants in water is uncontested (Inglezakis *et al*., 2004). Zeolite such as clinoptilolite (Inglezakis *et al.*, 2004; Haggerty and Bowman, 1994), seopite (Ladeira and Gonçalves, 2007) and montmorillonite(Chisholm-Brause et al., 2001) has been extensively studied for metal removal. Among the mentioned zeolites, the heulandite (clinoptilolite) and mordenite finds more industrial applications (Englert and Rubio, 2005).

Although the physicochemical properties of zeolite such as hydrophobicity, surface area (Oliveira *et al*., 2004), thermal stability and superior hydraulic property (Haggerty and Bowman, 1994) generally offers them better adsorption capacities for metal ions, it is the chemical composition, internal pore size (Zhan *et al*., 2003), ion exchange property and experimental set-up (Inglezakis and Grigoropoulou, 2004) for adsorption that ultimately determine the metal ion selectivity of zeolite (Erdem et al., 2004). Naturally available zeolites are generally considered as low-cost adsorbents (Oliveira *et al*., 2004; Shuibo *et al*., 2009; Zhang *et al*., 2009) due to their local abundance (Ibrahim *et al*., 2010), cost-free availability and high cation exchange capacity (Zhang *et al*., 2009).

2.12. Zeolite functionalisation

Adsorbents are mostly functionalised in chemistry and engineering for enhancement of water purification capacity of the adsorbent. Although functionalisation can be done to target dyes in water, zeolite functionalisation route is mostly employed to decontaminate water of the cations. Cations removal from wastewater using functionalised mesoporous material is a recent scientific development meant to combat water problems associated with metal ion contamination (Da and Sayari, 2012). Functionalisation can be done for a single functional group or many functional groups. Mostly, zeolite external surface functionalisation is achieved through surface silanols interactions with organosilanes of the type RnSiX(4–n).

Where R and X denotes a nonhydrolyzable moiety possessing the desired functionality and the reactive group (e.g. halogen or alkoxy), respectively (Brühwiler and Calzaferri, 2005).

Zeolite functionalisation for metal ion uptake can be effectively done by exploiting the known chemical interactions between functional groups and metals ions of interest. For instance, the removal of copper/gold and mercury would require target functionalising agents to be amine (Barquist, 2009) and sulphur (Kiefer and Höll, 2001) functional group containing reagents, respectively.

The metal ion–functional group pairing is important in AMD treatment with zeolite because functionalisation improves adsorbent surface adsorption capacity for specific target metal ions. In such functionalisation cases, zeolite mainly provides the support (Zhang *et al*., 2009) for the functionalising agent whereas the introduced functional group increases the adsorption affinity (Chen *et al*., 2003) and selectivity for targeted cations (Zhao *et al*., 2010).

Zeolite meant for use in water treatment is preferably functionalised for selective metal recovery or removal by coupling with organic group using condensation, esterification, and silylation methods (Asakura *et al*., 2014; Vassylyev *et al*., 2006). The resulting functionalised zeolites are called organic-inorganic zeolite hybrid (Zhan *et al*., 2003), organo-zeolite (Haggerty and Bowman, 1994) or metal-organic frameworks (MOFs) (Huang *et al*., 2010).

Zeolite surface modifications are made specifically for rational design and specific tailoring of their properties. Therefore, the effectiveness of organic group introduction and properties enhanced depends largely on the routes, reagents used, hydration and temperature conditions (Brühwiler and Calzaferri, 2005). Zeolite are characterised by both the small pore bearing internal surface and the external surface which is the exposed and available structural part for functionalisation (Vassylyev *et al*., 2006). Zeolite functionalisation methods include single pot grafting and postsynthetic grafting. The single pot grafting involves functionalising synthetic zeolite as they are being synthesised by co-condensation reaction whereas postsynthetic functionalisation methods is applied to already crystalized zeolite structures as in the case of natural zeolite functionalisation (Barquist, 2009).

Methylene (Lesthaeghe *et al*., 2006), 3- aminopropyltriethoxysilane (APTES) (Brühwiler and Calzaferri, 2005) and 3-mercaptopropyltrimethoxysilane (3-MPTMS) (Barquist, 2009) are examples of the previously used reagents for incorporation of useful functional groups for zeolite surface properties design. It was reported that over 30% of silicon group contained in zeolite were easily functionalised with methylene (Lesthaeghe *et al*., 2006).

The use of magnetic mesoporous silica (Li *et al*., 2011) or coupling of –SH (using 3-MPTMS) on silica (zeolite) or matrixes to enhance mercury (and other metals) adsorption capacity owing to the known strong binding affinity of thiol to mercury resulting in mercuric sulphide formation was also reported as an example of the effect of adsorbent functionalisation in water treatment (Fang *et al*., 2005).

The possible zeolite modification reactions are similar to those applying to other Metal – Organic frameworks or inorganic – organic hybrids. These reactions may include but not limited to covalent bonding, transformation with coordination bonding and step wise tandem modification as extensively highlighted in literature review (Wang and Cohen, 2009).

2.13. Silica Polyamine Composites

The silica polyamine composite (BPAP referred hereafter as SPC) used in this study is known to have superior properties for use in metal ion adsorption. Apart from the predominantly polar surface functional groups, SPC has some properties offering it advantages for use in inorganic polluted water, they include the stability against; shrinking/swelling, elevated temperatures, radiolytic decomposition and degrading life span (Beatty et al., 1999a). Silica polyamine composites have a zirconium functional group attached. Zirconium and uranium are known to react effectively to produce U-Zr metal alloys (Moore et al., 2015). Hence use of zirconium group containing adsorbent such as SPC can be a cognitive scientific breakthrough in uranium water remediation and recovery based researches. SPC previously showed better affinity order Cu(II) > Co(II) ≈ Ni(II) for removal of these metal ion from water compared to the commercially available resins meant for heavy metal (Beatty et al., 1999a).

Uranium removal using SPC showed positive results for simulated mine industrial water (Saad *et al*., 2014). SPC interaction with metal ions proved to be effective in the acidic pH range 2 – 4. Synthesis of SPC used was acquired from the US Patent 5,695,882. The synthesis of SPC basically involves anchoring organosilanes to the silica gel surfaces previously cleaned with an acid before humidifying to produce a monolayer of water on the silica surfaces. A small-chained anchor, $Cl_3Si(CH_2)_3Br$, is attached horizontally to the polymerized silica surface providing just few exposed silanols for anchoring with amine based polymers. This afford numerous amine groups "embedded" as polymers to act as metal ion chelators, hence increasing metal binding sites. Materials similar to the SPC were synthesised elsewhere using similar methods without first functionalising the silica material used in Patent 4,540,486S *(*Beatty *et al*., 1999b).

2.14. Principle of various technologies used for characterisation

Principle of Fourier Transformer infra-red

The Fourier Transformer infrared spectroscopy is a technological characterisation technique used particularly on its ability to provide information about possible bonds and functional groups forming a chemical structure by relying on the fact that most functional groups of organic molecules gives electro-magnetic radiation which lies in the spectral range 4000 to 400 cm-1. This FTIR spectroscopy region contains spectral lines that are typically narrow, distinct and are characteristic of the frequencies corresponding to the fundamental vibrations that are characteristic of bonds present in the chemical structure. Therefore, gives an advantage of identifying which specific groups can be functionalised in order to enhance the ability of the structure of interest to undergo certain chemical reactions (Doyle, 1992).

Principle of Thermogravimetric Analysis (TGA)

The Thermogravimetric analysis is a technique that employs the use of constant heat (temperature) increments to continuously degrade the sample of interest under nitrogen or synthetic air while the measuring the mass difference during the heating process. The loss of sample mass means that sample degradation is taking place while mass increase can mean that the sample is charging or the oxygen from synthetic air is reacting with the sample analyte (Bianca, 2001).

Principle of Zeta potential

When the electric field are applied to colloid matter charged particles or ions suspended in a solution, the particles migrate to the oppositely charged region by passing through a boundry known as surface of hydrodynamic shear or slipping plan. This particle distribution or migration is governed by the net charge at the particle surface. The potential that exist at this boundry is called zeta potential. This zeta potential can be used to identify the overall charge on the surface of the colloid material at given pH value. The zeta potential can therefore give an indication of possible chemical reaction between the surface of the material used and the analyte of interest, e.g. it can predicts whether uranium will flocculate, repel or adsorb on the zeolite surface at pH 9 or not (Salopek, 1992).

2.15. Environmental data modelling

The use of computational approaches has recently gained more application around the globe. One of the widely used geochemical computer code technique is pH Redox Equilibrium computer code (PHREEQC or Phreeqc). Phreeqc command can be used to design, describe, predict, estimate and interpret chemical processes. The environmental processes explainable through use of Phreeqc include AMD pathway, metal ion speciation and saturation probability in soil or aquatic environment. The model can be used for both quantitative and qualitative analysis. Qualitatively the model can be used to predict both the speciation of metal ions in a solution and the products formed from a given chemical reaction.

The qualitative application include among other possibilities the estimation of the amount of metal ion species existing at a given pH (concentration or temperature) range (Alberti *et al*, 2007) postulated that it is possible to predict the possible metal fraction to be sorbed under specific experimental conditions, Phreeqc code can in addition provide how much was removed through other processes such as precipitation and ion exchange.

Therefore Phreeqc can be a useful environmental tool in the establishment of the data base for effective removal mechanisms and chemical reactions involved in a chemical process and thus ensuring better metal pollutants removal techniques with minimised secondary contaminants. The validity of Phreeqc output is entirely tied to the Phreeqc input script. In a nutshell, Phreeqc follows the computational phrase "garbage in, garbage out". Phreeqc can be used for forward modelling when the reactants are known and only the possible results are to be predicted.

It can also be used in inverse modelling to determine the chemical reaction that took place and thus converting the reactant chemical composition to that of product chemical composition. In this study, phreeqc will be used mainly for speciation and forward modelling.

Chapter 3

Research aim and objectives:

This chapter concisely states the aim and specific objectives of the research study. These specific objectives were set as milestones necessary to focus the daily work of the research towards achieving the hypothesised research results.

3.1. Aim

The chemical properties of activated carbon, natural zeolites and silica polyamine make these adsorbents plausible water treatment materials for various pollutants. This study aimed to develop a cost efficient organo-inorganic zeolite hybrid that can be used to remove uranium from inorganic aqueous (AMD) systems and to compare its capability to that for activated carbon and silica polyamine composites.

3.2. Objectives

The above aim was accomplished by addressing the following specific objectives:

- Assessing the adsorption capability of activated carbon and silica polyamine composites for removal of U and other toxic elements from inorganic wastewater.
- Functionalising zeolite with amine and phosphate groups and assessing the capability of the resulting organo-zeolite for U removal from aqueous solutions.
- Assessing the effect of competing trace metals and oxyanions on uranium removal from wastewater.
- Elucidating the percentage removal of uranium attributed to ion exchange, adsorption and precipitation processes in activated carbon, natural zeolites and amine zeolites.

3.3. Questions

The research answered the following key questions:

- Is activated carbon, as the most commonly used adsorbent in water treatment, an effective adsorbent for removing U from mine contaminated water?
- Could functionalisation of zeolite improve adsorption capacity for U and other toxic elements and thereby providing an alternative cost-effective adsorbent?
- Does the presence of cations and oxyanions affect uranium uptake from water using aminophosphonated functionalised zeolite and silica polyamine composite?
- How much of the removed uranium occurred through adsorption, ion exchange or precipitation process in each adsorbent used?

3.4. Significant indicators of the study purpose

Most small scale uranium adsorption studies take lightly the dependence of uranium mobility on the presence of the oxyanions and trace metals making up the TDS. Consequently, most adsorption studies do not give a better reflection of the metal ion removal technique since in the real environment there is co-existence of various natural environmental wastewater processes that can cause different adsorbents to favour removal of metal ions through specific chemical and physical mechanisms depending on the chemical composition and adsorbent design (properties). The (adsorbent) zeolite natural availability and modification design (Jamil, 2011) determines the functionalised adsorbent cost efficiency (Yin, 2011) and surface group affinity (Ahamed, 2008) for metal ion adsorption (Yin, 2014).

In respect of the literature provided in chapter 2, two significant gaps were identified:

I. Although activated carbon, natural zeolite and amine functionalised zeolite have been used before for uranium removal, there is scanty information regarding the main fractional equilibrium mechanisms or process leading to highly effective uranium removal compared to the other co-existing environmental processes.

II. Uranium removal studies based on the use of aminophosphonated zeolite and silica polyamine composite in the presence of competing metal is scanty despite uranium and phosphate group being known to have high binding affinity for each other.

Nonetheless, the gaps exist despite the reports that uranium from mines and nuclear industries remains accessible at water point of use by human beings and its mobility is governed by the presence of TDS characterised largely by trace metals (Fox, 2006; Ulrich *et al*., 2006) and anions concentrations (Liu, 2013; Wang, 2012; Alberti, 2007).

Therefore, the current study was dedicated to the use of activated carbon, natural zeolites and silica polyamine composite for uranium removal from small scale AMD impacted drinking water in goldfields human settlements and to further quantify the adsorption capacities of some of the adsorbents in the presence of competing chemical species. Efforts were also put forth to elucidate fractions of processes involved in the uranium removal from the single metal aqueous solutions using some of the adsorbents. The outcomes shall benefit the South African water research fields and institutions responsible for either regulating the trace metals consumption or provide cheap alternative adsorbents.

3.5. Hypothesis

Amine and phosphate functionalisation of zeolites can effectively improve natural zeolite removal capacity and selectivity for hexavalent uranium from aqueous mine solutions. The uranium affinity of functionalised zeolite is better than that of untreated natural zeolites, activated carbon and silica polyamine composite. Aminophosphonated zeolite will have high adsorption capacity for uranium compared to amine functionalised zeolites.

3.6. Novelty

Although use of aminophosphate functionalised mesoporous silica material has been reported to effectively remove uranium from water (Tutu, 2013), the natural zeolite functionalisation with aminophosphate group and its use thereof as a cost effective adsorbent for hexavalent uranium cation is yet to be explored. The present study therefore is among the first if not the only study to by far prepare aminophosphonated natural zeolite for hexavalent uranium uptake from polluted water. Furthermore, in addition to effect of dissolved oxyanions on uranium removal using amine and phosphonated natural zeolite, the study provides insight information regarding the processes responsible for uranium removal and their corresponding partial percentages which is very scarce information even for the commonly used activated carbon.

Chapter 4

Research Methodology:

The chapter entails important information regarding the material and methods used to achieve the research objectives as outlined in chapter 3. The chapter further specifies the reagents, instruments, laboratory and mathematical approaches executed to elucidate and interpret the study results and discussions as highlighted in chapter 5. The major laboratory milestones were subdivided into the following undertaken research activities.

- Calcination of natural zeolites followed by their modification to amine and aminophosphonated functionalised natural zeolites.
- Characterisation of adsorbents using different characterisation techniques, namely; Fourier-transform infrared (FTIR), Brunauer, Emmett and Teller (BET) analysis, Thermo-gravimetric analysis (TGA), zeta potential and point of zero charge were also done to assess the surface charge.
- The effect of batch adsorption parameters such as metal ion aqueous solution pH, adsorbent dosage, metal ion initial concentration, adsorbent –adsorbate equilibration contact time, environmental temperature, cation and anions initial concentrations were evaluated for all adsorbents.
- Data treatment equations, mathematical data modelling, statistical approaches and computational data processing techniques that aided better analytical deductions from the obtained laboratory results were used as the last set as of this research approach.

4.1. Chemicals and reagents

The following reagents were used for adsorption studies; cation standard solutions of 1000 mg L-1 for ICP-OES method development, uranyl salt UO2(NO3)2•6H2O for stock solutions, nitric acid (65%, w/w), NaOH pellets were used for preparation of NaOH solutions as required and distilled water with 18.2 MΩ cm resistivity was supplied by Millipore-Q water system. The analytical grade salts of FeSO4(s), MnSO4(s), CaCO3(s) and Na2HPO3(s) were used for competition studies. The electrolyte used for point of zero charge was NaNO3(s). All centrifuge tubes, sample vials, volumetric flask and other apparatus were cleaned by soaking them in 30% (v/v) HNO3/water (deionised) when not in use and rinsed thoroughly with deionized water before use in the proceeding experiments. The zeolite functionalising reagents, namely; 3 – methylethoxyaminosilane and aminomethylphosphonic acid were purchased from Sigma Aldrich (Johannesburg, South Africa). Ethanol, methanol and toluene were also used during functionalised zeolite preparation. Sodium hydroxide (NaOH) pellets were used for preparing separate and varying concentrations of NaOH solutions for zeolite calcination and pH adjustments.

4.2. Preparation of solutions

The trace metal reagents used in this study for the analysis of their corresponding metal ions are $Hg(NO_3)_2$, and $UO_2(NO_3)_2.6H_2O$. The main group metal ion solutions were prepared from analytical grade salts of Na_2HNO_3 and $CaCO_3$. The solutions of anions evaluated were prepared by dissolving required amounts of the anions from their corresponding anionic salts, namely; Fe_2SO_4 ($-SO_4^{2-}$), $CaCO_3$ ($-CO_3^{2-}$), and H_3PO_4 ($-PO_4^{3-}$) (analytical grade). Stock solution of 1000 mg L^{-1} uranyl ion was prepared by dissolving appropriate amounts of analytical grade $UO_2(NO_3)_2.6H_2O$ salt in volumetric flask containing 1.0 L Millipore-Q water and HNO_3 in a ratio of 100:1 (v/v).

The required working solutions were freshly prepared from the 1000 mg L^{-1} uranyl ion stock solutions by pipetting calculated aliquots necessary to make the dilute working initial concentrations. When not in use, the stock solutions were stored in refrigerator with temperature set at 4°C.

4.3. Adsorbent preparation

4.3.1. 3-aminomethyltriethoxysilane zeolite functionalisation

The amine functionalised zeolite was synthesised according to procedure outlined in literature (Barquist, 2009). Natural zeolite was soaked in distilled water for 24 hours in order to remove trapped air within the porous channels of zeolite. After drying at ambient temperatures for 24 hours, approximately 75 g of natural zeolite were agitated for 24 h in 2 mol L^{-1} NaOH solution. The resulting zeolite with homogenous sodium surface was oven dried at 60°C for 18 hours before weighing out exactly 20 g into a 100 ml round bottomed flask equipped with a stirrer bar and thermometer. An amount of 60 ml toluene and 10 ml 3-aminotrimethoxysilane purchased from Sigma Aldrich (Johannesburg, South Africa) were added into the flask respectively. The flask was then clamped and refluxed for 24 h in a fume-hood using oil bath on a magnetic stirrer hot-plate. The temperature was maintained at 90-95°C throughout the refluxing process. The content were then cooled using running tap water, filtered and successively washed by applying about 40 mL of each of the mediums: toluene, ethanol, water, ethanol and water. The chemical composition and physical property characterisation of amine functionalised zeolite was done using BET and zeta potential.

4.3.2. (Aminomethyl) phosphonic acid functionalised zeolite

The natural zeolite 75 g granules (particle size; 500 µm – 2 mm) were calcined with 1 L of 2 mol L^{-1} NaOH solution for 24 h at 25^{o}C, filtered, washed with water and then oven dried at 95°C overnight.

Then (aminomethyl) phosphonic acid 15 mL was added dropwise into a 100 mL round bottomed flask containing a mixture of 15 g sodium zeolites (NaZ) and 60 mL toluene before refluxing for 24 h to afford the functionalised aminomethyl phosphonic acid zeolite (APZ) which were cooled, filtered and washed with water and ethanol following the procedure outlined in literature (Das et al., 2001) before drying at 95°C for 24 h. The commercially available orange silica polyamine composite (SPC or BPAP-1) synthesised according to procedure outlined by Beatty (Beatty et al., 2016) was used at received.

4.4. Instrumentation and characterisation of sorbents

All metal ions concentrations spectrometric analysis employed inductively coupled – optical emission spectroscopy (ICP-OES) Genesis model. The measurements of pH were performed using Mettler Toledo - Five Easy FE20. The chemical and elemental composition was assessed using x-ray fluorescence – XRF Model Axios max from Panalytical. The functional groups were determined using Fourier transformer infra-red – FTIR Model Tensor 27, Bruker (Germany). The Brunauer-Emmet-Teller (BET) analysis was carried out using Micrometrics Tri-Star surface area and porosity analyser. Surface zeta-potential and particle size were determined by zeta potential instrument using Zeta-Meter 3.0 system (Malvern ZS-90 Model). The point of zero charge (pH_{pzc}) was analysed using the drift method (Faur-Brasquet *et al*., 2002). The thermogravimetric analyses were achieved using Perkin Elmer TGA 6000. The automated mechanical shaker Model spomp8 from Labdesign was employed for sample agitation. The heating mantle IKAMAG RCT was utilised for providing heat during reflux reaction. Thermodynamic studies were done using WiseCube fuzzy control system.

4.5. Batch adsorption studies

4.5.1. Sample preparation

Batch studies were carried out for the assessment of the effect of aqueous solution initial pH for metal ion adsorption. In this study the effect of pH 2 to 11 ± 0.05 at T = 25 °C was examined for uranium removal using natural zeolites, amine zeolite, aminophosphate zeolite, silica polyamine composite and activated carbon using 10 mg L-1 uranium solution. The pH was adjusted using insignificant volumes of dilute HNO_3(aq) and NaOH(aq). In each adsorbent analysis, the pH giving highest adsorption efficiency was selected for use in determination of required adsorbent dosage for the determination of the effect of adsorbate concentration, contact time and for the development of adsorption isotherms, kinetics and thermodynamic models. A volume of 20 mL uranyl solution of 10 mg L^{-1} concentration was transferred into 50 mL centrifuge tubes containing different amount of the adsorbents in granular form. Dosages ranging from 25 mg to 1000 mg of each adsorbent sample were contacted with 20 mL of 10 mg L^{-1} uranyl solution prepared from $UO_2(NO_3)_2.6H_2O_{(s)}$ and controlled at various pH values. Solution pH was adjusted using dilute solutions of $NaOH_{(aq)}$ and $HNO_{3(aq)}$. The adsorbent-adsorbate solutions were stirred for 24 h at room temperature (21±2°C). The equilibrated samples were separated into solid and supernatant through gravitational filtration process using Whatman no.1 filter paper (Maidstone, England). The supernatant were analysed for uranium concentrations using an Inductively Coupled Plasma-Optical Emission Spectrophotometer (ICP-OES) Genesis model from spectraSA.

4.5.2. Parameter optimisation

During adsorption studies it is uncontestably important to evaluate the parameters that causes effective uptake of the metal ion by the adsorbent used (the phenomenon known as adsorption parameter optimisation). In this study the optimum operating conditions for uranium uptake were separately evaluated and compared thereafter. The parameters investigated included the aqueous solution pH, adsorbent dosage, contact time, solution temperature, initial concentration of uranium and that of the competing metals (and anions) in the sample solution.

The optimisation of parameters was done using a single factor method. In single factor adsorption method only one variable is investigated as a function of adsorption capacity. A minimum of three sample replicates were run for each sample analysis.

4.5.3. Batch adsorption competition studies

Equivalent uranium(VI) solutions of 30 mg L^{-1} were separately prepared and mixed with competing metals species in 250 mL volume of concentration ratios of U: metal salt; 6:1, 2:1, 1:1, and 1:4 mg L^{-1}. The shaking speed of 150 rpm was employed. The temperature used was 25 ± 2ºC for all adsorbents containing competing multi-metal solutions. The solution pH, equilibrating time and sorbent dosages used were those obtained as optimum batch adsorption conditions for uranium single metal solutions. Metal salts investigated are $FeSO_{4\,(aq)}$, $Na_2HPO_{3\,(aq)}$, $MnSO_{4\,(aq)}$ or $CaCO_{3\,(aq)}$. The resulting supernatant were analysed for metal ion concentrations using ICP-OES. Phreeqc interactive was used for uranyl ion speciation and corresponding concentrations in aqueous solution.

4.6. ICP-OES analysis

The uranium amounts of the solutions were measured directly using the wavelength U 409.5 nm as element line of the (inductively coupled plasma – optical emission spectroscopy) ICP-OES. The ICP-OES instrument was calibrated before each set of analysis using blank, 0.1, 0.5, 1.0 and 2.0 mg L^{-1} prepared from standards purchased from sigma Aldrich (Steiheim, Germany).

The average mean estimate of the sample replicates was taken as the uranium concentration in the aqueous solution. Appropriate solution dilutions were performed in case(s) where the analyte concentrations in the solution showed high amounts above the calibrated standards. The dilution factor of each diluted sample was taken into account during concentration calculations. Only sample replicates that displayed at most 10% relative standard deviations (rsd) for each sample run were considered throughout the ICP-OES data processing. The operating conditions of ICP-OES are listed in Table 4.1.

Table 4.1: Some operating conditions for ICP-OES parameters

Parameter	operating settings
Plasma power	1400 W
Nebulizer Gas flow	1 L m-1
Sample pump flow	1 mL m-1
Auxiliary gas flow	1 L m-1
Coolant gas flow	14 L m-1
Plasma Torch	Fix quartz EOP 2.5 mm
Nebulizer	Standard crossflow
Processing mode	Area
Spray Chamber	Single pass
Sample Aspiration rate	2 L min-1
Number of replicates	3

4.7. Data treatment

The statistical and mathematical methods were used to design, analyse, interpret and relate the data of some optimisable batch parameters to various patterns of chemical system.

In this study, data treatment was divided into three categories, namely: data processing, data modelling and data validation.

4.7.1. Data processing

In the concept of this study, data processing referred to the manipulation of adsorption set of data by using different known mathematical derivative equations in order to make meaningful automated, computerised or graphically displayed deductions (Rodbard, 1974). The proceeding statements of this chapter give a brief description of the adsorption data processing equations used in this study.

Removal efficiency or adsorption efficiency or efficiency

Adsorption efficiency refers to the percentage amount of metal ion removed by the adsorbent per initial total amount of the metal ion present in the aqueous solution.

The efficiency was calculated as percentage of metal ion removed using the equation 4.1:

$$\textit{Removal efficiency (\%)} = \frac{Ci - Ct}{Ci} \times 100 \quad (4.1)$$

$$\textit{Or (at equilibrium conditions) Removal efficiency (\%)} = \frac{Ci - Ce}{Ce} \times 100 \quad (4.2)$$

Where; C_i (mg L^{-1}) and C_t (mg L^{-1}) denotes the initial and residual metal concentration present in solution at time (t), respectively. In some literature *(Li et al*., 2011), C_i is denoted as C_0. At equilibrium conditions *Ct = C*e. Adsorption efficiency provides valuable information regarding the probability and selectivity of an adsorbent in removing a specific metal ion from a solution in a given time (Mellah, 2006):

Adsorption capacity

The adsorption capacity gives information regarding the metal ion amount removed from the aqueous solution at any time per unit gram of the adsorbent (Parab *et al*., 2005). Mathematically, adsorption capacity of an adsorbent can be easily defined as the product of the total adsorbed amount of metal ion concentration (mg L^{-1}) at any time (t) and the initial volume (L) of the metal ion solution per unit mass (g) of the adsorbent used (Guibal et al., 1992; Motsi *et al.*, 2009; Yang and Volesky, 1999) as expressed in equation 4.3:

$$qe = (C_i - C_e) \times \frac{V}{M} \quad (4.3)$$

Where q_e (mg g^{-1}) is the adsorption capacity, V (L) represents metal solution volume added and M (g) signifies adsorbent mass considered.

Metal ion selectivity

The metal ion selectivity (K) is the measure of adsorbent–adsorbate affinity or selectivity in a wide range of other trace metal ions. The metal ion selectivity evaluations were performed based upon the value of distribution coefficient (k_d) of each metal (Motsi *et al*., 2009).

In general, selectivity can be calculated using equation 4.4:

$$K_{(M^+)} = \frac{Kd(M+)}{Kd(B)} \quad (4.4)$$

This defines the distribution coefficient, general distribution coefficient of the metal ion and the total distribution coefficient of competing metal species. The uranium metal ion selectivity coefficient and distribution coefficient can therefore be calculated from equations 4.5 and 4.6 as a derivative expression of equations 4.4 (Tavengwa et al., 2015, 2014):

$$K_U = \frac{K_d(UO_2^{2+})}{K_d\, B} \quad (4.5)$$

Where K_U is the selectivity coefficient of the uranyl ion

$$K_d(M^+) = \frac{Ci-Ce}{CeM} \quad (4.6)$$

K values parameter implications;

K = 1, it means equal bounding of competing ions and uranyl ions

K >> 1 means the adsorbent favours uranyl ion or target metal

K < 1 means the adsorbent has low affinity for uranyl ion binding

Relative selectivity coefficient

The relative selectivity coefficient (K´) of the natural (untreated) zeolite against the functionalised zeolite was calculated using equation 4.7 (Tavengwa et al., 2014)

$$K' = \frac{KNZ}{KFZ} \quad (4.7)$$

Where KNZ refers to the selectivity coefficient of the natural zeolite adsorbent and KFZ can refer to selectivity coefficient of the functionalised zeolites such as amine zeolite or phosphate zeolite.

The relative selectivity coefficient is an important comparative adsorption parameter since it gives information about the enhanced effect of functionalising zeolite towards selectivity and adsorption affinity of the hybrid adsorbents.

4.7.2. Data validation

Critical parameters such as relative standard deviations, limit of detection (LOD), analysis of variance (ANOVA) and regression coefficient (R2) were used for method and results validation.

Limit of detection and limit of quantification

Limit of detection (LOD) or method detection limit (MDL) and limit of quantification (LOQ) of the chemical element or analyte were used as the important method performance characteristic for the validation of the data quality and quantity. The LOD was expressed as the sum of average concentration of a triplicate blank and three-fold standard deviation of the blank using equation 4.8 whereas the LOQ was calculated as the sum of the average blank concentration and ten-fold the standard deviation using equation 4.9:

$$LOD = Blank + 3sd(blank) \quad (4.8)$$

$$LOQ = Blank + 10sd(blank) \quad (4.9)$$

The LOD defines the minimum possible amount that the instrument can detect while LOQ refers to the minimum analyte concentration that can be computed with definite precision and accuracy of the set method test for a given analyte. Therefore, during the analysis if LOQ and LOD were very low, it was assumed that all chemical elements were determined with high reliability to produce conclusive, reproducible and accurate results.

Normalized standard deviation

The validity of data modelled using adsorption isotherms, kinetic and thermodynamics was evaluated by using a linear regression analysis.

The linearity of the linear regression equations was evaluated using the coefficient of determination (r^2) as the normalized standard deviation according to equation 4.10:

$$\Delta q(\%) = 100\sqrt{\frac{\sum_{i=1}^{n}\left[\frac{q_{\exp} - q_{calc}}{q_{\exp}}\right]^2}{n-1}} \quad (4.10)$$

Where Δq (%) denotes the normalized standard deviation, q_{cal} (mg g^{-1}) and q_{exp} (mg g^{-1}) represent calculated and experimental adsorption capacity data, respectively and n denotes the number of experimental data.

Estimated error

Like in many other studies involving sample analysis, the evaluations of the adsorption estimate mean of the sample metal ion concentrations are accompanied by errors. Therefore, the possible errors in this study were mathematically accounted for using scientific interpretation approach that takes into account the error from instrument, the sample volume and mass used. Owing to errors estimated, q_e was expressed mathematically as $q_e \pm e_4$ (where e_4 signifies the amount of estimated adsorption capacity taking into account the sum of possible errors involved).

Several steps were done in calculating the adsorption capacity error as pointed out in Harris (2007). The relative standard deviation with respect to the instrument (e_3) was calculated using equation 4.11. The percentage calculations of e_3 were performed according to equation 4.12, while the percentage adsorption capacity error (%e_4) was modelled using equation 4.13. The error compositions due to volume (eV) and the error composition due to mass (eM) of the sample solution were derived from equations 4.14 and 4.15. Thus the overall adsorption capacity error simplifies to equation 4.16:

$$e_3 = \sqrt{e_{12} + e_{22}} \quad (4.11)$$

Where; e_{12} and e_{22} refers to standard deviations of initial and final metal ion concentration, respectively.

$$\%e_3 = (e_3/C_e) \times 100 \quad (4.12)$$

Where C_e is the equilibrium concentration

$$\%e_4 = \sqrt{\%e_3 + \%e_V + \%e_M} \quad (4.13)$$

Where $\%e_V$ and $\%e_M$ are the error compositions due to the volume and the mass of the sample solution, respectively

$$\%e_v = 0.5\frac{SD(50mL)}{V\ (mL)} \times 100 \quad (4.14)$$

Where SD (50 mL) is the standard deviation error associated with the 50 mL measuring cylinder and V is the volume of the sample solution

$$\%e_m = 0.11\frac{SD\ (balance)mg}{m(mg)} \times 100 \quad (4.15)$$

Where SD (balance) is the standard deviation error associated with the measuring balance and m is the mass of the sample

$$e_4 = \frac{\%e_4 \times qe}{100} \quad (4.16)$$

Where q_e remains the adsorption capacity of the sorbent

Linear regression

The coefficient of determination (R^2) was used to evaluate the degree of linearity when predicting if the obtained data fitted the calibration curve of the models or methods used. If the R^2 value lied between 0 and 1, then the data was considered to fit the model if R^2 lied much closer to 1 and the calculated adsorption capacity shows consistency (i.e. equivalent) to experimental adsorption capacity. If the data did not fit the model or calibration curve, then it was concluded that the model cannot be used to predict the behaviour of the data modelled. The applicability of each of the adsorption models was carried out using the correlation coefficient (r). The error associated with models was calculated using equation 4.10:

One way ANOVA

Owing to the sensitivity and depth of water pollution by metal ions it is always best to state the nature of the difference between any two separate adsorption samples results.

The F critical statistical calculations and p-value calculations at 95% confidence level were used to deduce if the difference between any of the two or more adsorption interval, points or measurements were of significant difference using one way ANOVA. If the P value was greater than 0.05, the difference was considered insignificant. If less than 0.05, then the difference was considered significant.

Outlier testing

Sometimes the data obtained present range of values containing one or more values that are not easy to accept or reject as part of the median analysis. Hence the statistical outlier testing technique known as Test for Outliers (Q-test) was employed. Owing to the nature of this study and the current economic instabilities the Q-test was preferred method to decide on the relevancy of possible outlier data as opposed to the traditional and time consuming technique which involves increasing the number of replicates. If Qexp > Qcrit (obtained from statistical tables) then the questionable result were subject for rejection.

4.7.2. Adsorption data modelling

Generally adsorptions data models can establish mechanisms regarding selectivity of adsorbents for different metal ions or quantitative compare factors that influences adsorption capacity. In this study, the models used estimate the contribution of varied mechanisms are kinetics, isotherms, thermodynamics and Phreeqc models..

Kinetic modelling

Modelling of adsorption kinetics is fundamental in elucidating the controlling adsorption mechanisms (Mellah et al., 2006) on the basis of adsorption data variation of metal ions concentrations between the boundary conditions; $q_t = 0$ at $t = 0$ and $q_t = q_t$ at $t = t$. The commonly applied kinetic models are linearised pseudo first-order 4.17 for physisorption and pseudo second-order for chemisorption 4.18:

$$\log(qe - qt) = \log qe - \frac{k_1}{2.303} t \quad (4.17)$$

$$\frac{t}{qt} = \frac{1}{K_2 q_e^2} + \frac{1}{q_e} t \quad (4.18)$$

Where k_1 (min^{-1}) is the rate constant of pseudo first order and can be determined from the slope of the plot of $\log(q_e - q_t)$ against time (min), k_2 (g mg min^{-1}) is the rate constant of pseudo-second-order and can be obtained from the intercept of the plot of t/q_t v/s time (min). However, Elovich equation 4.19 was used herein to confirm chemisorption (Wu *et al*., 2009a; Robbins, 1992).

$$q_t = b\ln(ab) + b\ln t \quad (4.19)$$

Where b is a constant and a is an initial chemisorption rate constant. The fractional kinetic model equation 4.20 derived from the Freundlich was used to assess the extent of chemisorption.

$$q_t = at^b \quad \text{Or} \quad lnq_t = lna + b\ lnt \quad (4.20)$$

Where *a*,*b* and *ab* are constants and specific sorption rate at t = 1, respectively. Since the zeolite materials are porous in nature, it was important to assess the surface porosity effect on the rate mechanism, hence this factor was assed using intraparticle diffusion equation 4.21:

$$q_t = \frac{1}{4} k_{id} t^{1/2} + C \quad (4.21)$$

where ki_d (mg g^{-1} $min^{-1/2}$) is intraparticle diffusion rate constant and C (mg g^{-1}) is a constant.

Isotherm modelling

The mathematical incorporation of isotherm parameters that express the surface properties and affinity of the sorbent helps in designing the interaction between the metal ions and adsorbent at a given pH and concentration for application in real water systems.

The widely used sorption isotherms are namely, the Langmuir, Freundlich, Dubinin–Radushkevich (D–R) models, TEMKIN and Brunauer-Emmet-Teller (BET) (Sprynskyy, 2011).

Langmuir isotherm

Langmuir model is a common adsorption isotherm that utilizes equation 4.22 (Özeroğlu and Metin, 2012; Shuibo *et al*., 2009):

$$q = q_{m1}\frac{b.C_e}{b.C_e+1} \tag{4.22}$$

Where q_{m1} (mg g^{-1}) and b (L g^{-1}) are the saturated monolayer sorption and saturated sorption equilibrium constant, respectively. Langmuir isotherm predicts that a solid surface with a monolayer is formed at saturation (Parab *et al*., 2005), that is there is homogeneity without uranium transmigration (Han *et al*., 2007). When the sorption process proceeds through a monolayer metal uptake, the plot of $1/q$e against $1/C_e$ yield a linear equation with a slope given by $(1/bQ_i)$ and intercept $1/Q_i$. The model utilises dimensionless separation factor (R_L) to predict the affinity of an adsorbent for adsorbate adsorption (Mellah *et al*., 2006) from equation 4.23:

$$R_L = (\frac{1}{1+bC_i}) \tag{4.23}$$

Freundlich isotherm

The Freundlich isotherm was predicted using equation 4.24:

$$\ln q_e = \ln K_F + \frac{1}{n} lnC_e \quad (4.24)$$

Where, K_F *and* n are Freundlich sorption capacity constant and sorption intensity constant. The Freundlich model predicts the probability of a heterogeneous infinite coverage on exponential active sites (Özeroğlu and Metin, 2012; Shuibo *et al*., 2009). In simple this modelled suggests that the ratio of metal ion solutes adsorbed to the solutes concentration is a function of the solution.

Therefore, if an adsorption process proceeds on a heterogeneous surface then when adsorption data is fitted on the plot of ln q_e versus ln C_e to give a straight line, a slope of *(1/n)* and intercept of log K_F results.

Dubinin–Radushkevich (D–R) models

The Dubinin–Radushkevich (D–R) isotherms were also used to predict adsorption mechanisms as physisorption or chemisorption by employing equation 4.25:

$$\ln q_e = q_{m3} - K\varepsilon^2 \quad (4.25)$$

Where K, q_{m3} and ε represent adsorption energy constant, theoretical saturation capacity and Polanyi potential (ε) as expressed from equation 4.26:

$$\varepsilon = RTln(1 + \frac{1}{C_e}) \quad (4.26)$$

Where *R* is the ideal gas constant (8.314 J mol^{-1} K^{-1}) and *T* is the absolute temperature in kelvins (K) and the activation energy of adsorption process *(E*a*)* was calculated from equation 4.27:

$$E_a = 1/(-2K)^{-1/2} \quad (4.27)$$

Brunauer-emmet-teller (BET)

The BET adsorption isotherm was used to estimates the surface area of the system as a function of pore diameter (Gelb and Gubbins, 1998).

The Brunauer-Emmett-Teller equations for multimolecular adsorption are currently used with some derivations or substitutions owing to the never more than half filled adsorbent pores that could not be accounted for by the BET expression (Pickett, 1945). In order for BET equation to be in good agreement with the data some researchers (Sprynskyy *et al.,* 2011) consider using initial concentration in state of saturation concentration within the BET models.

The porous surface and microporosity contributions were estimated by computing equation 4.28 and equation.4.29 (Theoretical, 1974), respectively.

$$q = q_m K_{BET} \frac{(\frac{C_e}{C_i})}{1-(\frac{C_e}{C_i})}[1 + (K_{BET} - 1)(\frac{C_e}{C_i})] \quad (4.28)$$

$$k_d = \frac{q_e}{C_e} \quad (4.29)$$

Where k_{BET}, q_{m2}, q and k_d are the BET adsorption isotherm (L/mg), complete surface monolayer metal ion concentration (mg L^{-1}), theoretical isotherm saturation capacity (mg g^{-1}) and C- isotherm distribution coefficient, respectively.

TEMKIN

The Temkin isotherm modelling was investigated using equation 4.30 which was linearised to give equation 31:

$$qe = RTb \ln(AC_e) \quad (4.30)$$

$$q_e = B \ln A + B \, lnC_e \quad (4.31)$$

The value of B was further calculated using equation 4.32:

$$B = RT/b \quad (4.32)$$

Where *b* denotes the Temkin constant related to heat of sorption (in J/mol) and A denotes the Temkin isotherm constant (in L/g). The values of A and B can be obtained from the plot of q_e versus ln C_e. The Temkin isotherms equation assumes that sorption energy decrease linearly with an increase in the degree of completion of the optional centres of an adsorbent (Hameed and Daud, 2008). The model takes into account the adsorbent-adsorbate interaction by assuming that the heat of adsorption of all molecules in the layer decreases linearly with coverage *(*Dada *et al*., 2012; Kalavathy *et al*., 2005).

This implies that the adsorption of metal ions on molecules present on the layer occurs uniformly with a continuous decrease until some maximum binding energy is reached because of the equal distribution of binding energies.

Thermodynamic modelling

Thermodynamic mechanisms as function of temperature were elucidated by relating the thermodynamic parameter; ΔG° (Gibbs free energy change) to entropy change (Δ*S°)* and enthalpy change (Δ*H°)* according to equation 4.33 and equation 4.34:

$$\Delta G = -RT \ln \left(\frac{q_e}{C_e}\right) \quad (4.33)$$

$$\ln K_D \, or \ln \left(q_e / C_e\right) = \frac{\Delta S^0}{R} - \frac{\Delta H^0}{RT} \quad (4.34)$$

4.7.3. Geochemical modelling

The PHREEQC was used to distinctively determine the effective metal ion removal processes, that is, it was used to establish whether uranium removal occurred through adsorption, precipitation, ion exchange etc. This is very important since in natural environment the aforementioned geochemical processes may occur concurrently. Addition of the chemical processes responsible for effectively high removal of metal ion may or may not lead to secondary toxicants. The PHREEQC model enables us to predict in advance the probability of secondary contaminants because it provides information regarding the metal speciation, mobility, complex formation probability, saturation index and chemical reaction pathways.

Using the information acquired from the model, the bioavailability, and toxicity of the metal ion post removal process can be estimated. It is important to note that this natural processes simulator assumes thermodynamic and kinetic equilibrium in all the chemical reaction analysis. The PHREEQC code models data on the basis of the computational concept "*garbage in, garbage out*".

This means that the reliability of the data interpreted on the *output script* by the PHREEQC is purely dependent on how good (how close the data simulates the environmental conditions) the *input script* modelled is.

Where *input* script and *output* script refers to "the data put into PHREEQC before running the program" and "the data read as results from PHREEQC after running the program" respectively. In this study a geochemical computer code known as PHREEQC interactive model was used for assessment of the environmental implications of uranium removal under the solutions conditions outlined in the corresponding study manuscripts.

Chapter 5

Results and Discussion

The results and discussions given in 5.1 and 5.2 are based on the specific background of the case study 5.1 and case study 5.2 as outlined under abstract section.

5.1. Results and discussion

Removal of uranium(VI) from small scale drinking water: comparative study using activated carbon, natural zeolite and amine functionalized zeolite.

This subsection compares the extent of various adsorption mechanisms involved in uranium removal from batch aqueous solutions using activated carbon, natural zeolite and amine functionalised zeolites as solid adsorbents materials. The specific theoretical background for this precedes the outcomes of this subsection.

5.1.1 Background

Radioactive uranium wastes constitute a global aquatic ecosystem problem (Sharma *et al*., 2014; Parab *et al*., 2005). In human, uranium can cause neurological defects, cancer, chemical mutation and renal failure (Özeroğlu and Metin, 2012). Major uranium sources are nuclear power generation stations and mining sites (Bister *et al*., 2015). Uranium compounds identified at mine fields include: uraninite (UO_2), brannerite (UTi_2O_6) (Tutu *et al*., 2012; Frimmel, 2003) and uranyl sulphates ($UO_2SO_{4(aq)}$), ($UO_2SO_4.3H_2O_{(s)}$), schoepite (a uranyl hydroxide). The hazardousness of this radiotoxic and non-biodegradable radioactive isotope is promoted by enormous half-life, high solubility and varied speciation over a wide pH ranges. Uranium species identified in aqueous medium includes, in acidic; UO_2^{2+}, $(UO)_2(OH)_2^{2+}$, UO_2OH^+, near neutral; $UO_2(OH)$, UO_2CO_3, and in alkaline; $UO_2(CO_3)_2^{2-}$, $UO_2(CO_3)_4^{3-}$ (Kalin *et al*., 2004). The commonly used adsorbent for inorganic pollutants is the cost inefficient activated carbon which is not easily applicable for small scale water systems. Therefore, a need for alternative cost effective small scale adsorbents (Ríos *et al*., 2008) for inorganic water toxins has been identified (Babel and Kurniawan, 2003).

To date, adsorbents such as talc (Sprynskyy *et al*., 2011), phosphonated cross-linked polyethylenimine (Saad *et al*., 2015), silica polyamine composite (Tutu *et al*., 2013) filamentous green algae - *Oedogonium* sp. (Bakatula *et al.*, 2014), maghemite nanoparticles (Etale *et al*, 2014), coir pith (Parab *et al*., 2005) and zeolite have been explored as possible easily reusable and highly selective alternative of activated carbon for inorganic pollutants removal (Mellah *et al*., 2006). However, most uranyl ion adsorption studies only assess the kinetic and isotherm model of best fit without giving further evaluations on the extent of contribution of each equilibrium kinetic and isotherm mechanism involved during uptake.

If kinetic and isotherms mechanisms are confined to the line of best fit then the applicability of such developed adsorbents is limited because sometime two or more different mechanisms such as coagulation, adsorption, ion-exchange, coprecipitation, particle or film diffusion and other varied chemisorption in real aquatic environment can occur concurrently and interdependently (Ho and Mckay, 2002; Lee *et al*., 2002).

Therefore, in the present study, the chemical properties of natural zeolite were modified with 3-aminopropyltrimethoxysilane to improve their uranyl ion adsorption selectivity. Zeolite were chosen to provide solid support because they comprise high ion exchange and molecular sieve properties that enable easy modifications that enhances sorption selectivity (Jamil *et al*., 2011; Ibrahim *et al*., 2010; Motsi *et al*., 2009). The probability of uranium adsorption onto amine zeolite hybrid (AMZ) was then compared to that of activated carbon (AC) and natural (unmodified) zeolite (NZ) in batch studies. The contribution of varied mechanisms was estimated by kinetics, isotherms, thermodynamics and Phreeqc models.

5.1.2. Results and Discussion

Characterisation

Most characterisation techniques were successfully utilized previously in elucidating the properties of various activated carbon (AC) (Zacaroni *et al*., 2015), natural zeolite (NZ) and amine functionalised zeolite (AMZ) (Bakatula *et al*., 2015). In this study; AC, NZ and AMZ were characterised and the XRF mineral composition results are shown in Table 5.1. The loaded and unloaded activated carbon XRF results are not shown because the entire material decomposed completely to 100% loss on ignition. This means that activated carbon is entirely composed of organic material with lower thermal stability than that of solid zeolite material.

The XRF analysis revealed that the unloaded natural zeolites were montmorillonite since the sum of silicates, iron and aluminium oxides exceeded 78%. Montmorillonite structural composition is reportedly advantageous for inner-sphere monodentate/bidentate and outer-sphere monodentate/bidentate binding of uranyl ion to SiO_x surface groups (Sylwester *et al*, 2000).

Table 5.1: Mineralogical composition of natural zeolites and amine functionalised zeolites

Adsorbent	NZ		AMZ	
XRF; Mineral (%)	unloaded	loaded	unloaded	loaded
SiO_2	77,91	67,79	66,11	67,02
Al_2O_3	12,95	11,36	11,60	11,37
Fe_2O_3	0,13	0,11	0,12	0,11
FeO	1,04	0,91	0,96	0,94
MnO	0,02	0,02	0,02	0,02
MgO	0,76	0,70	0,83	0,76
CaO	0,89	1,03	1,34	1,19
Na_2O	2,74	2,65	3,11	2,56
K_2O	3,59	3,49	3,61	3,62
TiO2	0,15	0,13	0,14	0,13
P_2O_5	0.02	0.03	0.03	0.02
LOI	-	11,60	12,61	12,16

In **Table 5.2**, the functionalisation reduced the microporosity of natural zeolites by a factor of 13 from 0.003 nm for NZ to 0.0003 nm microporosity for AMZ. This means that the amine capping agent blocks the zeolite pores during functionalisation. The BET surface area of NZ is reduced from 19 m^2 g representing external surface area of 12 m^2 g to the total of 6 m^2 g surface areas corresponding almost entirely to the external surface.

The main reason for pore and surface reduction can be attributed to pores of zeolites functionalisation with organic compound that blocks the inner zeolite pores and covers the external surface. Similar BET surface and microporosity reduction were reported for magnetic iron zeolite (Oliveira *et al*., 2004). It can be expected that if the uranyl uptake is entirely attributed to surface area, then the external surface area of AC shall contribute 15 times that of NZ and 30 time that of AMZ because the external surface area order is AC (184 m^2 g) > NZ (12 m^2 g) > NMZ (6 m^2 g). The number of active sites introduced was 4.5 mmols but only 2.5 mmols (56%) were occupied, meaning that the rest of the active sites were strongly embedded inside the zeolite pores as shown by an increasing pore diameter and decreasing micropore volume of natural zeolites after functionalisation. There was high loss on ignition (LOI) for unloaded AMZ compared to NZ meaning that functionalisation with organic group was successful. There was complete loss of activated carbon on ignition affirming that activated carbon was completely made of organic functional groups. The CEC of AMZ before adsorption is higher than that of unloaded NZ, loaded NZ and loaded AMZ. According to the CEC values, it can be postulated that most of the Na^+ introduced during zeolite calcination remained (high CEC for unloaded NZ and loaded AMZ) not exchanged during functionalisation but were exchanged (low CEC for loaded AMZ) after batch adsorption studies. The natural zeolite zeta potential was -0.143 compared to 0.023 for AMZ and 0.076 for AC. This means that natural zeolite can undergo strong electrostatic ion exchange interactions compared to AMZ and AC which are almost neutral. The zeta potential studies further showed that the particle distribution of MAZ was not evenly dispersed. This means uranyl ion adsorption may not be evenly adsorbed by different sites of the AMZ surfaces.

Table 5.2: Some of the important physicochemical properties displayed by natural zeolite, activated carbon and amine zeolites.

Adsorbent property	NZ		AMZ		AC
	unloaded	loaded	unloaded	loaded	loaded
Total surface area (m^2/g)	19.02		6.65		708.22
Ext-surface area (m^2/g	12.73		6.65		184.91
C	-347.24		78.87		-94.48
Qm (cm^3/g)	4.37		1.43		162.69
Micropore volume (cm^3/g)	0.003		0.00023		0.26
Pore diameter (nm)	21.21		31.23		2.42
Particle size	≤ 2 mm		≤ 2 mm		≤500 μm
Zeta potential (mV)	-0.143		0.023		0.076
Active sites - N (mmols)	-	-	4.5	2.5	-
CEC (meq 100 g^{-1})	24.10	23.32	26.78	23.38	-

Batch studies

Effect of pH on uranium removal

The aqueous solution pH and concentration determines uranium speciation, solubility and removal efficiency (Figure 5.1). The observed uranium adsorption efficiency of 92% for AC at pH 2 which remained above 78% at pH 3 can be attributed to the interactions occurring at the AC surface functional groups with the hydrolysed uranyl ion species such as UO_2^{2+} and UO_2OH^+ (Figure 5.1) existing freely below and around pH 3. The decrease in adsorption efficiency with an increase in pH beyond 3 (Figure 5.1) may be explained by poor electrostatic interaction of AC hydrophobic surface towards dissolved neutral and negatively charged soluble uranyl species such as UO_2OH_2, $(UO_2)_2(OH)_2^{2+}$, $(UO_2)_3(OH)_5^+$, and $(UO_2)_2(OH)_7^+$.

Uranium removal efficiency by NZ was lower than 35% in acidic medium possibly owing to the elevated amount of H^+ proton with high ion exchange affinity than UO_2^{2+} towards metal ions Na^+, Mg^{2+} and Ca^{2+} present in the pore of the zeolite, hence leaving more UO_2^{2+} in solution.

The maximum adsorption efficiency of 70% reached at pH 4 can be attributed to the decrease in free H^+ protons in the solution as pH increases allowing more UO_2^{2+} to diffuse into the zeolite pore channels and undergo ion exchange with various alkali metal ions. Although AMZ showed about 87% uranium removal efficiency at pH 2, 4 and 11, there was over 70% removal efficiency throughout the entire pH range investigated. The AMZ efficiency at all other pH values had no significant removal efficiency difference with respect to the high removal occurring at pH 4. This can be attributed to the possible high affinity of capping groups to the uranyl ion. All adsorbents showed lowest efficiency at pH 9 probably owing to the existence of the water soluble negatively charged species $(UO_2)_3(OH)_7^-$, $UO_2(OH)_3^-$ and $UO_2(OH)_4^-$ which have very low adsorption affinity.

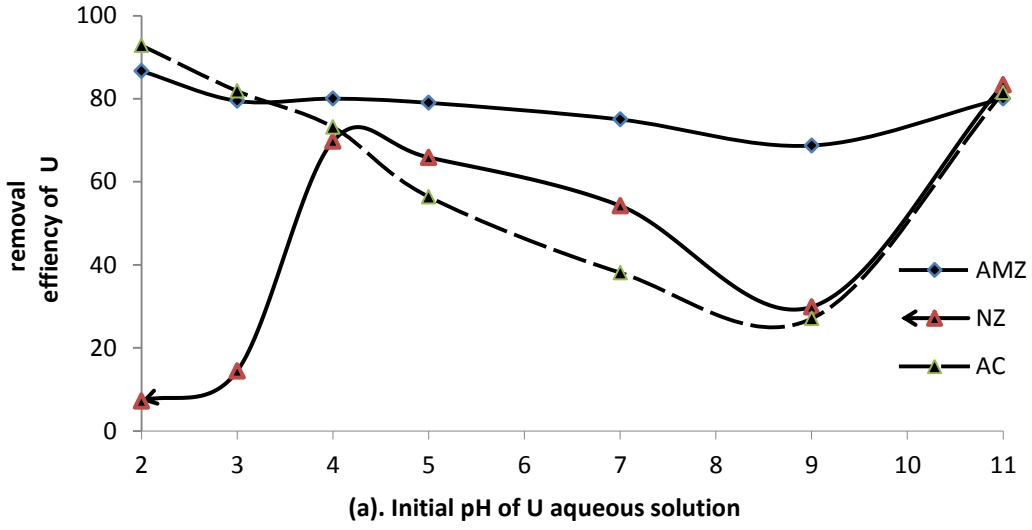

Figure 5.1: Adsorption of U(VI) from 10 mg L^{-1} U aqueous solution at different pH and T = 25 ± 1°C over 24 h mixing time at 150 rpm shaking speed.

Effect of adsorbent dosage

To investigate the effect of mass on adsorption capacity, the values of adsorbent masses investigated were 25, 60, 250, 500 and 1000 mg. The results showed that increasing AC and NZ dosage increased the removal efficiency of uranyl ion until the optimum removal efficiency was reached at 500 mg (Figure 5.2). Although, Figure 5.2 shows that the optimum dosage may lie between 250 and 5000 mg dosages, the ANOVA analysis proved that optimum adsorption was reached at 500 mg. The results imply that the removal efficiency for AC and NZ depends on the number of active sites exposed to uranyl ion in solution relative to the dosage used. The removal efficiency for AMZ was higher than that of NZ and increased with subsequent dosage increments implying that increasing AMZ presented more active sites for uranyl ion binding. The mass of 500 mg used corresponded to removal efficiency of 94, 88 and 54% for AC, AMZ and NZ, respectively.

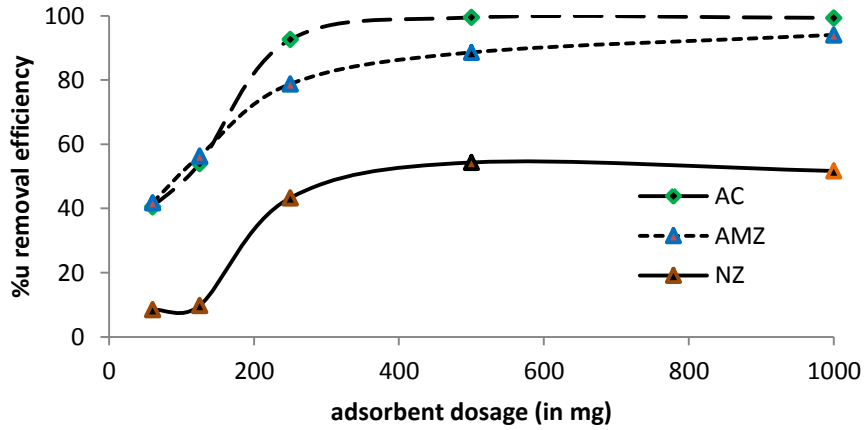

Figure 5.2: Effect of adsorbent dosage increase on adsorption efficiency of 10 mg L^{-1} uranium(VI) using AC, NZ and AMZ as the adsorbents at pH 3, 4 and 4, respectively.

Effect of contact time on uranium adsorption

The removal efficiency of activated carbon and natural zeolite increased rapidly with time where over 90 and 65% of the uranyl ion is removed during the first 60 (Figure 5.3). The adsorption equilibrium contact times were statistically proven to be significantly different until 360 min for AC and 1400 min for NZ. Previous study (Mellah, 2006) reported similar rapid uranium (IV) uptake of over 70% for activated carbon within 60 min.

According to study (Kouraim et al., 2015), some fractions of the 65% uranium removed in the first 5 min can be attributed to some hydrophobicity of activated carbon and coagulation. The removal efficiency of uranium (IV) for amine zeolite increased gradually with time until reaching an optimum removal efficiency of over 78% at 360 min equilibrating time.

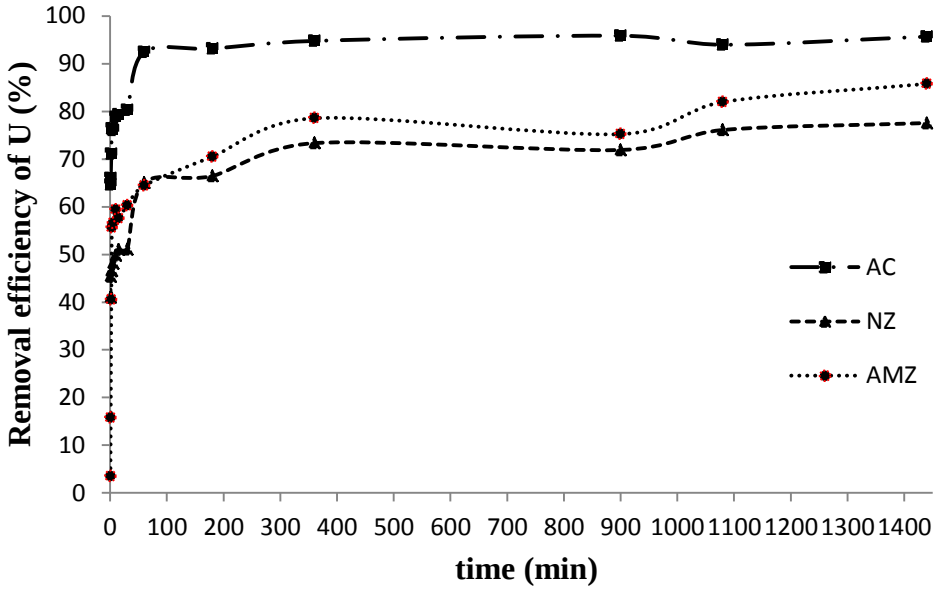

Figure 5.3: The plot of time versus adsorption efficiency as function of contact time.

Kinetics

The linearized plots of pseudo first-order (Figure 5.4*:* a, c, e) and pseudo second-order (Figure 5.4*:* b, d, f) used to determine both the rate constants (k_1 *and* k_2) of some of the kinetic model investigated and the loaded amount of uranium (IV) at equilibrium (q_{e1} and q_{e2}) for each adsorbent used are illustrated in Figure 5.4.

The pseudo first-order and pseudo second-order kinetics correlations was nearly R^2 = 0.9 for all adsorbents. However, the calculated adsorption capacity of pseudo second-order ($q_{e2,\ cal}$) was much closer to experimental adsorption capacity ($q_{e,\ exp}$) than q_{e1} giving the normalized standard deviation of q_1 = 49, 30, 43% compared to q_2 = 8, 1, 11% for AC, NZ and AMZ, respectively (Table 5.3).

This implies that physisorption and chemisorption mechanisms occurred complimentarily. However experimental data and *q* best fitted pseudo-second order which is a kinetic model related to chemisorption through involvement of uranium electrons transfer or sharing with the adsorbent (Kouraim *et al*., 2015). The adsorption rate constant (k_2) mechanisms favouring the order similar to that shown by dosage analysis, i.e. AC > AMZ > NZ.

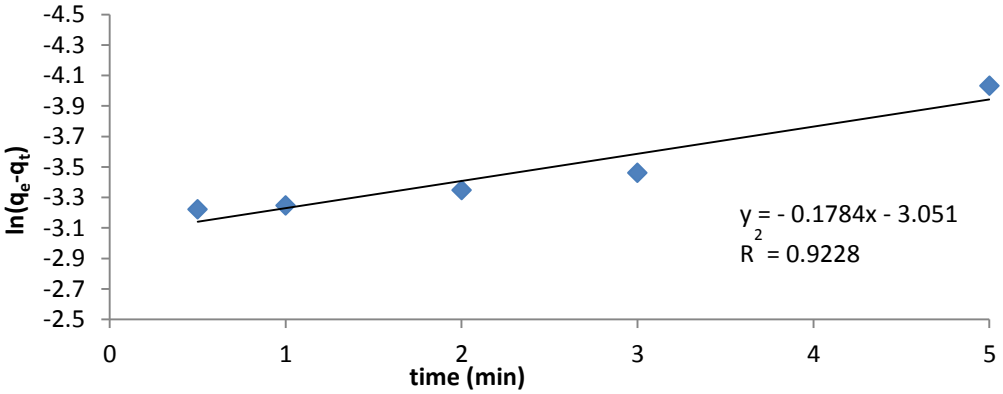

Figure 5.4 (a): Linearised Pseudo first-order for activated carbon on uranium

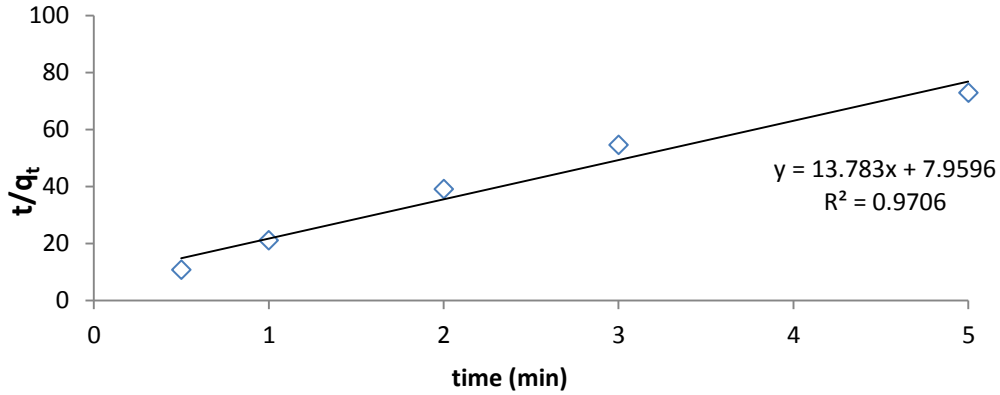

Figure 5.4 (b): Linearised Pseudo second-order for activated carbon on U

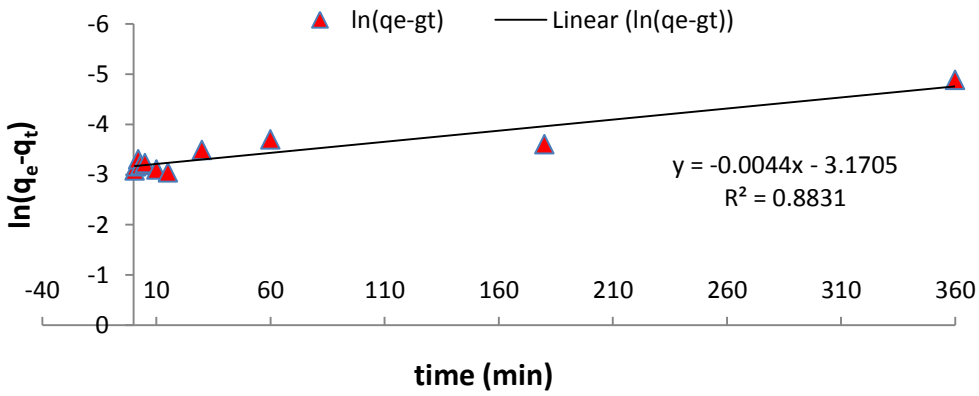

Figure 5.4 (c): Linearised Pseudo first-order for natural zeolite on U

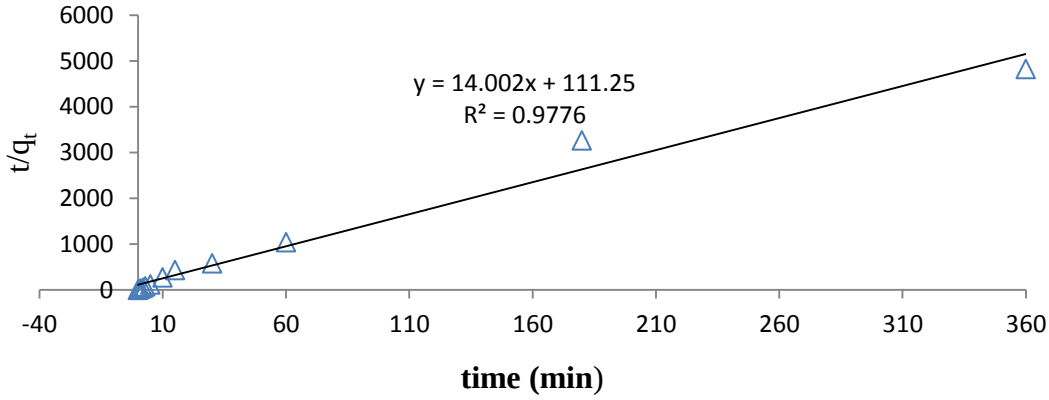

Figure 5.4 (d): Linearised Pseudo second-order for natural zeolite on U

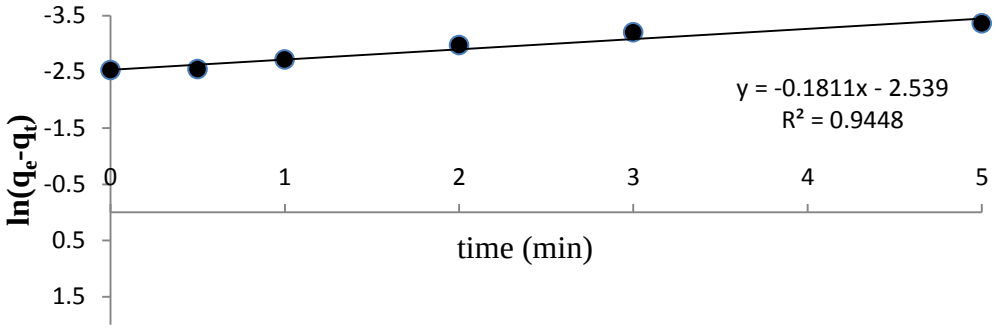

Figure 5.4 (e): Linearised Pseudo first-order for amine zeolite on U

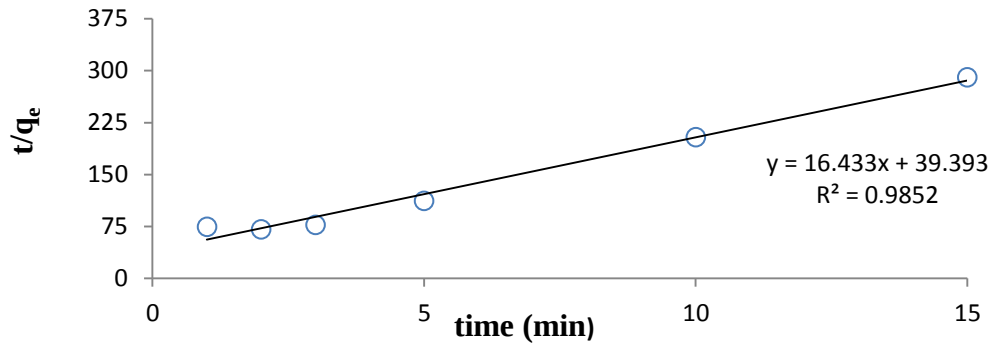

Figure 5.4 (f): Linearised Pseudo second-order for amine zeolite on U.

However, the chemisorption order can be concluded as AMZ > NZ > AC as accounted for by the Elovich chemisorption model. Furthermore, Elovich *a*-value increased from a = 5.01 for NZ to a = 17.86 for AMZ suggesting that chemisorption rate mechanism increased after functionalisation. The intraparticle parameters; I_d and RC order was AMZ ≥ AC > NZ while the R^2 showed that functionalisation reduced zeolite correlation to intraparticle diffusion. These orders suggests the occurrence of high intraparticle diffusion mechanism zeolite characterised by high pore diameter of 21.21 nm compared to 2.42 nm for AC which still experienced some uranyl ion diffusion into the inner walls better than AMZ whose uranium adsorption mechanism was likely to be controlled by external mass transfer as opposed to intraparticle diffusion because the AMZ pores were almost completely blocked by functionalisation (Table. 5.2). All intraparticle diffusion graphs did not pass through the origin implying that diffusion was not the main rate controlling mechanisms. The correlation coefficient (R^2) for NZ is higher while the R^2 from Elovich is high for AMZ. This means that there was high chemisorption increased chemisorption and reduced physisorption for AMZ in comparison to NZ.

The high positive values of intercept of the linear intraparticle diffusion indicate that physisorption mechanism through diffusion increases in the order AC > NZ > AMZ.

The fractional power model fitted the data in the order NZ > AC > AMZ at unit contact time as reflected by *ab* values. However, at equilibrium the order is AMZ > NZ > AC as per R^2 values. The ratio ab/q_t after 1 min contact time estimated uranyl ion removal efficiency through chemisorption using NZ, AMZ and AC as 86, 13, and 10%. These results are consistent with the observed slow uptake of U ion by AMZ, followed by NZ then higher for AC in the first few minutes since a chemical equilibrium generally is a slow step causing a delay in uranium uptake in NZ and AMZ compared to the efficiency of adsorbents that physically capture the metal ions in the first minute and only adsorbing 10% of the uranium through chemisorption. The high removal of uranyl ion using NZ than AMZ for the first few minutes can be attributed to nature of chemisorption involved in uranyl-adsorbent binding because the chemical ion-exchange in NZ with negative zeta potential is electrostatically energetic than binding of uranium on amine group surface that need some energy to establishment equilibrium before chemical bonding. Furthermore, the higher AMZ efficiency compared to NZ as time increases can be attributed to the fact that uptake mechanisms are affected differently with an increasing loaded metal ion concentration (Giles *et al*,. 1974).

Table 5.3: kinetic models calculated parameters for U sorption onto AC, NZ and AMZ.

Model	Parameter	Adsorbent		
		AC	NZ	AMZ
Experimental	$q_{e,\ exp.}$ (mg g^{-1})	0,086	0.074	0.080
Pseudo first-order	$q_{e1,\ cal.}$ (mg g^{-1})	8.89×10^{-4}	6.75×10^{-4}	28.9×10^{-4}
	R_1^2	0.923	0.883	0.945
	K_1 (min^{-1})	0.41	0.010	0.417
	Δq_1 (%)	49	30	43
Pseudo second-order	R_2^2	0.97	0.97	0.98
	K_2 (g.mg^{-1} min^{-1})	23.84	1.787	6.845
	$q_{e2,\ cal.}$ (mg g^{-1})	0.073	0.071	0.0609
	Δq_2 (%)	8	1	11
Elovich	R_3^2	0.79	0.81	0.94
Intraparticle diffusion	a	226.47	5.07	17.86
	β	217.39	196.08	0.038
	I_d	0.05	0.04	0.05
	K_p	0.0009	0. 001	0.001
Fractional model	RC (%)	68.49	56.33	82
	R_4^2	0.75	0.83	0.78
	ab	0.0048	0.0347	0.0037
	a_2	0.037	0.034	1.05

Effect of concentration

Concentration studies in Figure 5.5 showed an increasing adsorption capacity with an increasing uranyl ion concentration for AMZ. adsorption capacity for AC and NZ increased until reaching saturation at initial uranyl concentration of 10 mg L^{-1} and 20 mg L^{-1} corresponding to about 72% and 67% removal efficiency, respectively. It was observed that the adsorption capacity for AMZ is the only one that increased with an increasing uranyl concentration.

The amount of uranyl ion sorbed by AC and AMZ were statistically comparable after using 30 mg L^{-1} uranium solution. Therefore, amine modified zeolite (AMZ) adsorbs U(VI) similarly to activated carbon (AC) but better than unmodified natural zeolite (NZ).

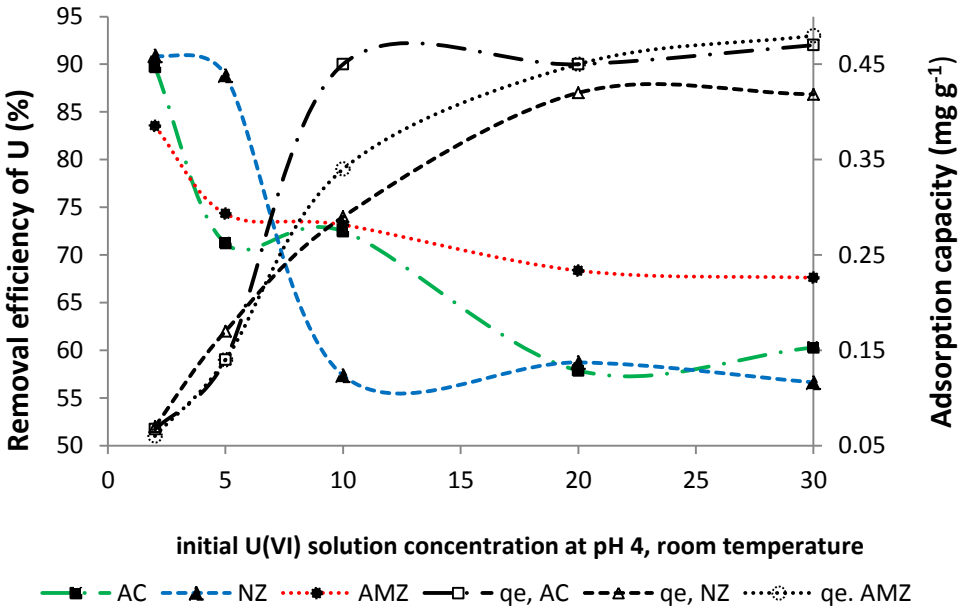

Figure 5.5: Effect of U(VI) concentration on adsorption capacity and adsorption efficiency.

Isotherms

The equilibrium adsorption isotherm data (Table 5.4) showed that Freundlich n values were in the range $1 < n < 10$ while Langmuir dimensionless R_L values were between 0 and 1 signifying that some fractions of uranyl ions were favourably adsorbed on specific sites whilst some involved electron participation. However, coefficient correlations (R^2) best fitted Freundlich model the most following the order (AMZ > NZ ≥ AC) similar to that displayed by pseudo second-order kinetic model. This suggests that there was more adsorption on more than one active site through electron participation (Abdi *et al*., 2014), respectively.

It can therefore be deduced that sorption of uranyl ion depended on both homogenous and heterogeneous mechanisms which translate to stepwise occurrence of sorption mechanism on a single specific site and also on more than one specific site, respectively.

In Figure 5.5 the efficiency of uranium adsorption using AMZ increases with increasing concentration until 10 mg L^{-1} U was added, beyond which adsorption capacity decreased with an increasing concentration. This phenomenon can be related to cooperative adsorption of uranyl ions below 10 mg L^{-1} and thereby followed with a decline in further creation of heterogeneous adsorption active sites due to stable number of sites possibly created and available for binding through Langmuir mechanism at high concentration. The R^2 results of BET isotherms in Table 5.4, shows that the involvement effect of pores on adsorption mechanisms was of the order NZ > AC > AMZ which shows no direct link to one particular surface properties, hence suggesting that BET isotherm influence on adsorption was a combination of all surface porosity properties. The C-isotherm distribution coefficient; $K_d = q_e/C_e$ gave correlation (R^2) order; AMZ > NZ > AC, which is quantitatively and qualitatively similar to that displayed by Freundlich isotherm. The observed C– isotherm correlation order is consistent to experimental distribution coefficient ($k_{d,\ exp}$) and its relative distribution error ($\%\Delta q$) was 0.4% for AC, 4.2% for NZ and 0.13% for AMZ. Therefore, the ratios $X_m/q_{e,\ exp}$, $q_m/q_{e,\ exp}$ and the difference $q_{e,\ exp} - q_{e,\ BET\ (qe,\ C\text{-}isotherm)}$ were used to estimate the removal efficiency related to BET isotherm accounting for overall porosity, C-isotherm representing microspores and Freundlich isotherm as exponential chemical actives sites model. The theoretical estimations revealed that the removal efficiency contribution related to BET, C –isotherm and Freundlich mechanisms for AC was about 93%, 9% and 7%, for NZ was 15%, 61% and 39% and for AMZ was ≈ 0%, 2.8%, and 97%. According to these estimations the functionalisation of zeolites increased the uranyl adsorption through functional groups that promoted Freundlich chemisorption mechanisms.

Therefore, the 2.8% taken up by AMZ through C-isotherm may be related to the low microporosity observed in BET surface property analysis in Table 5.2 and the lower adsorption in the first 5 min of kinetic studies as illustrated in Figure 5.3. The Dubinin-Radushkevich energies were not used to predict the mechanisms involved as chemisorption or physisorption because the correlation coefficient showed that the data did not fit this isotherm model.

Table 5.4: Adsorption isotherm parameters calculated for AC, NZ and AMZ.

	Langmuir				*Freundlich*		
	R^2	q_m (mg g^{-1})	b (L mg^{-1})	R_L	R^2	K_F	n
AC	*0.85*	*0.65*	*0.32*	*0.20*	*0.95*	*6.58*	*1.78*
NZ	*0.87*	*0. 50*	*0. 72*	*0.07*	*0.94*	*0.18*	*2.28*
AMZ	*0.92*	*0.79*	*0.22*	*0.95*	*0.99*	*0.13*	*1.47*

	Dubinin-Radushkevich			*Brunauer-emmet-teller (BET)*		
	E_s (kJ mol^{-1})	X_m (mol g^{-1})	B (kJ^2/mol^2)	R	q_m	C
AC	*2.50*	*0.34*	*0.084*	*0.86*	*0.42*	*12.30*
NZ	*2.60*	*0.38*	*0.0739*	*0.91*	*0.31*	*16.76*
AMZ	*1.83*	*0.38*	*0.15*	*0.82*	*0.72*	*14.57*

	C - Isotherm			*Batch*	
	R	$K_{d,\,exp}$ ($L\ g^{-1}$)	$K_{d,\,cal}$($L\ g^{-1}$)	$q_{e,\,cal}$	$q_{e,\,exp}$
AC	*0.91*	*0.059*	*0. 052*	*0.089*	*0.452*
NZ	*0.93*	*0.066*	*0.0468*	*0.093*	*0.506*
AMZ	*0.99*	*0.069*	*0.0725*	*0.042*	*0.480*

Effect of temperature

Figure 5.6 indicate that temperature affect uranium(VI) adsorption efficiency of granular activated carbon since uranium uptake efficiently increased with an increase in temperature until reaching the optimum removal efficiency of 77% at T = 303.15 K before decreasing to a constant removal of 60% at higher temperatures.

The plot further shows that uranium removal efficiency of natural zeolite and functionalised zeolites are favoured at lower temperatures suggesting that their adsorption mechanisms favour exothermic nature. Moreover, the natural zeolite efficiency for uranium removal decreases insignificantly with an increase in temperature, whereas that there is no observed changes on amine functionalised zeolites removal efficiency as temperature increases. The decrease in uranyl ion removal efficiency for NZ can be attributed to the deforming zeolytic structure and pore size as temperature increases.

The activated carbon decrease in efficiency can be attributed to the loss of pore shape with increasing temperature since about 93% uranyl uptake mechanisms in this adsorbent were related to BET. It is generally expected that the uranium adsorption efficiency of AMZ increases at low temperatures and decrease at high temperatures because chemisorption was the dominant equilibrium adsorption mechanism. However, In this study there was no significant decrease in adsorption efficiency with an increasing temperature using AMZ, this can be explained by the mechanism involved for removal of uranyl ion as being dependent mostly on the functional groups that do not decompose at temperatures explored and do not depend largely on the mesoporous channels related to BET mechanisms of the crystal structure arrangement (especially at low temperatures).

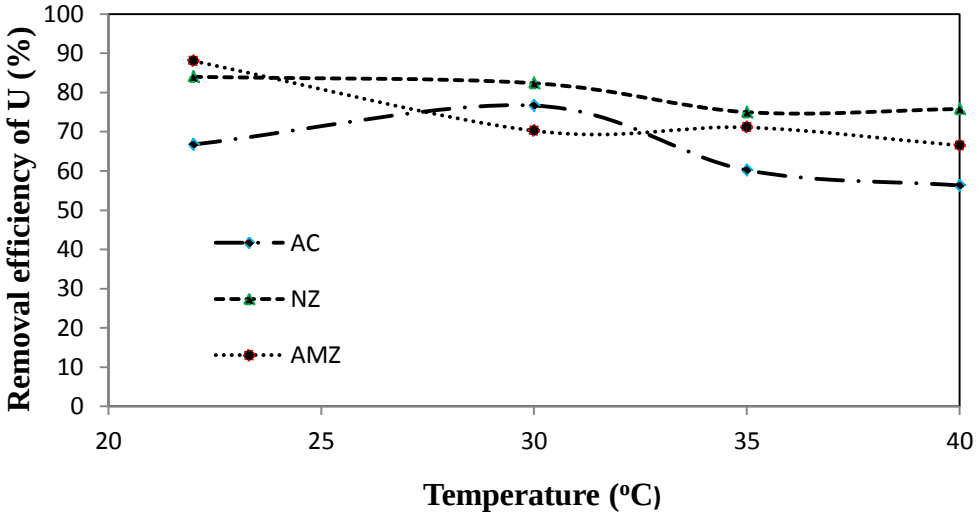

Figure 5.7: Adsorption efficiency of AC (t = 6 h), NZ (t = 21 h) and AMZ (t = 6 h) for uranium(VI) in 10 mg L^{-1} aqueous solution.

Thermodynamics

The negative thermodynamic enthalpy change (ΔH°) calculated from the slope of Van't Hoff linear equation of ln K_d versus 1/T plot were - 20.30, -28.76 and - 45.86 kJ mol^{-1} for AC, NZ and AMZ, respectively (Table 5.5). This suggest that the adsorption mechanisms were exothermically favoured in the order AMZ > NZ > AC. The positive Gibbs free energy change (ΔG°) in all adsorbents reflects that the uranyl ion adsorption mechanisms are non-spontaneous. The non-spontaneity of the mechanisms is in agreement with the long equilibrating times of 6 h and 21 h for AC, AMZ and NZ respectively.

The negative entropy change (ΔS°) of adsorption implies that the uranyl ions adsorbed less randomly on the adsorbent surfaces. The calculated ΔS° values were - 0.09, -0.11 and -0.17 kJ.$mol^{-1}K^{-1}$ for AC, NZ and AMZ respectively, suggesting that the decrease in randomness followed the order AC > NZ > AMZ. This decreasing randomness order was also observed in the isotherm models wherein AMZ followed both Langmuir (homogenous adsorption) and Freundlich models despite AMZ being the modified successor of NZ which followed Freundlich (heterogeneous adsorption) model. Since not all activated sodium zeolite –OH groups are replaced by $–NH_2$ group during functionalisation, therefore it can be assumed that the AMZ surface is microporous and characterised by –OH and $-NH_2$ binding sites which in turn favours a characteristic heterogeneous Freundlich models. However, as the $–NH_2$ functional groups are occupied, the mechanisms seems to be proceeding through micropores diffusion and complexing with the inner –OH group resulting in an almost homogenous mechanistic processes that increases the correlation of Langmuir which is a homogenous surface prediction model.

Table 5.5: Thermodynamic parameters of U adsorption using AC, NZ and AMZ adsorbent

	$\Delta H°$	$\Delta S°$	$\Delta G°$			
	kJ mol^{-1}	*kJ(mol K)$^{-1}$*	*kJ mol^{-1}*			
			295.15 K	*303.15 K*	*308.15 K*	*313.15 K*
AC	-20.30	*-0.09*	*5.86*	*6.59*	*7.03*	*7.47*
NZ	-28.76	*-0.11*	*3.42*	*4.30*	*4.84*	*5.39*
AMZ	-45.86	-0.17	*3.82*	*5.17*	*6.01*	*6.85*

5.1.3. Conclusions

The study comparatively focused on the nature of uranyl ion sorption mechanisms onto activated carbon, natural zeolite and 3-aminopropyltriethoxysilane functionalised zeolite from batch aqueous solutions. The batch sorption parameters, pH, dosage, time, concentration and temperature showed different influence on different uranium(VI) adsorbents. The uranyl ion 10 mg L^{-1} solution adsorption capacity of AC, NZ and AMZ was experimentally determined to be 0.452, 0.506 and 0.480 mg g^{-1} at optimum operating batch parameters pH 3, 4 and 4, contact time of 6 h, 21 h, and 6 h, temperature of 20^{o}C, shaking speed of 150 rpm using 500 mg dosage for each adsorbent. The kinetic and isotherm models signified that the chemisorption mechanisms occurred prevalently compared to physisorption mechanisms for all adsorbents. The thermodynamic evaluations showed that equilibrium mechanisms were exothermically feasible, non-spontaneous in nature and sorption onto all adsorbents occurred randomly at temperature range 22 - 40^{o}C. The theoretical estimations revealed that the removal efficiency contribution of active sites for AC were of the order; BET-isotherm (mesoporous intraparticle diffusion) > C – isotherm (microporous intraparticle diffusion) > Freundlich (through a heterogeneous uranyl ion binding), for NZ was BET > Freundlich > C – isotherm and for AMZ was only two mechanisms were dominantly involved

in the order Freundlich >> C –isotherm. Therefore, amine zeolite functionalisation can be recommended for high uranyl ion adsorption capacity since it caused adsorption changes with coverage over distinct set of active site as seen from better correlation to chemisorption binding models.

5.2. Results and discussion

Removal of radioactive uranium(VI) from inorganic wastewater using aminotrimethyl phosphonic acid zeolites and silica polyamine composite

This chapter 5 section compares the use of aminomethyl phosphonic acid functionalised natural zeolites and silica polyamine composite for the uptake of uranyl ion from aqueous solutions in the presence competing ionic species. The specific theoretical background is given before a detailed results and discussion subsection.

5.2.1. Background

Heavy metals from industry (Davidescu *et al*., 2013; Ibrahim *et al*., 2010), phosphate fertilizers (Elser and Bennett, 2011), metal plating, mining and nuclear power generation (Beatty *et al*., 1999a), sewage plants (Donat, 2009), pesticide and oil transportation (Tutu *et al*., 2013) pollutes the aquatic environment and consequently endangers all forms of life (Misaelides, 2011). Uranium is one such highly toxic, non-biodegradable and radioactive heavy metal (Tutu 2013). The major uranium sources are nuclear power plants and mining wastes (Kütahyalı and Eral, 2004; Yang and Volesky, 1999; Guibal *et al*.,1992). The human health effects of uranium includes organismic central nervous system (CNS) problems, bone and DNA deformation (Jiang, 2006), electrophysiological changes (Briner and Murray, 2005), chemical mutagens and cancer (Saad *et al*., 2015).

High uranium concentrations from 1 mg L^{-1} to 14 mg L^{-1} were reported for areas within mine site proximity (Saad *et al*., 2015; Ladeira and Gonçalves, 2007) while natural environment have lower uranium content (Kalin *et al*., 2004). Therefore continued mining, ^{238}U toxicity (Yang and Volesky, 1999) and long half-life of about 4.5×10^{9} years coupled with need for rapid growth in metal recovery for nuclear electricity production *(*Beatty *et al.*, 1999a*;* Faur-Brasquet *et al*., 2002) constitute a major concern for tailoring low cost adsorbents such as zeolites for uranium(VI) uptake (Tawanda *et al.*, 2014; Yin *et al*., 2014).

Zeolites are solid porous aluminosilicates with low metal ion selectivity (Figueiredo and Quintelas, 2014). However, zeolites surfaces can be functionalised to improve their metal ion selectivity. Different synthetic phosphate-ligated or functionalised materials have since been investigated for metal sorption selectivity (Saad *et al*., 2015; Yin *et al*., 2014; Deepatana and Valix, 2008; Kiefer and Höll, 2001). Nevertheless, to the best knowledge of the author, uranium adsorption using phosphate ligated natural zeolite in the presence of iron, phosphates, manganese and calcium salts is a rarely explored field.

This is despite, (1) the metal salts and organic acids known to determine environmental uranium migration and distribution (Kantar, 2007) and (2), uranium(VI) known to have high propensity to selectively form water insoluble multidentate complexes with silicates and phosphates via the Lewis acid-base coordination (Yin *et al*., 2011; Sirola *et al*., 2008).

Therefore, the present work aimed to produce (aminomethyl) phosphonic acid functionalised zeolite and further compared it to silica polyamine composite for uranium adsorption efficacy in the presence of some competing metal species. The data was also modelled for speciation, kinetics, isotherms and thermodynamics in order to elucidate the adsorption mechanism involved.

5.2.2. Results and discussion

Characterisation

Functional group analysis using FTIR

The reduced intensity at 3676 cm^{-1} vibrations reported to correspond to Mg-OH (Sprynskyy *et al*., 2011) (Figure 5.8) indicates a successful activation of natural zeolites to afford sodium zeolites by replacing Mg with Na. The asymmetric stretching vibrations of NaZ around 1039 cm^{-1} corresponding to Si-O-Si and Si-O-Al bridging bonds while the overlaps from 1022 and 1076 cm^{-1} through to 1100 cm^{-1} in both APZ and SPC signifies an organic-inorganic Si-O-Si group hybridisation at molecular level (Nagarale *et al*. 2004). The hybridization can also be confirmed by the APZ bending -CH band at 2988, 2931, 2981 cm^{-1} and the low strength band secondary –NH group at 3274 cm^{-1}, 3608 cm^{-1} in APZ and at 3433, 3450 cm^{-1} for SPC (Su, Lu *et al*. 2010). The phosphorylation can be confirmed by the vibrations at 1400 cm^{-1}. Therefore the change in NaZ spectral vibrations at 1400 cm^{-1} to APZ intensity that is superimposable to phosphonated silica polyamine composite at 1400 cm^{-1} wavenumber suggests a successful phosphorylation of sodium zeolites to aminomethyl phosphonic acid.

The decrease in the NaOH broad vibrations from 3400 cm^{-1} wavelength of NaZ suggests that the acidic bronsted bridging -OH group vibrations from 3170 to 3564 cm^{-1} were involved in phosphorylation of zeolites with PO-H low bands observed at 1967, 2032 and 2164 cm^{-1} (Li 2005).

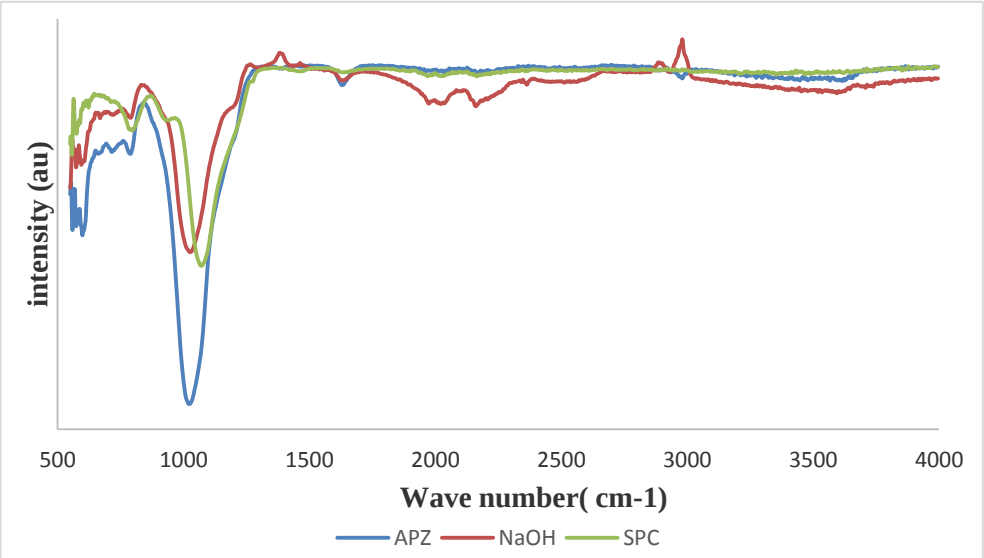

Figure 5.8: The FTIR spectrum profile of NaZ (NaOH), APZ and SPC.

Thermo-stability analysis

The observed TGA profile (Figure 5.9) inflations of silica polyamine composite can be linked to water evaporation at temperatures below 110^{o}C, amino propyl group degradation in the ranges 110^{o}C to 300^{o}C giving 5% inflation and –CH group oxidation process at thermal range of 300-804^{o}C giving 19% inflation, respectively (Su, Lu *et al*. 2010). The NaZ and APZ also showed water loss below 110^{o}C. The weight loss observed in Figure 5.9 at temperatures below 110^{o}C is of the order APZ > NaZ > SPC. This water retention decreasing trend is in agreement with the observed decreasing intensity trend of H-O-H (water molecules) vibrations at 1637 cm^{-1} of FTIR spectrum in Figure 5.8.

The insignificant weight loss difference between sodium zeolites and phosphonated zeolites in the ranges 250 – 500^{o}C suggests that the functionalised zeolites –PO_3H_2 bond retained high thermal stability (Nagarale *et al*., 2004).

In the temperature ranges of 500^{o}C – 900^{o}C, the phosphonated zeolites lost 2% more compared to weight higher than the sodium zeolites. This observation can be attributed to loss of –CH group related to inorganic-organic hybridisation that formed Si-O-CH bond around 1100 cm^{-1} vibrations of the FTIR spectrum (Figure 5.8) (Saravanan and Aparna, 2015). Hence, there is an increased non-reversible zeolytic structural deformation with an increasing thermal exposure.

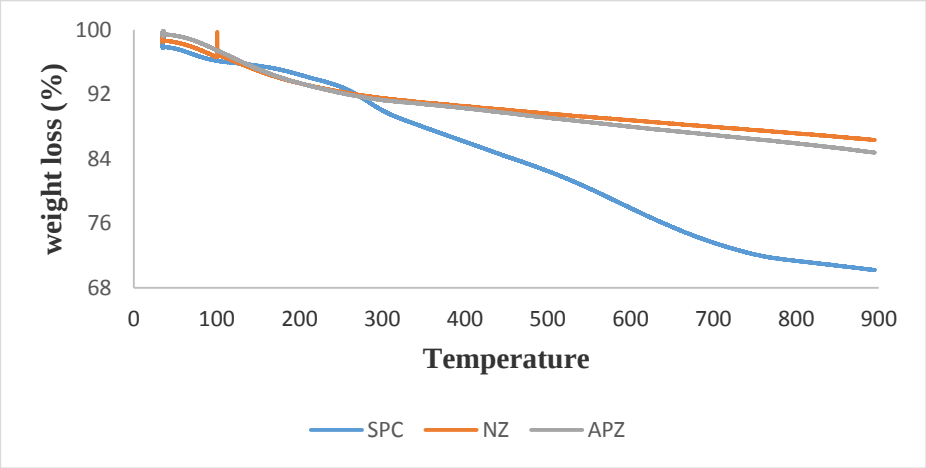

Figure 5.9: Thermogravimetric curves of NaZ, APZ and SPC

Other surface properties of NaZ (NZ as referred in Figure 5.9), APZ and SPC

Different surface properties of APZ and SPC are presented in Table 5.6. The BET results showed that the BJH pore volume was of the order SPC > NaZ > APZ. The pore volume order confirms the easy dehydration process occurring in SPC adsorbent characterised by the mesoporous volume of 0.73 nm in comparison to the more hydrophilic APZ characterised by the microporous volume of 0.04 nm. According to literature (Ye *et al*., 2007), the large pore size and the capability of pore walls to have chemical or physical interaction with the adsorbate increases the adsorption capacity through diffusion process.

In addition, the overall surface charge can be used to predict the adsorbent-adsorbate interaction mechanisms and electrostatics. This implies that below the point of zero charges (pH_{phz}) of pH 7.3 and 3.02, the APZ and SPC adsorbents are positively charged, respectively and it further means that the uranyl ion species uptake will depend on the uranium speciation and charge in conjunction with adsorbent surface point of zero charge. The low pH_{phz} for SPC also known as BPAP 1 can be linked to high amine and phosphate elemental composition that amounts to 3.36 N% and 4.34 P% according to literature (Hughes and Rosenberg, 2007; Tutu et al., 2013). The BJH average pore diameter of APZ (64.27 m^2/g) and a total surface area of 13.23 m^2/g in comparison to SPC (13.69 m^2/g) with large total surface area of 189.75 m^2/g and external surface area of 194.82 m^2/g means that there is high probability of active sites exposed for metal binding than in APZ (Saleh *et al*., 2016).

Table 5.6: Physicochemical properties of aminophosphonated zeolite and Silica polyamine composite before batch adsorption studies

Adsorbent properties	Adsorbent	
	APZ	SPC
Total surface area – BET (m^2/g)	13.23	189.75
External surface area (m^2/g)	-	194.82
BJH Pore volume (cm^3/g)	0.04	0.73
BJH pore diameter (nm)	64.27	13.69
Point of zero charge (pH_{PHC})	7.3±02	3±02
Particle size (mm)	$0.5 < 2$	$0.25 \leq 0.5$
Zeta potential	0.0857	-0.0346

Batch adsorption studies

Effect of initial pH

The silica polyamine composite (SPC) removes uranyl ion almost completely throughout the pH range evaluated (5.2.3). This observation coincide with the characterisation results in a number of ways; (1) there is large number of negative

active sites -NH_2, - OH (Tutu, 2013) and - PO_3 (Mark, 2007) as observed in FTIR vibrations and TGA inflations corresponding to these functional groups. The SPC small particle size and point of zero charge (pH_{pzc}) at low pH equalling 3±02 can be responsible for the binding of both the competing protonation H^+ atoms and the hydrolysed UO_2^{2+}, UO_2OH^+ ion species existing freely below pH 3 (Figure 5.11), (2) The continued high efficiency beyond pH_{pzc} 3±02 can be associated to the electrostatic attraction of negatively charged SPC surface beyond the point of zero charge as reflected by the zeta potential of – 0.0346 (Table 5.6) at acidic pH beyond 3 and positively charged $UO_2(OH)_2$, UO_2^{2+} , UO_2OH^+ and $(UO_2)_2(OH)_2^{2+}$ ion species (Figure 5.10 and 5.2.4) as depicted by phreeqc results and (3) the SPC surface pendant ligand shielding by a polymer matrix promote uranyl ion adsorption and some metal ions in basic conditions as reported (Hughes and Rosenberg, 2007). In contrast, the optimum efficiency of aminophosphonated zeolite (APZ) in acidic and basic conditions occurs at pH 4 and 9 respectively. Elevated amounts of UO_2^{2+} and UO_2OH^+ are left in solution due to high protonation process around pH 2 to 3 which promotes high zeolytic structure affinity for small sized H^+ protons ion exchange (zeolite 2009). The maximum q_e of 0.75 mg g^{-1} at pH 4 can be attributed to the decrease in hydrogen-uranium protonation competition that leaves more APZ negative centres –NH_2 and –PO_3 exposed for UO_2^{2+} and UO_2OH^+ coordination. The existence of bulky $(UO_2)_3(OH)_5^+$ and $(UO_2)_2(OH)_7^+$ ion species with restricted mobility in water may account for the significant uranyl ion removal efficiency drop for APZ at pH 5. It is expected that the electrostatic repulsion between negatively charged APZ surfaces beyond pH_{pzc} = 7.4 and the anionic species $(UO_2)_3(OH)_7^-$, $UO_2(OH)_3^-$, $UO_2(OH)_4^-$ existing at pH 9 will reduce adsorption, hence the high removal at pH 9 can be attributed to precipitation of hydroxyl uranium complexes into the zeolytic pores since no ion exchange was recorded for both XRF analysis. The dependence of uranium adsorption on the initial pH was similarly reported (Rosenberg *et al*., 2016).

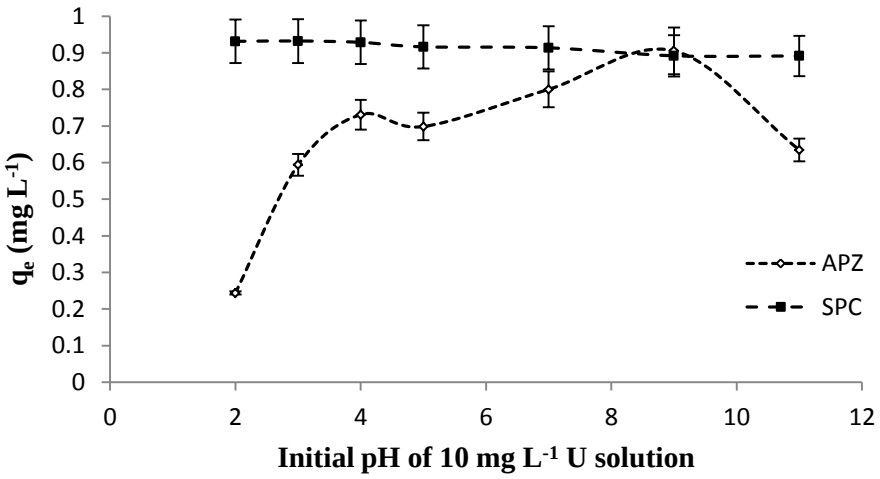

Figure 5.10: Effect of pH_i on 10 mg L^{-1} U adsorption capacity at room temperature for 24 h (n=3, SD =RSD × q_e).

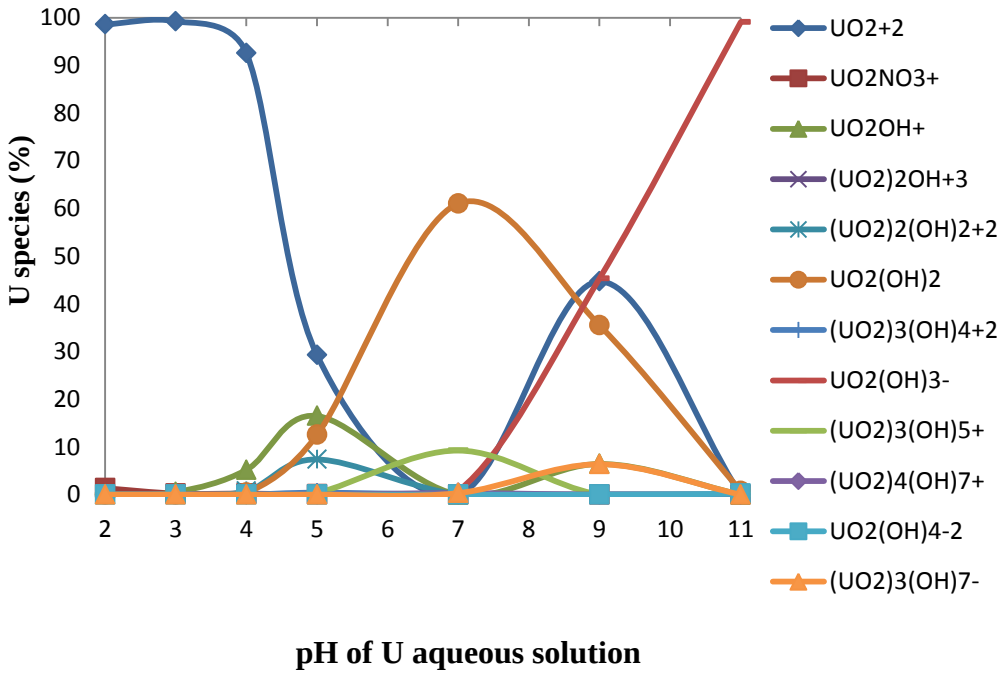

Figure 5.11: Speciation of U in 10 mg L^{-1} U aqueous solution at T = 25 °C, Eh = 4 using Phreeqc code interactive modelling version.

Effect of dosage on uranium adsorption capacity SPC and APZ

The SPC dosage results indicated an almost complete mass removal of 10 mg L^{-1} uranyl ion corresponding to atleast 99 % removal efficiency (*Figure 5.12*). The SPC dosage of 25 mg was then used for the subsequent analysis of the effect of other batch parameters on removal efficiency of uranium. The removal efficiency increased with an increase in APZ dosage until active sites saturation was reached at 100 mg dosage. The observed slight decrease in APZ adsorption efficiency beyond 100 mg suggests that the binding of UO_2^{2+} ion concentration onto APZ is dependent on the APZ dosage increments for as much as the active sites are not shielding from being exposed to uranyl ion in the solution due to APZ dose increase. Similar trends were reported for uranium removal using activated carbon (Mellah *et al*., 2006) and ammonium modified zeolite (Bakatula *et al*., 2015).

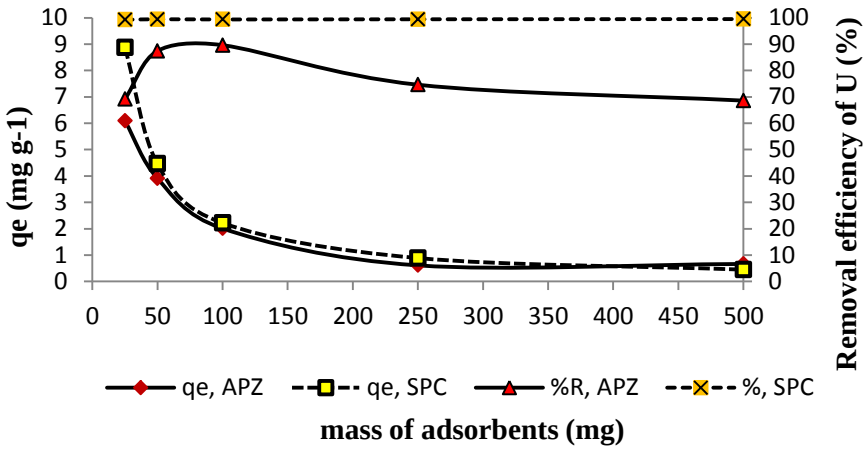

Figure 5.12: Effect of dosage on 10 mg L^{-1} U adsorption capacity at T =25°C, pH_i 4 and t = 24 h (n = 6, sd = rsd × qe, p-value at 95% confidence level)

Effect of contact time

In Figure 5.13, the results showed significant uranyl ion adsorption of about 92% by SPC and 62% by APZ in the first 5 min and 30 min, respectively. The observed rapid removal of uranium can be attributed to the high number of vacant

–NH and -PO_3 active sites available at the beginning of the adsorbent-adsorbate contact time. In addition, the high SPC efficiency can be linked to the large number of different negative active sites ligands with high affinity for uranyl ion and the small particle size allowing faster movement in solution in contrast to the low active sites, microporosity and slow mobility presented by the large APZ particles which do not promote easy uranyl ion diffusion into the small inner pores for inside wall interactions. The equilibrium removal efficiency of 95 % in SPC was achieved within 60 min but for APZ it efficiency of above 78% was achieved after 360 min. In APZ samples the equilibrium time can be linked to the decrease in the available active sites for uranyl ion uptake and the inclusion of the second phase mechanism which proceeded slowly after 30 min. In SPC samples the results may reflect the uranyl ion depletion from the solution owing to enormous uptake by large number of active sites as represented by the large weight loss in TGA.

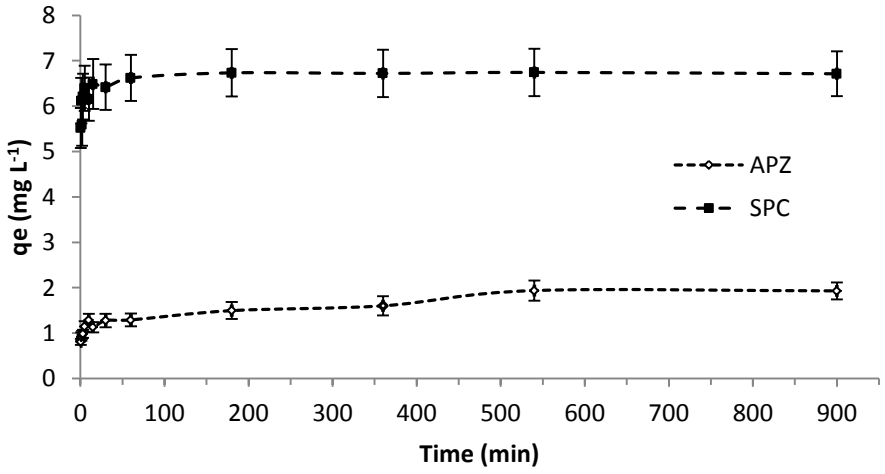

Figure 5.13: The plot of 10 mg L^{-1} U(VI) concentration adsorption efficiency versus contact time (n = 3, sd = rsd ×qe, p value at 95 %).

Kinetic modelling

The Pseudo first-order equation 4.17 and Pseudo second-order equation 4.18 were used to elucidate the adsorption controlling mechanisms (Fu *et al*., 2015).

$$\ln(q_{e1} - qt) = \ln q_{e1} - k_1 t \quad (4.17)$$

$$\frac{t}{q_{e2}} = \frac{1}{k_2 q_{e2}^2} + \frac{1}{q_{e2}} t \quad (4.18)$$

where k_1 (min^{-1}) and k_2 (g mg min^{-1}) are pseudo first-order and pseudo second-order rate constants from the plots of ln ($q_e - q_t$) v/s t and t/q_t v/s t, respectively.

The SPC and APZ data best fitted pseudo second-order kinetics with correlation coefficient (R^2) of 1 and 0.99, respectively (Table. 6.1). The theoretical adsorption capacity ($q_{e2,\ cal}$ mg g^{-1} = 1.92 for APZ and 6.75 for) and experimental ($q_{e2,\ exp}$ = mg g^{-1}1.93 for APZ and 6.74 SPC) were equivalent and displayed a normalized standard deviation of 0.03% and 0.15% for SPC and APZ data, respectively. Since the pseudo second-order model fundamentally assumes that chemisorption is involved (Sari and Tuzen, 2009), the plausibility of this model was further assessed using Elovich kinetic model that makes an assumption that for chemisorption the adsorption decreases with increasing contact time. The Elovich R^2 = 0.92 for APZ data confirmed that uranyl ion was chemically adsorbed onto APZ surfaces. Although SPC data correlated to Elovich model better than pseudo first-order, the low Elovich R^2 of 0.77 suggests that chemisorption is not the only rate determining mechanism involved. The deductions coincides with the implications that of high *b* value when related to the extent of surface coverage for APZ compared to SPC because increasing mass for APZ increased active sites for uranium chemisorption but mass increase in SPC did not show any significant effect. The effect of porosity difference as shown in BET results (Table 5.6) for uranyl ion removal was assessed using intraparticle diffusion kinetic model by plotting q_t v/s $t^{1/2}$ (Wu et al., 2009b). Since, $I_d > 0$ (Table 5.7.), then it can be deduced that intraparticle diffusion and external mass transfer were involved in rate determining mechanisms. Nonetheless, it must be noted that according to the coefficient of determination (R^2) value of 0.33, this model does not fit the SPC data best compared to R^2 = 0.78 for APZ which is better suited by this model, hence this deduction can be reserved for SPC analysis. Furthermore, the low relative coefficient (RC = 57.5%) of APZ implies that the intraparticle diffusion was the adsorption dominant rate limiting step. The high relative coefficient of SPC (RC = 91.9%) could signify that the external mass transfer was massively involved in rate determining steps.

Generally, if above 90% of metal ion is removed in the first 5 min, then the uptake might be associated with conglomeration or aggregation. These results are consistent with the microporous APZ structure that is likely to delay the diffusion of uranyl ion into the inner zeolite walls and thereby causing the observed two step reaction rate in APZ samples (Figure 5.13) as compared to the mesoporous SPC silica material that allows easy diffusion into inner walls for adsorption and therefore suggesting that the availability of mass transfer in the form of uranium availability in solution determines the adsorption rate.

Table 5.7: Kinetic parameters of U adsorption using SPC and APZ adsorbents

	Pseudo first-order model			***Pseudo second=order model***		
	R^2	k_1 (min^{-1})	q_{e1} ($mg\ g^{-1}$)	R^2	k_2 ($g\ mg^{-1}\ min^{-1}$)	q_e ($mg\ g^{-1}$)
APZ	0.72	0.04	13.56	0,99	0.04	1.92
SPC	0.88	0,050	5.85	1.00	0.04	6.75
	Intraparticle diffusion mode			***Elovich***		
	Kp ($mol \cdot kg^{-1} \cdot min^{-0.5}$)	Id ($mg\ L^{-1}$)	RC (%)	R^2	b	R^2
APZ	*0.0007*	1.1	57.5	0.78	7.09	0.92
SPC	*0.0005*	6.2	91.9	0.33	6.81	0.77

Effect of the initial uranyl ion concentration on adsorption capacity

In Figure 5.14, increasing initial uranyl ion concentration increased adsorption capacity of APZ and SPC. However, the adsorption efficiencies drop slightly at higher concentrations. The observations can be attributed to the availability of enormous vacant uranium ion binding sites, –NH, $–PO_3$ and pores. This trend is consistent with the time effect data that best fitted Elovich kinetics as a model that predicts that in chemisorption mechanism the adsorption capacity increases with an increasing concentration while the efficiency continuously drops with further concentration increments. The continuous increase in adsorption capacity until saturation levels can be linked to uranyl ion adsorption on the heterogeneous

functional groups until the pores are also occupied with hydroxyl uranium complexes (Kouraim *et al.*, 2015) and this can be validated if the adsorption data best fit BET isotherm.

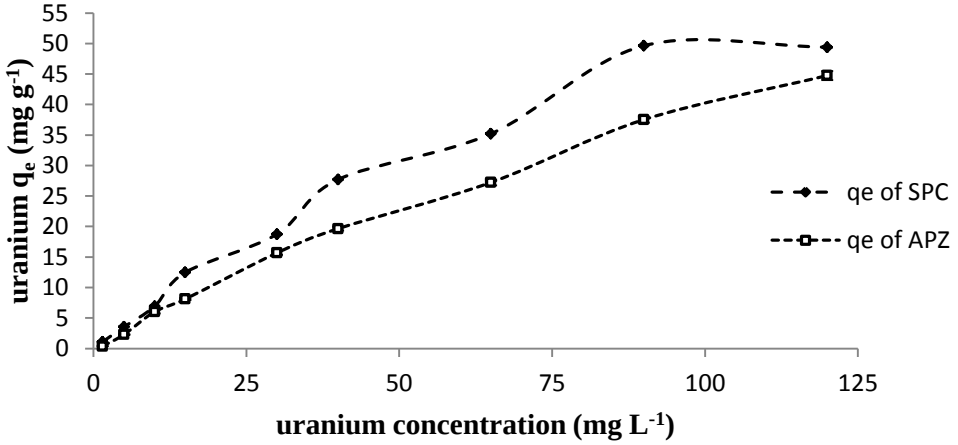

Figure 5.14: Effect of initial uranium (IV) concentration on adsorption capacity of 100 mg APZ (at t = h) and 20 mg SPC (at t = 1 h) at pH 4, 25 ^{o}C and 150 rpm.

Isotherm modelling

Different Isotherms models were used to calculate various parameters and to further describe the equilibrium mechanisms on the basis of adsorbent surface properties and metal ion affinity (Table 5.8). The widely used Langmuir isotherm predicts homogenous adsorption using equation 4.22:

$$q = q_{m1} \frac{b.C_e}{b.C_e+1} \quad (4.22)$$

The poor Langmuir R^2 of 0.76 suggests that the model cannot be used to predict the feasibility of uranium adsorption onto both APZ and SPC. The Freundlich isotherm was also evaluated by plotting ln q_e v/s ln C_e which gave the slope of 1/n (n - intensity constant) and intercept of log K_F (sorption capacity constant) when the data was fitted into equation 4.24:

$$\ln q_e = \ln K_F + \frac{1}{n} \ln C_e \quad (4.24)$$

where n and K_F are the intensity and sorption capacity constants, respectively.

The Freundlich isotherm best fitted both SPC and APZ data with equal correlation coefficient (R^2) of 0.98. Therefore, predicting that a heterogeneous adsorption mechanism was greatly involved for uranyl adsorption onto both adsorbents. The n values obtained suggest that adsorption is feasible but because n ≈ 1 it can also be deduced that this linearity corresponds to the almost linear adsorption trend observed in Figure 5.14. The Dubinin–Radushkevich (D–R) isotherm was also used to predict whether adsorption occurred chemically or physically using equation 4.25:

$$\ln q_e = q_{m3} - K\varepsilon^2 \quad (4.25)$$

Where the values of q_m and K can be read from the plot of ln q_e versus ε^2, where(ε) denotes the Polanyi potential described statistically in equation 4.26.

The D-R isotherm could not be used to fully explain the adsorption mechanisms due to poor correlation. Although the Es < 8 kJ mol^{-1} suggested there existed some physisorption mechanisms, the D-R model could not be used to predict the equilibrium mechanisms due to low coefficient of determination (R^2 = 0.4) for both APZ and SPC. Another isotherm model used for porous adsorbents is BET. The high R^2 values of SPC = 0.93 and APZ 0.95 =0.95 (Table 5.8) confirms that the uranyl ion adsorption was also affected by the BJH pore volumes calculated from BET surface analysis shown in Table 5.6.

Table 5.8: Isotherm parameter of U adsorption using SPC and APZ adsorbent

Isotherms	Langmuir				Freundlich		
parameter	R	R_L (L mg^{-1})	q_m (mg L^{-1})	*b*	R	K_F	n
SPC	0.22	0.84	285.71	0.002	0.96	3.20	0.98
APZ	0,69	0,83	129.87	0,004	0.96	3.95	0.97
	Dubinin-Radushkevich				BET		
	R^2	X_m	β	E_s	R		
SPC	0.40	2.37	0.17	1.70	0.93		
APZ	0.40	1.07	0.14	1.89	0.95		

The effect of temperature on the uranium adsorption capacity

The effect of temperature ranging from 22 to 40°C was assessed for uranium adsorption capacity using 30 mg L^{-1} uranium concentrations (Figure 5.15). An increase in temperature decreased U(VI) uptake from q_e = 9.5 mg g^{-1} to 8.2 mg for SPC and from 2.2 mg g^{-1} to 1.1 mg g^{-1} for APZ. In both adsorbents, the removal efficiency showed significant decrease from 35°C. This observation can be attributed to the change in both uranyl ion species and the structural surface functional group under this temperature conditions. About 50 % removal efficiency and adsorption capacity decrease observed for APZ can be attributed to the previously reported findings that high temperature collapses the zeolytic framework leading to the porosity decrease (Motsi 2009), thus decreasing the effectiveness of zeolites for uranium capture. The decreasing adsorption capacities with increases temperature suggest that the equilibrium mechanisms were exothermically favoured.

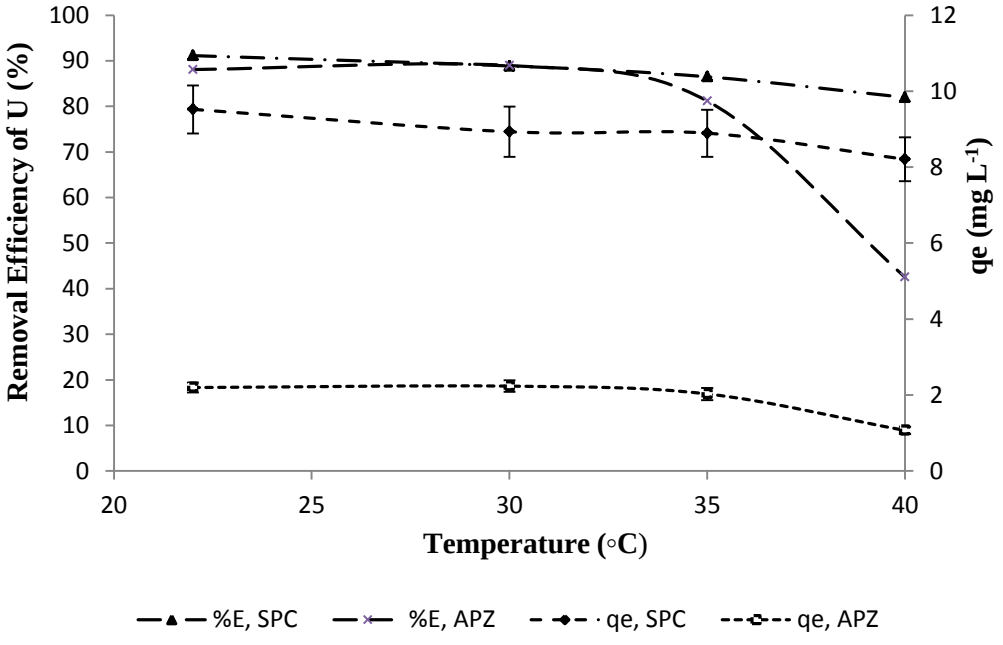

Figure 5.15: Effect of temperature on 30 mg L^{-1} uranium removal efficiency and adsorption capacity (n = 3, sd = $e_4 \times q_e$, p –value at 95% confidence level)

Thermodynamic modelling

The essential thermodynamic parameter enthalpy change (ΔH°) negative values reaffirms that both mechanisms are exothermic (Table 5.9). The large negative Gibbs free energy change (ΔG°) imply that UO_2^{2+} ion adsorption was favourable and spontaneous for SPC while positive ΔG for APZ signifies a deteriorating adsorption feasibility of U(VI) onto APZ with an increase in temperature (Fig 6.10). The ΔG° becomes less negative for SPC and increases its positivity for APZ implying that uranium adsorption was not favourable at higher temperatures investigated. The negative entropy change (ΔS°) values suggest that UO_2^{2+} ions were orderly adsorbed onto the adsorbent-adsorbate interface.

Table 5.9: Thermodynamic parameters of U adsorption using SPC and APZ

	$\Delta H°$	$\Delta S°$	$\Delta G°$		
	kJ mol^{-1}	*kJ(mol K)$^{-1}$*	*kJ mol^{-1}*		
			295.15 K	*308.15 K*	*313.15 K*
SPC	- 31.44	-0.09	-5,73	-4,24	-4,23
APZ	-82.17	-0.27	2.35	4.81	6.71

Effect of competing ionic species

The results of competing metal effect are expressed in the form of metal ion selectivity in Table 5.10. An increase in both $CaCO_3$ and $MnSO_4$ concentration decreased the SPC efficiency for uranium removal until 15 mg L^{-1} competing metal concentrations were used, beyond which the adsorption capacity remained statistically constant. These results (Table 5.10) can be related to the likely precipitation of uranium as UO_2CO_3 (Log K= 5.4, SI = - 1.66) and $UO_2(OH)_2$ (log K = 5.4, SI = - 1.52) which do not easily adsorb. The pH increase after contacting $CaCO_3$ and uranium to APZ suggests that the low efficiency for APZ was due to formation of $Ca_2UO_2(CO_3)_3^0$ and $Ca_2UO_2(CO_3)_2^2$ (Appendix A1) species that do not easily adsorb on silica material.

In the case of $MnSO_4$ it can mean that the $SO4^{2-}$ bind slightly better to uranium than manganese as seen by the log K = -3.20 for $U(OH)_2SO_4$ and log K = – 5.71 for $Mn_2(SO_4)_3$ indicating that manganese is less likely to bind to sulphate compared to uranium which then remain in solution as $U(OH)_2SO_4$ (Appendix A1). In SPC tests the pores are large enough to influence non chemisorption by trapping the small cation of manganese compared to large uranium nucleus and thereby leaving more uranium sulphate in solution. The optimum adsorption capacities of 5.9 mg g^{-1} and 16 mg g^{-1} corresponding to removal efficiency of 99% APZ and 89% SPC were reached for phosphate ions competing samples, respectively. The was an almost complete uranyl ion adsorption observed for APZ with increasing Na_2HPO_4 content added while the SPC samples adsorption capacity decreased randomly with an increasing phosphate ion. The phreeqc calculated saturation index of $UO_2(HPO_4)_2^{2-}$ equals – 7.79 with species activity log IAP = – 59.37, implied that the ionic strength and cationic radius affected uranium uptake since the abundantly available competing protons H^+ and Na^+ with small radius move fasters in solution and hence binds to active sites without binding to uranium since the log K = – 47.41 for the two autunites; $H_2(UO_2)_2(PO_4)_2$ and $Na_2(UO_2)_2(PO_4)_2$ means their formation probability is very low (Appendix A1). Similar results were reported for competing $NaNO_3$ for copper and uranium adsorption by peat and other functionalised mesoporous silica material, respectively; the ionic strength was said to highly affect the outer-sphere complexes such as those of uranium (Ho and Mckay, 2002). The increase in APZ adsorption in the presence of phosphate competing ionic species therefore suggests that the inner complex PO_4^{2-} binds first to the phosphate group immobilised on the zeolite surface resulting in an increase in active sites before uranium can attach onto the PO_4^{2-}group to form UO_2HPO_4 complex (Wang *et al*., 2014). The results in Table 5.10, shows that adsorption selectivity for APZ was of the order Na > Mn ≥ U > Ca > Fe while the SPC selectivity order was Fe > Ca > Mn > U > Na. The selectivity coefficient value of 1.06 shows that Mn^{2+} and U(VI) are equally preferred for binding by SPC.

Furthermore the results show that Mn^{2+} is adsorbed through a Langmuir model. Therefore, Mn compete with uranium for binding on one of the active sites available for metal uptake and thereby reduce uranium binding insignificantly compared to the cations that proceeds through mechanisms that best fitted Freundlich model. The lowest selectivity coefficients of uranium were observed for competing Fe^{2+} in both cases. This can be attributed to the adsorption of Fe ion on more than one active site as indicated that its adsorption data best fitting Freundlich isotherm, consequently contesting the binding of uranium on various active sites. In addition iron exist in various oxidation state and complexation forms (Appendix A1), hence offering it better chance to be adsorbed by different rate determining active sites. The decrease in uranium removal in the presence of Ca can be attributed to the carbonate ion presented by the dissolution of Calcium as $CaCO_3$ thereby forming uranium carbonate. The results generally show that uranium removal is greatly decreased by competing metal in SPC samples than in APZ samples.

Table 5.10: The metal ion distribution coefficient and selectivity coefficient

	Metals	K_dU	K_{M+}	*K*	M^+ *isotherms*
SPC	U/Fe	0,0047	1,31	0,0036	Freundlich
APZ	U/Fe	0,014	0,93	0,015	Freundlich
SPC	U/Mn	0,0027	0,0025	1,06	Langmuir
APZ	U/Mn	0,031	0,00069	44,12	Langmuir
SPC	U/Ca	0,0027	0,021	0,13	Langmuir
APZ	U/Ca	0,020	0,0014	14,64	Freundlich

5.2.3. Conclusion

The APZ and SPC can be used to effectively remove uranium from small (batch) scale aqueous inorganic wastewaters since the adsorption efficiency of atleast 98% and 78% were observed for SPC at all pH range and APZ at pH 4 using 10 mg L^{-1} solution, respectively. The highest adsorption capacity of 49 mg g^{-1} and 44 mg g^{-1} were reached at pH 4 using 100 mg L^{-1} U concentration onto 25 mg and 100 mg for 1 h and 6 h contact time onto SPC and APZ, respectively. The thermodynamic models indicated that the uranyl ion was feasible, spontaneous and occurred exothermically for both APZ and SPC. The increasing temperature lead to random adsorption of uranium by APZ but the order increased for SPC with increasing temperature. The kinetic and isotherm models showed that the sorption occurred chemically. The diffusion models revealed that the pore size diameters were involved in the reaction mechanisms for both adsorbents. The phosphate functionalised zeolites removal efficiency of uranium was enhanced greatly by the presence of disodium phosphate. The APZ is well suited for competing salts water type compared to SPC which was mostly affected by the presence of competing species evaluated in this adsorption study.

Chapter 6

Summary of general conclusions and future work

This chapter gives a summary of the study outputs based on the adsorption capability of activated carbon, natural zeolites, amine zeolite, phosphate zeolite and silica polyamine composite for uranyl ion in aqueous solution. The chapter further recommend the possible future related research areas to be undertaken.

6.1. Summary of general conclusions

The reflux functionalisation method proved to be a plausible route for successfully incorporating organic moieties into the zeolite surfaces such that the uranyl ion adsorption selectivity can be enhanced, especially when the capping agent is a phosphate group ligand. The amine group functionalised zeolites and phosphate group functionalised zeolites were used in their granular form and they were easy to handle during batch applications since they do not require the use techniques such as ultrafiltration because they are at least 2 mm in size. The FTIR vibration showed that zeolite functionalisation with the phosphate and amine groups was successfully achieved while the TGA analysis indicated that the structural thermal stability of the zeolite was almost completely retained at ambient temperature. The BET analysis showed that the introduction of amine groups resulted in external surface functionalisation and internal pore blockage which in turn reduced the surface area of the amine functionalised zeolite.

The uranium removal using phosphate group ligated silica adsorbent material such as silica polyamine composite and aminomethyl phosphonic acid zeolite provide high affinity for uranium-phosphate complexation which promotes high uranium removal efficiency. Activated carbon removes uranium better than untreated natural zeolite but adsorbs uranium weakly compared to phosphate ligated natural zeolite. The predominant adsorption of uranyl ion by phosphate group based adsorbents is due to the property of the phosphate group ligand which enables them to form multidentate complexes when they come into contact with different uranium species.

The uranium coordination is favours chemical adsorption mechanisms largely dependent on speciation, competing metal species, the charge of the ligand type and size of the ion acting as the active site; this makes pH the most important parameter during uranium adsorption. The relative selectivity of adsorbents was of the order towards: SPC > APZ >>> AC≥ AMZ > NZ.

6.2. Future work

- There is a need to evaluate the effectiveness of zeolites functionalised using microwave technique since this route has been recently recommended in literature as a better route to introduce the capping agents inside the inner zeolite structure by supercritical processes. Therefore, this means the negativity caused by pore blockage when using the reflux method can possibly be avoided and hence increase the number of active sites (organic groups) of the inner surfaces of the functionalised zeolites.

- In order to confirm the applicability of the outcomes of the work presented in the studies 5.1 and 5.2 further evaluation based on column studies are necessary since they closely represent real aquatic environmental conditions. If the same material synthesised performs adequately in column systems they will have to be further used and monitored in an open real water area designed for remediation purposes.

- The use of zeolite in nanoparticle form can also be assessed. This is to ensure that the surface area increases which according to most literature studies may influence an increase in kinetic energy or collision between target metal ion and the adsorbent active site and thereby increasing the adsorption probability.

- Analysis of the chemical composition of real water samples from a known uranium-contaminated water system should be conducted. Perform speciation and forward modelling and assess the surface exchange reactions using Phreeqc in order to predict the mechanisms responsible for the results that will be obtained when these adsorbents are tested in real water column studies.

6.3. References

Abdi, M.R., Shakur, H.R., Rezaee Ebrahim Saraee, K., Sadeghi, M., 2014. Effective removal of uranium ions from drinking water using CuO/X zeolite based nanocomposites: Effects of nano concentration and cation exchange. J. Radioanal. Nucl. Chem. 300, 1217–1225. doi:10.1007/s10967-014-3092-3.

Adams, N., Spoor, N., 1974. Kidney and bone retention functions in the human metabolism of uranium. Phys. Med. Biol. 19, 460.

Akcil, A., Koldas, S., 2006. Acid Mine Drainage (AMD): causes, treatment and case studies. J. Clean. Prod. 14, 1139–1145. doi:10.1016/j.jclepro.2004.09.006.

Alberti, G., Biesuz, R., Pesavento, M., 2007. Determination of the total concentration and speciation of Uranium in natural waters by the Resin Titration method. Microchemical. J. 86, 166–173. doi:10.1016/j.microc.2007.02.004.

Asakura, Y., Takayama, R., Shibue, T., Kuroda, K., 2014. Topotactic conversion of β-helix-layered silicate into AST-type zeolite through successive interlayer modifications. Chem. - A Eur. J. 20, 1893–1900. doi:10.1002/chem.201303368.

Asikainen, M., Kahlos, H., 1979. Anomalously high concentrations of uranium, radium and radon in water from drilled wells in the Helsinki region. Geochim. Cosmochim. Acta 43, 1681–1686.

Arnold, T., Baumann, N., Krawczyk-B??rsch, E., Brockmann, S., Zimmermann, U., Jenk, U., Weiβ, S., 2011. Identification of the uranium speciation in an underground acid mine drainage environment. Geochim. Cosmochim. Acta 75, 2200–2212. doi:10.1016/j.gca.2011.01.037

Babel, S., Kurniawan, T.A., 2003. Low-cost adsorbents for heavy metals uptake from contaminated water: a review. J. Hazard. Mater. 97, 219–243. doi:10.1016/S0304-3894(02)00263-7.

Bakatula, E.N., Cukrowska, E.M., Weiersbye, I.M., Mihaly-cozmuta, L., Peter, A., Tutu, H., 2014. Biosorption of trace elements from aqueous systems in gold

mining sites by the filamentous green algae (*Oedogonium sp*.). J. Geochemical Explor. 144, 492–503. doi:10.1016/j.gexplo.2014.02.017.

Bakatula, E.N., Cukrowska, E.M., Chimuka, L., Tutu, H., 2012. Characterization of cyanide in a natural stream impacted by gold mining activities in the Witwatersrand Basin, South Africa. Toxicol. Environ. Chem. 94, 7–19. doi:10.1080/02772248.2011.638637

Bakatula, E.N., Mosai, A.K., Tutu, H., 2015. Removal of Uranium from Aqueous Solutions using Ammonium-modified Zeolite. South African J. Chem. 165– 171. doi:10.17159/0379-4350/2015/v68a23.

Bargar, J.R., Reitmeyer, R., Davis, J.A., 1999. Spectroscopic confirmation of uranium (VI)-carbonato adsorption complexes on hematite. Environ. Sci. Technol. 33, 2481–2484.

Barquist, K.N., 2009. Synthesis and environmental adsorption applications of functionalized zeolites and iron oxides/zeolite composites, PhD Thesis, University of Iowa, Iowa city

Beatty, S.T., Fischer, R.J., Hagers, D.L., Rosenberg, E., 1999a. A Comparative Study of the Removal of Heavy Metal Ions from Water Using a Silica−Polyamine Composite and a Polystyrene Chelator Resin. Ind. Eng. Chem. Res. 38, 4402–4408. doi:10.1021/ie9903386.

Beatty, S.T., Fischer, R.J., Rosenberg, E., Pang, D., 1999b. Comparison of novel and patented silica-polyamine composite materials as aqueous heavy metal ion recovery materials. Sep. Sci. Technol. 34, 2723–2739.

Belli, K.M., Dichristina, T.J., Cappellen, P. Van, 2015. Effects of aqueous uranyl speciation on the kinetics of microbial uranium reduction. Geochim. Cosmochim. Acta 157, 109–124. doi:10.1016/j.gca.2015.02.006.

Bernhard, G., Geipel, G., Brendler, V., Nitsche, H., 1998. Uranium speciation in waters of different uranium mining areas. J. Alloys Compd. 271, 201–205.

Bianca, T., 2001. Differential Scanning Calorimetry (DSC) and Thermogravimetry Analysis (TGA) 2–3.

Bister, S., Birkhan, J., Lüllau, T., Bunka, M., Solle, A., Stieghorst, C., Riebe, B., Michel, R., Walther, C., 2015. Impact of former uranium mining activities on the floodplains of the Mulde River , Saxony , Germany. J. Environ. Radioact. 144, 21–31. doi:10.1016/j.jenvrad.2015.02.024.

Brierley, C.L., 1990. Bioremediation of metal contaminated surface and groundwaters. Geomicrobiol. J. 8, 201–223.

Briner, W., Murray, J., 2005. Effects of short-term and long-term depleted uranium exposure on open-field behavior and brain lipid oxidation in rats. Neurotoxicol. Teratol. 27, 135–144. doi:10.1016/j.ntt.2004.09.001

Brühwiler, D., Calzaferri, G., 2005. Selective functionalization of the external surface of zeolite L. Comptes Rendus Chim. 8, 391–398. doi:10.1016/j.crci.2004.11.008.

Campbell, K.M., Gallegos, T.J., Landa, E.R., 2015. Applied Geochemistry Biogeochemical aspects of uranium mineralization, mining, milling, and remediation. Appl. Geochemistry 57, 206–235. doi:10.1016/j.apgeochem.2014.07.022.

Chen, J.P., Wu, S., Chong, K., 2003. Surface modification of a granular activated carbon by citric acid for enhancement of copper adsorption. Carbon 41, 1979–1986.

Chisholm-brause, C.J., Berg, J.M., Matzner, R.A., Morris, D.E., 2001. Uranium (VI) Sorption Complexes on Montmorillonite as a Function of Solution Chemistry. Journal of Colloid and Interface Science 233, 38–49. doi:10.1006/jcis.2000.7227.

Cozmuta, L.M., Cozmuta, A.M., Peter, A., Nicula, C., Nsimba, E.B., Tutu, H., 2012. The influence of pH on the adsorption of lead by Na-clinoptilolite : Kinetic and equilibrium studies. Water SA 38, 269–278.

Crafford, D., 2010. Bioaccumulation of non-essential trace metals in tissues and organs of Clarias gariepinus (sharptooth catfish) from the Vaal River system – strontium , aluminium , lead and nickel. Water SA 36 (5), 621–640.

Da, E., Sayari, A., 2012. Adsorption of heavy metals on amine-functionalized SBA-15 prepared by co-condensation : Applications to real water samples. Des. 285, 62–67. doi:10.1016/j.desal.2011.09.034.

Dada, A., Olalekan, A., Olatunya, A., Dada, O., 2012. Langmuir, Freundlich, Temkin and Dubinin–Radushkevich isotherms studies of equilibrium sorption of Zn^{2+} unto phosphoric acid modified rice husk. J. Appl. Chem. 3, 38–45.

Das, D., Lee, J.F., Cheng, S., 2001. Sulfonic acid functionalized mesoporous MCM-41 silica as a convenient catalyst for Bisphenol-A synthesis. Chem. Commun. (Camb). 2178–2179. doi:10.1039/b107155f.

Dash, R.R., Balomajumder, C., Kumar, A., 2009. Removal of cyanide from water and wastewater using granular activated carbon. Chem. Eng. J. 146, 408–413. doi:10.1016/j.cej.2008.06.021

Davidescu, C.M., Ciopec, M., Negrea, A., Popa, A., Lupa, L., Dragan, E.S., Ardelean, R., Ilia, G., Iliescu, S., 2013. Synthesis, characterization, and Ni(II) ion sorption properties of poly(styrene-co-divinylbenzene) functionalized with aminophosphonic acid groups. Polym. Bull. 70, 277– 291. doi:10.1007/s00289-012-0801-3.

Deepatana, A., Valix, M., 2008. Steric hindrance effect on adsorption of metal – organic complexes onto aminophosphonate chelating resin. Des. 218, 297–303.

Donat, R., 2009. The removal of uranium(VI) from aqueous solutions onto natural sepiolite. J. Chem. Thermodyn. 41, 829–835. doi:10.1016/j.jct.2009.01.009.

Doyle, W.M., 1992. Principles and applications of Fourier transform infrared (FTIR) process analysis, 2, 11–41.

Dudev, M., Wang, J., Dudev, T., Lim, C., 2006. Factors governing the metal coordination number in metal complexes from Cambridge Structural Database analyses. J. Phys. Chem. B 110, 1889–1895.

Elser, J., Bennett, E., 2011. Phosphorus cycle: A broken biogeochemical cycle. Nature 478, 29–31. doi:10.1038/478029a.

Englert, A., Rubio, J., 2005. Characterization and environmental application of a Chilean natural zeolite. Int. J. Miner. Process. 75, 21–29.

Erdem, E., Karapinar, N., Donat, R., 2004. The removal of heavy metal cations by natural zeolites. J. Colloid Interface Sci. 280, 309–314. doi:10.1016/j.jcis.2004.08.028

Fagan, P.A., Haddad, P.R., 1991. Determination of free cyanide in gold cyanidation process liquors by ion-interaction chromatography with post-column derivatization. J. Chromatography A. 550, 559–571.

Falconer, D.M., Craw, D., Youngson, J.H., Faure, K., 2006. Gold and sulphide minerals in Tertiary quartz pebble conglomerate gold placers , Southland , New Zealand 28, 525–545. doi:10.1016/j.oregeorev.2005.03.009.

Fang, G.-Z., Tan, J., Yan, X.-P., 2005. An ion-imprinted functionalized silica gel sorbent prepared by a surface imprinting technique combined with a sol-gel process for selective solid-phase extraction of cadmium(II). Anal. Chem. 77, 1734–1739.

Faur-Brasquet, C., Kadirvelu, K., Le Cloirec, P., 2002. Removal of metal ions from aqueous solution by adsorption onto activated carbon cloths: Adsorption competition with organic matter. Carbon 40, 2387–2392. doi:10.1016/S0008-6223(02)00117-3.

Figueiredo, H., Quintelas, C., 2014. Tailored zeolites for the removal of metal oxyanions: Overcoming intrinsic limitations of zeolites. J. Hazard. Mater. 274, 287–299. doi:10.1016/j.jhazmat.2014.04.012.

Fox, P.M., Davis, J.A., Zachara, J.M., 2006. The effect of calcium on aqueous uranium(VI) speciation and adsorption to ferrihydrite and quartz. Geochim. Cosmochim. Acta 70, 1379–1387. doi:10.1016/j.gca.2005.11.027.

Frimmel, H.E., 2003. Detrital origin of hydrothermal Witwatersrand gold - A review Detrital origin of hydrothermal Witwatersrand gold - a review. Terra Nov. 9, 192–197. doi:10.1046/j.1365-3121.1997.d01-23.x.

Fu, J., Chen, Z., Wang, M., Liu, S., Zhang, J., Zhang, J., Han, R., Xu, Q., 2015. Adsorption of methylene blue by a high-efficiency adsorbent (polydopamine microspheres): Kinetics, isotherm, thermodynamics and mechanism analysis. Chem. Eng. J. 259, 53–61. doi:10.1016/j.cej.2014.07.101.

Gelb, L.D., Gubbins, K., 1998. Characterization of porous glasses: Simulation models, adsorption isotherms, and the Brunauer-Emmett-Teller analysis method. Langmuir 14, 2097–2111.

Giles, C.H., Smith, D., Huitson, A., 1974. A General Treatment and Classification of the Solute Adsorption Isotherm; I thereoretical. J. Colloid Interface Sci 47, 766–778.

Gregusova, M., Docekal, B., 2011. Analytica Chimica Acta New resin gel for uranium determination by diffusive gradient in thin films technique. Anal.Chim. Acta 684, 142–146. doi:10.1016/j.aca.2010.11.002.

Groudev, S., Georgiev, P., Spasova, I., Nicolova, M., 2008. Hydrometallurgy Bioremediation of acid mine drainage in a uranium deposit. J. Hydromet. 94, 93–99. doi:10.1016/j.hydromet.2008.05.023.

Grové, D., Harris, C., 2010. O- and H-isotope study of the Carbon Leader Reef at the Tau Tona and Savuka mines (Western Deep Levels), South Africa: Implications for the origin and evolution of Witwatersrand Basin fluids. South African J. Geol. 113, 73–86. doi:10.2113/gssajg.113.1-73

Guibal, E., Roulph, C., Le Cloirec, P., 1992. Uranium biosorption by a filamentous fungus *Mucor miehei* pH effect on mechanisms and performances of uptake. Water Res. 26, 1139–1145. doi:10.1016/0043-1354(92)90151-S.

Haggerty, G.M., Bowman, R.S., 1994. Sorption of Chromate and Other Inorganic Anions by Organo-Zeolite. Environ. Sei. Techno 28, 452–458.

Hameed, B., Daud, F., 2008. Adsorption studies of basic dye on activated carbon derived from agricultural waste: *Hevea brasiliensis* seed coat. Chem. Eng. J. 139, 48–55.

Han, R., Zou, W., Wang, Y., Zhu, L., 2007. Removal of uranium(VI) from aqueous solutions by manganese oxide coated zeolite: discussion of adsorption isotherms and pH effect. J. Environ. Radioact. 93, 127–143. doi:10.1016/j.jenvrad.2006.12.003.

Harris, D.C., 2007. Quantitative Chemical Analysis, 7th edition, W.H. Freeman and Company, New York, USA.

Hnizdo, E., Murray, J., Klempman, S., 1997. Lung cancer in relation to exposure to silica dust, silicosis and uranium production in South African gold miners. Thorax 52, 271–275.

Ho, Y.S., Mckay, G., 2002. Application of Kinetic Models to the Sorption of Copper(II) on to Peat. Adsorption Science and Technology. 20 (8), 797–815.

Horzum, N., Shahwan, T., Parlak, O., Demir, M.M., 2012. Synthesis of amidoximated polyacrylonitrile fibers and its application for sorption of aqueous uranyl ions under continuous flow. Chem. Eng. J. 213, 41–49. doi:10.1016/j.cej.2012.09.114.

Huang, A., Dou, W., Caro, J., 2010. Steam-stable zeolitic imidazolate framework ZIF-90 membrane with hydrogen selectivity through covalent functionalization. J. Am. Chem. Soc. 132, 15562–15564.

Hughes, M. a., Rosenberg, E., 2007. Characterization and Applications of Poly Acetate Modified Silica Polyamine Composites. Sep. Sci. Technol. 42, 261– 283. doi:10.1080/01496390601070141.

Ibrahim, H.S., Jamil, T.S., Hegazy, E.Z., 2010. Application of zeolite prepared from Egyptian kaolin for the removal of heavy metals: II. Isotherm models. J. Hazard. Mater. 182, 842–847. doi:10.1016/j.jhazmat.2010.06.118.

Inglezakis, V.J., Grigoropoulou, H., 2004. Effects of operating conditions on the removal of heavy metals by zeolite in fixed bed reactors. J. Hazard. Mater. B 112, 37–43. doi:10.1016/j.jhazmat.2004.02.052.

Inglezakis, V.J., Loizidou, M.M., Grigoropoulou, H.P., 2004. Ion exchange studies on natural and modified zeolites and the concept of exchange site accessibility. J. Colloid Interface Sci 275, 570–576. doi:10.1016/j.jcis.2004.02.070.

Jamil, T.S., Gad-allah, T.A., Ibrahim, H.S., Saleh, T.S., 2011. Adsorption and isothermal models of atrazine by zeolite prepared from Egyptian kaolin. Solid State Sci. 13, 198–203. doi:10.1016/j.solidstatesciences.2010.11.014.

Jiang, G.C.-T., 2006. Neurotoxicity of Depleted Uranium. Biol. Trace Elem. Res. 110, 1–17. doi:10.1385/BTER:110:1:1.

Johnson, D.B., Hallberg, K.B., 2005. Acid mine drainage remediation options : a review. Science of the Total Environment 338, 3–14. doi:10.1016/j.scitotenv.2004.09.002.

Kalavathy, M.H., Karthikeyan, T., Rajgopal, S., Miranda, L.R., 2005. Kinetic and isotherm studies of Cu (II) adsorption onto H_3PO_4 - activated rubber wood sawdust. J. Colloid Interface Sci. 292, 354–362.

Kalin, M., Wheeler, W.N., Meinrath, G., 2004. The removal of uranium from mining waste water using algal/microbial biomass. J. Environ. Radioact. 78, 151–177. doi:10.1016/j.jenvrad.2004.05.002.

Kantar, C., 2007. Heterogeneous processes affecting metal ion transport in the presence of organic ligands: Reactive transport modelling. Earth-Science Rev. 81, 175–198. doi:10.1016/j.earscirev.2006.11.001.

Karpas, Z., 2014. Analytical Chemistry of Uranium: Environmental, Forensic, Nuclear, and Toxicological Applications. Taylor & Francis.

Kiefer, R., Höll, W.H., 2001. Sorption of Heavy Metals onto Selective Ion-Exchange Resins with Aminophosphonated Functional Groups. Ind. Eng. Chem. Res. 40, 4570–4576. doi:10.1021/ie010182l.

Kouraim, M.N., Farag, N.M., Sadeak, S.A., Gado, M.A., 2015. Extraction of uranium using impregnated hydrophobic water hyacinth roots. International Journal of Chemical Studies 2, 10–19.

Kraemer, L.D., Evans, D., 2012. Uranium bioaccumulation in a freshwater ecosystem: Impact of feeding ecology. Aquat. Toxicol. 124–125, 163–170. doi:10.1016/j.aquatox.2012.08.012.

Kütahyalı, C., Eral, M., 2004. Selective adsorption of uranium from aqueous solutions using activated carbon prepared from charcoal by chemical activation. Sep. Purif. Technol. 40, 109–114. doi:10.1016/j.seppur.2004.01.011.

Ladeira, A.C.Q., Gonçalves, C.R., 2007. Influence of anionic species on uranium separation from acid mine water using strong base resins. J. Hazard. Mater. 148, 499–504. doi:10.1016/j.jhazmat.2007.03.003.

Langmuir, D., 1978. Uranium solution-mineral equilibria at low temperatures with applications to sedimentary ore deposits. Geochim. Cosmochim. Acta 42, 547–569.

Lee, G., Bigham, J.M., Faure, G., 2002. Removal of trace metals by coprecipitation with Fe, Al and Mn from natural waters contaminated with acid mine drainage in the Ducktown Mining District, Tennessee. Appl. Geochemistry 17, 569–581. doi:10.1016/S0883-2927(01)00125-1.

Lee, K.-H., Matzapetakis, M., Mitra, S., Marsh, E.N.G., Pecoraro, V.L., 2004. Control of metal coordination number in de novo designed peptides through subtle sequence modifications. J. Am. Chem. Soc. 126, 9178–9179.

Leigh, D.S., 1994. Mercury contamination and floodplain sedimentation from former gold mines in north Georgia. JAWRA, 30, 739–748.

Lesthaeghe, D., Delcour, G., Speybroeck, V. Van, Marin, G.B., Waroquier, M., 2006. Theoretical study on the alteration of fundamental zeolite properties by methylene functionalization. J. micromeso 96, 350–356. doi:10.1016/j.micromeso.2006.07.020.

Li, G., Zhao, Z., Liu, J., Jiang, G., 2011. Effective heavy metal removal from aqueous systems by thiol functionalized magnetic mesoporous silica. J. Hazard. Mater. 192, 277–283. doi:10.1016/j.jhazmat.2011.05.015.

Lundin Jr, F.E., Lloyd, J.W., Smith, E.M., 1969. Mortality of Uranium Miners in Relation to Radiation Exposure, Hard-rock Mining and Cigarette Smoking-1950 Through September 1967. Health Phys. 16, 571–578.

Mandal, S., Roy, D., Chaudhari, R. V, Sastry, M., 2004. Pt and Pd nanoparticles immobilized on amine-functionalized zeolite: excellent catalysts for hydrogenation and heck reactions. Chem. Mater. 16, 3714–3724.

Martínez-Torrents, A., Meca, S., Baumann, N., Martí, V., Giménez, J., De Pablo, J., Casas, I., 2013. Uranium speciation studies at alkaline pH and in the presence of hydrogen peroxide using time-resolved laser-induced fluorescence spectroscopy. Polyhedron 55, 92–101. doi:10.1016/j.poly.2013.02.075

McCarthy, T.S., 2011. The impact of acid mine drainage in South Africa. S. Afr. J. Sci. 107, 1–7. doi:10.4102/sajs.v107i5/6.712.

Mellah, A., Chegrouche, S., Barkat, M., 2006. The removal of uranium(VI) from aqueous solutions onto activated carbon: Kinetic and thermodynamic investigations. J. Colloid Interface Sci. 296, 434–441. doi:10.1016/j.jcis.2005.09.045.

Misaelides, P., 2011. Application of natural zeolites in environmental remediation: A short review. Microporous Mesoporous Mater. 144, 15–18. doi:10.1016/j.micromeso.2011.03.024.

Monser, L., Adhoum, N., 2002. Modified activated carbon for the removal of copper, zinc, chromium and cyanide from wastewater. Sep. Purif. Technol. 26, 137–146. doi:10.1016/S1383-5866(01)00155-1.

Moore, A.P., Beeler, B., Deo, C., Baskes, M.I., Okuniewski, M.A., 2015. Atomistic modeling of high temperature uranium-zirconium alloy structure and thermodynamics. J. Nucl. Mater. 467, 802–819. doi:10.1016/j.jnucmat.2015.10.016.

Motsi, T., Rowson, N.A., Simmons, M.J.H., 2009. Adsorption of heavy metals from acid mine drainage by natural zeolite. Int. J. Miner. Process. 92, 42–48. doi:10.1016/j.minpro.2009.02.005

Mugisidi, D., Ranaldo, A., Soedarsono, J.W., Hikam, M., 2007. Modification of activated carbon using sodium acetate and its regeneration using sodium hydroxide for the adsorption of copper from aqueous solution. Carbon 45, 1081–1084. doi:10.1016/j.carbon.2006.12.009.

Nagarale, R.K., Gohil, G.S., Shahi, V.K., Rangarajan, R., 2004. Organic - Inorganic Hybrid Membrane : Thermally Stable Cation-Exchange Membrane Prepared by the Sol - Gel Method. Macromolecules 10023–10030.

Naicker, K., Cukrowska, E., McCarthy, T.S., 2003. Acid mine drainage arising from gold mining activity in Johannesburg, South Africa and environs. Environ. Pollut. 122, 29–40. doi:10.1016/S0269-7491(02)00281-6.

Neves, M.O., Figueiredo, V.R., Abreu, M.M., 2012. Transfer of U, Al and Mn in the water-soil-plant (*Solanum tuberosum* L.) system near a former uranium mining are a (Cunha Baixa, Portugal) and implications to human health. Sci. Total Environ. 416, 156–163. doi:10.1016/j.scitotenv.2011.11.065.

Nguyen Trung, C., Begun, G., Palmer, D.A., 1992. Aqueous uranium complexes. 2. Raman spectroscopic study of the complex formation of the dioxouranium (VI) ion with a variety of inorganic and organic ligands. Inorg. Chem. 31, 5280–5287.

Oliveira, L.C.A., Petkowicz, D.I., Smaniotto, A., Pergher, S.B.C., 2004. Magnetic zeolites: A new adsorbent for removal of metallic contaminants from water. Water Res. 38, 3699–3704. doi:10.1016/j.watres.2004.06.008.

Özeroğlu, C., Metin, N., 2012. Adsorption of uranium ions by crosslinked polyester resin functionalized with acrylic acid from aqueous solutions. J. Radioanal. Nucl. Chem. 291, 923–935. doi:10.1007/s10967-011-1533-9.

Palanivelu Saravanan, Sridhar Aparna, S.A.K. and D.D., 2015. Studies on Biocide Encapsulated Zeolite-epoxy Nano Hybrid Coatings on Mild Steel. Curr. Bionanotechnol. 1, 37–50. doi:10.2174/2213529401666150304234007.

Parab, H., Joshi, S., Shenoy, N., Verma, R., Lali, A., Sudersanan, M., 2005. Uranium removal from aqueous solution by coir pith: Equilibrium and kinetic studies. Bioresour. Technol. 96, 1241–1248. doi:10.1016/j.biortech.2004.10.016.

Pickett, G., 1945. Modification of the Brunauer—Emmett—Teller Theory of Multimolecular Adsorption. J. Am. Chem. Soc. 67, 1958–1962.

Ríos, C.A., Williams, C.D., Roberts, C.L., 2008. Removal of heavy metals from acid mine drainage (AMD) using coal fly ash, natural clinker and synthetic zeolites. J. Hazard. Mater. 156, 23–35. doi:10.1016/j.jhazmat.2007.11.123.

Robbins, M.O., 1970.Comments on the Elovich equation. J. Catalysis. 16, 126-128.

Rodbard, D., 1974. Statistical quality control and routine data processing for radioimmunoassays and immunoradiometric assays. Clin. Chem. 20, 1255–1270.

Rosenberg, E., Pinson, G., Tsosie, R., Tutu, H., Cukrowska, E., 2016. Uranium remediation by ion exchange and sorption methods: A critical review. Johnson Matthey Technol. Rev. 60, 59–77. doi:10.1595/205651316X690178.

Rosner, T., van Schalkwyk, A., 2000. The environmental impact of gold mine tailings footprints in the Johannesburg region, South Africa. Bull. Eng. Geol. Environ. 59, 137–148. doi:10.1007/s100640000037.

Rui-Zhong, H., Wen-Chao, S., Xian-Wu, B., Guang-Zhi, T., Hofstra, A.H., 2002. Geology and geochemistry of Carlin-type gold deposits in China. Miner. Depos. 37, 378–392. doi:10.1007/s00126-001-0242-7

Saad, D.M., Cukrowska, E., Tutu, H., 2015. Column adsorption studies for the removal of U by phosphonated cross-linked polyethylenimine: modelling and optimization. Appl. Water Sci. 5, 57–63. doi:10.1007/s13201-014-0162-1.

Saad, D.M.G., Cukrowska, E.M., Tutu, H., 2014. Engineered Materials for the Containment of Uranium and Other Toxic Elements in Mine-polluted Water 654–657.

Saccomanno, G., Huth, G.C., Auerbach, O., Kuschner, M., 1988. Relationship of radioactive radon daughters and cigarette smoking in the genesis of lung cancer in uranium miners. Cancer 62, 1402–1408. doi:10.1002/1097-0142(19881001)62:7<1402::AID-CNCR2820620727>3.0.CO;2-K

Saeed, S.M., Shaker, I.M., 2008. Assessment of heavy metals pollution in water and sediments and their effect on Oreochromis niloticus in the Northern Delta Lakes, Egypt. 8th Int. Symp. Tilapia Aquac. 475–490.

Saleh, T.A., Naeemullah, Tuzen, M., Sarı, A., 2016. Polyethylenimine modified activated carbon as novel magnetic adsorbent for the removal of uranium from aqueous solution. Chem. Eng. Res. Des. 117, 218–227. doi:10.1016/j.cherd.2016.10.030.

Salopek, B., Krasic. D., Filipovic. S., 1992. Measurement and application of zeta-potential. Engeneering .4, 4–8.

Samet, J.M., Kutvirt, D.M., Waxweiler, R.J., Key, C.R., 1984. Uranium mining and lung cancer in Navajo men. N. Engl. J. Med. 310, 1481–1484.

Sanding, A., Bruno, J., 1992. The solubility of (UO 2) 3 (PO 4) 2• 4H 2 O (s) and the formation of U(VI) phosphate complexes: Their influence in uranium speciation in natural waters. Geochim. Cosmochim. Acta 56, 4135–4145.

Sari, A., Tuzen, M., 2009. Kinetic and equilibrium studies of biosorption of Pb(II) and Cd(II) from aqueous solution by macrofungus (*Amanita rubescens*) biomass. J. Hazard. Mater. 164, 1004–1011. doi:10.1016/j.jhazmat.2008.09.002.

Scislewski, A., Zuddas, P., 2013. Risk Evaluation of Uranium Mining: A New Kinetic Approach. Procedia Earth Planet. Sci. 7, 778–781. doi:10.1016/j.proeps.2013.03.195.

Semião, A.J., Rossiter, H.M., Schäfer, A.I., 2010. Impact of organic matter and speciation on the behaviour of uranium in submerged ultrafiltration. J. Memb. Sci. 348, 174–180.

Sharma, S., Singh, B., Manchanda, V.K., 2014. Phytoremediation: role of terrestrial plants and aquatic macrophytes in the remediation of radionuclides and heavy metal contaminated soil and water. Environ. Sci. Pollut. Res. 22, 946–962. doi:10.1007/s11356-014-3635-8.

Shin, Y., Zemanian, T.S., Fryxell, G.E., Wang, L.Q., Liu, J., 2000. Supercritical processing of functionalized size selective microporous materials. Microporous Mesoporous Mater. 37, 49–56. doi:10.1016/S1387-1811(99)00192-4.

Shrivastava, A., Sharma, J., Soni, V., 2013. Various electroanalytical methods for the determination of uranium in different matrices. Bull. Fac. Pharmacy, Cairo Univ. 51, 113–129.

Shuibo, X., Chun, Z., Xinghuo, Z., Jing, Y., Xiaojian, Z., Jingsong, W., 2009. Removal of uranium (VI) from aqueous solution by adsorption of hematite. J. Environ. Radioact. 100, 162–166. doi:10.1016/j.jenvrad.2008.09.008.

Sirola, K., Laatikainen, M., Lahtinen, M., Paatero, E., 2008. Removal of copper and nickel from concentrated ZnSO4 solutions with silica-supported chelating adsorbents. Sep. Purif. Technol. 64, 88–100. doi:10.1016/j.seppur.2008.08.001.

Sladkov, V., 2013. Uranyl complexation with acetate studied by means of affinity capillary electrophoresis. J. Chromatogr. A 1289, 133–138.

Sprynskyy, M., Kowalkowski, T., Tutu, H., Cukrowska, E.M., Buszewski, B., 2015. Ionic liquid modified diatomite as a new effective adsorbent for uranium ions removal from aqueous solution. Colloids Surfaces A Physicochem. Eng. Asp. 465, 159–167. doi:10.1016/j.colsurfa.2014.10.042.

Sprynskyy, M., Kowalkowski, T., Tutu, H., Cukrowska, E.M., Buszewski, B., 2011. Adsorption performance of talc for uranium removal from aqueous solution. Chem. Eng. J. 171, 1185–1193. doi:10.1016/j.cej.2011.05.022.

Sutton, M., Burastero, S.R., 2004. Uranium (VI) solubility and speciation in simulated elemental human biological fluids. Chem. Res. Toxicol. 17, 1468–1480.

Sylwester, E.R., Hudson, E.A., Allen, P.G., 2000. The structure of uranium (VI) sorption complexes on silica, alumina, and montmorillonite. Geochim. Cosmochim. Acta 64, 2431–2438. doi:10.1016/S0016-7037(00)00376-8

Tawanda, N., Ewa, T., Chimuka, L., 2014. Sequestration of U (VI) from aqueous solutions using precipitate ion imprinted polymers endowed with oleic acid functionalized magnetite J. Radioanal Nucl Chem. 933–943. doi:10.1007/s10967-014-3878-3.

Tavengwa, N.T., Cukrowska, E., Chimuka, L., 2015. Selective Adsorption of Uranium(VI) on $NaHCO_3$ Leached Composite Methacryloxypropyltrimethoxysilane Coated Magnetic Ion-imprinted Polymers Prepared by Precipitation Polymerization. S. Afr. J. Chem 68, 61–68. doi:10.17159/0379-4350/2015/v68a10

Tavengwa, N.T., Cukrowska, E., Chimuka, L., 2014. Synthesis of bulk ion-imprinted polymers (IIPs) embedded with oleic acid coated Fe3O4 for selective extraction of hexavalent uranium. Water SA 40, 623–630. doi:10.4314/wsa.v40i4.7

Tucker, R.F., Viljoen, R.P., Viljoen, M.J., 2016. A Review of the Witwatersrand Basin - The World's Greatest Goldfield. Episodes 39, 105. doi:10.18814/epiiugs/2016/v39i2/95771

Tutu, H., Bakatula, E., Dlamini, S., Rosenberg, E., Kailasam, V., Cukrowska, E.M., 2013. Kinetic, equilibrium and thermodynamic modelling of the sorption of metals from aqueous solution by a silica polyamine composite. Water SA 39, 437–444.

Tutu, H., Cukrowska, E., Mccarthy, T.S., Mphephu, N.F., Hart, R., 2012. Determination and modelling of geochemical speciation of uranium in gold mine polluted land in South Africa. 8th Int. Congr. Mine Water Environ. Johannesburg, South Africa 137–155.

Tutu, H., McCarthy, T.S., Cukrowska, E., 2008. The chemical characteristics of acid mine drainage with particular reference to sources, distribution and remediation: The Witwatersrand Basin, South Africa as a case study. Appl. Geochemistry 23, 3666–3684. doi:10.1016/j.apgeochem.2008.09.002.

Ulrich, K.-U., Rossberg, A., Foerstendorf, H., Zänker, H., Scheinost, A.C., 2006. Molecular characterization of uranium(VI) sorption complexes on iron(III)-rich acid mine water colloids. Geochim. Cosmochim. Acta 70, 5469–5487.

Vassylyev, O., Chen, J., Hall, G.S., Khinast, J.G., 2006. Efficient surface functionalization of zeolites via esterification. Microporous Mesoporous Mater. 92, 101–108. doi:10.1016/j.micromeso.2005.10.030.

Vidaud, C., Dedieu, A., Basset, C., Plantevin, S., Dany, I., Pible, O., Quéméneur, E., 2005. Screening of human serum proteins for uranium binding. Chem. Res. Toxicol. 18, 946–953.

Wall, J.D., Krumholz, L.R., 2006. Uranium reduction. Annu. Rev. Microbiol. 60, 149–166.

Wan, B., Fleming, J.T., Schultz, T.W., Sayler, G.S., 2006. In vitro immune toxicity of depleted uranium: Effects on murine macrophages, $CD4^+$ T cells, and gene expression profiles. Environ. Health Perspect. 114, 85–91. doi:10.1016/j.patrec.2005.07.005

Wang, S., Zhu, Z., 2006. Characterisation and environmental application of an Australian natural zeolite for basic dye removal from aqueous solution. J. Hazard. Mater. 136, 946–952.

Wang, X., Ni, S., Shi, Z., 2014. Uranium distribution in the sediment of the Mianyuan River near a phosphate mining region in China and the related uranium speciation in water. Chemie der Erde - Geochemistry 74, 661–669. doi:10.1016/j.chemer.2014.03.001.

Wang, Y.-L., Song, L.-J., Zhu, L., Guo, B.-L., Chen, S.-W., Wu, W.-S., 2014. Removal of uranium(VI) from aqueous solution using iminodiacetic acid derivative functionalized SBA-15 as adsorbents. Dalton Trans. 43, 3739–49. doi:10.1039/c3dt52610k.

Wang, Z., Cohen, S.M., 2009. Metal – organic frameworks issue Postsynthetic modification of metal – organic frameworks. Chem. Soc. Rev. doi:10.1039/b802258p

Wu, F.C., Tseng, R.L., Juang, R.S., 2009a. Characteristics of Elovich equation used for the analysis of adsorption kinetics in dye-chitosan systems. Chem. Eng. J. 150, 366–373. doi:10.1016/j.cej.2009.01.014.

Wu, F.C., Tseng, R.L., Juang, R.S., 2009b. Initial behavior of intraparticle diffusion model used in the description of adsorption kinetics. Chem. Eng. J. 153, 1–8. doi:10.1016/j.cej.2009.04.042.

Wu, F.C., Tseng, R.L., Juang, R.S., 2009. Characteristics of Elovich equation used for the analysis of adsorption kinetics in dye-chitosan systems. Chem. Eng. J. 150, 366–373. doi:10.1016/j.cej.2009.01.014

Yang, J., Volesky, B., 1999. Biosorption of uranium on Sargassum biomass. Water Res. 33, 3357–3363. doi:10.1016/S0043-1354(99)00043-3

Yazici, E.Y., Deveci, H., Alp, I., 2009. Treatment of cyanide effluents by oxidation and adsorption in batch and column studies. J. Hazard. Mater. 166, 1362–1366. doi:10.1016/j.jhazmat.2008.12.050.

Ye, C., Gong, Q.M., Lu, F.P., Liang, J., 2007. Adsorption of uraemic toxins on carbon nanotubes. Sep. Purif. Technol. 58, 2–6. doi:10.1016/j.seppur.2007.07.003.

Yin, P., Tian, Y., Wang, Z., Qu, R., Liu, X., Xu, Q., Tang, Q., 2011. Synthesis of functionalized silica gel with poly(diethylenetriamine bis(methylene phosphonic acid)) and its adsorption properties of transition metal ions. Mater. Chem. Phys. 129, 168–175. doi:10.1016/j.matchemphys.2011.03.067.

Yin, P., Xu, M., Liu, W., Qu, R., Liu, X., Xu, Q., 2014. High efficient adsorption of gold ions onto the novel functional composite silica microspheres encapsulated by organophosphonated polystyrene. J. Ind. Eng. Chem. 20, 379–390. doi:10.1016/j.jiec.2013.04.032.

Zacaroni, L.M., Magriotis, Z.M., Cardoso, M. das G., Santiago, W.D., Mendonça, J.G., Vieira, S.S., Nelson, D.L., 2015. Natural clay and commercial activated charcoal: Properties and application for the removal of copper from cachaca. Food Control 47, 536–544. doi:10.1016/j.foodcont.2014.07.035.

Zamora, M.L.L., Zielinski, J.M., Moodie, G.B., Falcomer, R. a F., Hunt, W.C., Capello, K., 2009. Uranium in drinking water: renal effects of long-term ingestion by an aboriginal community. Arch. Environ. Occup. Health 64, 228–41. doi:10.1080/19338240903241267.

Zhan, B., White, M.A., Lumsden, M., 2003. Bonding of Organic Amino , Vinyl , and Acryl Groups to Nanometer-Sized NaX Zeolite Crystal Surfaces. Langmuir. 4205– 4210.

Zhang, X.-Y., Wang, Q.-C., Zhang, S.-Q., Sun, X.-J., Zhang, Z.-S., 2009. Stabilization/solidification (S/S) of mercury-contaminated hazardous wastes using thiol-functionalized zeolite and Portland cement. J. Hazard. Mater. 168, 1575–1580.

Zhao, Y., Liu, C., Feng, M., Chen, Z., Li, S., Tian, G., Wang, L., Huang, J., Li, S., 2010. Solid phase extraction of uranium(VI) onto benzoylthiourea-anchored activated carbon. J. Hazard. Mater. 176, 119–124. doi:10.1016/j.jhazmat.2009.11.005.

Zhou, L., Wang, Y., Zou, H., Liang, X., Zeng, K., Liu, Z., Adesina, A.A., 2016. Biosorption characteristics of uranium(VI) and thorium(IV) ions from aqueous solution using CaCl2-modified Giant Kelp biomass. J. Radioanal. Nucl. Chem. 307, 635–644. doi:10.1007/s10967-015-4166-6.

Zobel, C.R., Beer, M., 1961. Electron stains. I. Chemical studies on the interaction of DNA with uranyl salts. J. Biophys. Biochem. Cytol. 10, 335– 46.

Appendix A1

Phreeqc input scripts for uranium and competing species

SOLUTION 1: Uranium and $FeSO_{4(aq)}$

```
temp        25
pH          4
pe          4
redox       pe
units       mg/L
density     1
Fe          30
U           30
S(6)        30
End
```

SOLUTION 2：Uranium and $MnSO_{4(aq)}$

```
temp        25
pH          4
pe          4
redox       pe
units       mg/L
density     1
Mn          30
U           30
S(6)        30
End
```

SOLUTION 3: Uranium and $NaHPO_{4(aq)}$

temp	25
pH	4
pe	4
redox	pe
units	mg/L
density	1
Na	30
U	30
P	30
End	

SOLUTION 4: Uranium and $CaCO_{3(aq)}$

temp	25
pH	4
pe	4
redox	pe
units	mg/L
density	1
Ca	30
C(4)	30
U	30
End	

Phreeqc output scripts for uranium and competing species

SOLUTION 1: uranium and $FeSO_{4(aq)}$

Solution composition

Species	Molality
Fe	5.372×10^{-04}
S(6)	3.123×10^{-04}
U	1.260×10^{-04}

Saturation indices

Species	Molality	SI	Log IAP	Log K
$UO_2(OH)_2$:H_20	1.705×10^{-06}	-1.52	3.88	5.40
$U(OH)_2SO_4$	2.412×10^{-05}	-11.53	-14.73	-3.20
$UO_2(OH)_2$	9.271×10^{-05}	-1.66	3.88	5.54
$FeSO_4$:$7H_2O$	1.71×10^{-05}	-4.81	-7.02	-2.21
SO_4^{2-}	2.687×10^{-4}	-	-	-

SOLUTION 2: Uranium and $MnSO_{4(aq)}$

Solution composition

Species	Molality
Mn	5.461×10^{-04}
S(6)	3.123×10^{-04}
U	1.260×10^{-04}

Saturation indices

Species	Molality	SI	Log IAP	Log K
$UO_2(OH)_2$	1.705×10^{-06}	-1.66	1.88	5.54
$U(OH)_2SO_4$/ $UO_2(SO_4)_2^{2-}$	6.333×10^{-08}	-11.53	-14.73	-3.20
$Mn_2(SO_4)_3$	2.685×10^{-04}	-54.98	-60.69	-5.71
$MnSO_4$	1.736×10^{-05}	-9.68×10^{-05}	-7.01	2.67
UO_2	9.276×10^{-5}	1.72	-3.08	-4.80

Phreeqc output scripts for uranium and competing species

SOLUTION 3：Uranium and $NaHPO_{4(aq)}$

Solution composition

Species	Molality
Na	1.305×10^{-03}
P	9.868×10^{-04}
U	1.260×10^{-04}

Saturation indices

Species	Molality	SI	Log IAP	Log K
$H_2(UO_2)_2(PO_4)_2$	9.306×10^{-12}	-9.46	-57.39	-47.93
$Na_2(OU_2)_2(PO_4)_2$	-	-7.79	-55.20	-47.41
$UO_2(HPO4)_2^{2-}$	1.260×10^{-4}	-7.07	-62.37	-55.30
UO_2HPO_4	3.268×10^{-9}	-4.50	-16.35	-11.85
$U(OH)_2^{2+}$	7.251×10^{-20}	-7.52	-1.98	5.54
UO_2	1.23×10^{-10}	-4.14	-8.94	-4.80
$NaHPO_4^-$	1.086×10^{-9}	-	-	-

SOLUTION 4：Uranium and $CaCO_{3(aq)}$

Solution composition

Species	Molality
C (4)	4.917×10^{-04}
Ca	7.486×10^{-04}
U	1.260×10^{-04}

Saturation indices

Species	Molality	SI	Log IAP	Log K
$CaCO_3$ (aragonite)	-	-6.86	-15.20	-8.34
$CaCO_3$ (calcite)	1.063×10^{-12}	-6.72	-15.20	-8.48
$UO_2(CO_3)_2^{2-}$	1.18×10^{-11}	-	-	-
UO_2 (uraninite)	1.134×10^{-4}	1.81	-2.99	-4.80
$UO_2(OH)_2$	3.271×10^{-12}	-1.57	3.97	5.54
UO_2CO_3	4.087×10^{-7}	-1.57	-16.02	-14.45
$Ca(OH)_2$	-	-18.01	4.79	22.80
$UO_2(OH)_2$:H_20 (schoepite)	2.554×10^{-6}	-1.43	3.97	5.40